Republic of Iraq
Ministry of Higher Education
and Scientific Research
University of Babylon
College of Materials Engineering
Department of Ceramic and Building Materials

Studying the Effect of Mg^{+2} and Cu^{+2} on the Bioactivity and Antibacterial of Powder and Bulk Hydroxyapatite

A Thesis

Submitted to the Conical of the College of Materials Engineering / University of Babylon in Partial Fulfillment of the Requirements for the degree of Master in Materials Engineering/ Ceramic

By

Aala Suhail Najim Aboud

(B.Sc. Ceramic and Building Materials , 2018)

Supervised by

Assist. Prof.
Dr. Israa Khahtan Sabree

Assist. Prof.
Dr. Firas Jabbar Hmood

2022 A.D **1444 A.H**

وزارة التعليم العـــــالي والبحث العلمي
جـــــــامـــــعـــــة بـــــابـــــــل
كـــلـــيـــة هـــنـــدســـــــــة الـــمـــواد
قـــســـم هندسة السيراميك و مواد البناء

دراسة تأثير Mg^{+2} وCu^{+2} على الفعالية الحيوية والمضاد للبكتريا على خواص الهـــايدروكســي ابتايــت المسحوق والمشكل

رسالة

مقدمة الى قسم هندسة السيراميك/كليه هندسه المواد/ جامعة بابل كجزء من متطلبات نيل درجة الماجستير في هندسة المواد / السيراميك

من قبل

الاء سهيل نجم عبود

بإشراف

أ.م.د. اسراء قحطان صبري

أ.م.د. فراس جبار حمود

هـ ١٤٤٤ م ٢٠٢٢

بِسْمِ اللَّهِ الرَّحْمَنِ الرَّحِيمِ

﴿وَيَسْأَلُونَكَ عَنِ الرُّوحِ قُلِ الرُّوحُ مِنْ أَمْرِ رَبِّي وَمَا أُوتِيتُم مِّن الْعِلْمِ إِلاَّ قَلِيلاً﴾

صدق الله العلي العظيم

{ سورة الإسراء / أية 85}

Supervisor Certification

We certify that this thesis entitled (**Studying the Effect of Mg^{+2} and Cu^{+2} on the Bioactivity and Antibacterial of Powders and Bulk Hydroxyapatite**) had been carried out under our supervision at the university of Babylon/ college of material's engineering/department ceramic and building materials in partial fulfillment of the requirements for the degree of Master in Material's Engineering/ ceramic and building materials.

Signature:

Asst. Prof. Israa Khahtan Sabree (PhD)

(supervisor)

Date: / / 2022

Signature:

Asst. Prof. Firas Jabbar Hmood (PhD)

(supervisor)

Date: / / 2022

Examining Committee Certification

We certify that we had read this thesis entitled **(Studying the Effect of Mg^{+2} and Cu^{+2} on the Bioactivity and Antibacterial of Powders and Bulk Hydroxyapatite)** and as an examination committee examined the student (**Aala Suhail Najim)** in its contents and that in our opinion it meets the standard of a thesis and is adequate for the award of the degree of master of science in materials engineering/ ceramic and building materials.

Signature:
Prof.Elham Abd Al Majeed (PhD)
(Committee Chair)
Date: / / 2022

Signature:
Asst. Prof. Shaimaʹa J. Kareem (PhD)
(Member)
Date: / / 2022

Signature:
Asst. Prof. Fatimah J. AL-Hasani (PhD)
(Member)
Date: / / 2022

Signature:
Asst. Prof. Israa Khahtan Sabree (PhD)
(Supervisor)
Date: / / 2022

Signature:
Asst. Prof. Firas Jabbar Hmood (PhD)
(Supervisor)
Date: / / 2022

Approval of Head of the Ceramic and building materials Department

Signature:

Prof. Mohsin Abbas Aswad (PhD)

Date: / / 2022

Approval of Dean of the Materials Engineering Collage

Signature:

Prof. Imad Ali Disher (PhD)

Date: / / 2022

Dedication

To my father that is

the light of my way.

To the greatest woman in

the world my mother.

To My lovely family

with my love

and respect.

Aala

2022

Acknowledgment

Praise be to Allah, Lord of the Creation.

Graduate life would not have been the same without the people who have generously helped me. On this very page, I would like to express my deep gratitude to them.

My first and foremost thanks go to my supervisors ***Dr.Israa*** *and* ***Dr.Firas*** *for their guidance throughout the course of my postgraduate studies and their suggestions and comments on my research were invaluable. I have learnt and benefitted from their valuable knowledge.*

*Thanks to the dean of materials engineering collage for his support**.** I also would like to thank the staff of materials engineering college specially the ceramic and building materials department in University of Babylon.*

I also would like to thank the staff of ceramic and building materials laboratories at the University of Babylon. The support and understanding of my family is deeply appreciated. Their love has been for me a powerful source of inspiration and energy, support and encouragement that have made all of this possible.

Abstract

Abstract

Hydroxyapatite [$Ca_{10}(PO_4)_6(OH)_2$] is one of the most widely used bioceramic materials in medical applications as a result of its high biocompatibility, non-toxicity, high bone bonding ability and osteoconductivity. Pure and Co-doped hydroxyapatite with Cu^{+2}, Mg^{+2} ions powders were prepared using the wet chemical Co-precipitation method at room temperature . Three stoichiometric compositions of the co-doped HA were prepared by substituting calcium ions with the doping metal ions according to the proportions (Mg^{+2} :Cu^{+2}): (0.5:0.5, 0.75:0.25 and 0.25:0.75)

The dried filtered powders were calcinated at 800°C for 2h. The structure was characterized and identified using XRD and TEM means. The biological features i.e. antibacterial activity and toxicity toward osteoblast cells have been also investigated. The XRD analysis reviled that the fabricated co-doped HA had one phase and did not show any other secondary phases. from the XRD analysis the main peaks of all doped HA show a slight shift.

While the TEM images indicated that incorporation of Cu^{2+} and Mg^{2+} has altered the size and shape of the resulting HA crystals, which the nanoparticles appears to be longitudinal in shape with size less than 100nm. Moreover, all the stoichiometric ratio of Cu^{2+} and Mg^{2+} improved the antibacterial activity of HA specially of HA-4 [$(Mg_{0.25,}\ Cu_{0.75})Ca_9(PO_4)_6(OH)_2$] has showed higher inhibition activity toward bacteria cells. On the other hand, switching the stoichiometric ratio of Mg and Cu i.e. HA-3 [$(Mg_{0.75},\ Cu_{0.25})Ca_9(PO_4)_6(OH)_2$] has appeared superior role to increase cell proliferation even more than the pure hydroxyapatite.

In this study modern and simple sintering technique has been involved known as the cold sintering (CSM) method. In which the sintering temperature

does not go more than 300 °C under external applied pressure. The result of XRD for bulk HA fabricated using CSM show that there is no phases of CaO or TTC are formed in addition to the hydroxyapatite structure.

The density of pure Cold sintered hydroxyapatite were measured to be 2.6972 g/cm^3 in comparison to 2.9433 g/cm^3 for HA sintered by traditional sintering. Introducing of metal ions has changed the density according to their ratio in the structure of HA. For instance, Cold sintered HA-4 exhibits density of 2.8792 g/cm^3. In the same context, the result of microhardness has changed with the fabrication route, on one hand, and with the chemical composition on the other hand. The hardness of pure HA prepared using traditional sintering was measured to be 323.83HV in comparison to 224.86 HV for HA sintered by CSM .Bio-degradation results showed that HA biodegrades increased as the number of days increases, and the obtaining results indicate that pure HA had the lowest rate of degradation, also increasing the Mg content in the HA structure significantly enhanced the degradation.

Table of Contents

Table of Contents

List of Tables

List of Figures

List of Symbols and Abbreviations

Symbols	Meaning	Units
HA	Hydroxyapatite	
SEM	Scanning Electron Microscope	
TEM	Transmission Electron Microscope	
FTIR	Fourier-transform Infrared spectroscopy	
XRD	X-Ray Diffraction	
EDX	Energy-Dispersive X-ray analysis	
α-TCP	Alpha Tricalcium phosphate	
β-TCP	Beta Tricalcium phosphate	
TTCP	Tetra Tricalcium phosphate;	
TGA	Thermo Gravimetrical Analysis	
DTA	Differential Thermal Analysis	
Tris	Tris (hydroxymethyl) aminomethane	
E.Coli	Escherichia coli	
S.aureu	Staphylococcus aureus	
DBM	Demineralized Bone Matrix	
SA	Surface Area	mm^2
T	Temperature	°C
TS	Traditional Sintering	
CSM	Cold Sintering Method	
ρ	Density	g/cm^3
Hv	Vickers Hardness	Kgf, MPa
ΔW	Weight Loss	g
Xc	Crystallinity	%
rpm	Round Per Minute	
ROS	Reactive oxygen species	

Chapter One

Introduction

Chapter One

Introduction

1.1 General View

Bioceramics are materials that have good biocompatibility with human body tissues. They used as alternatives to repair damaged parts of the human skeleton. Calcium phosphates are the safest choice among them for a variety of pharmaceutical applications, including tissue engineering, drug delivery, and dental applications. Hydroxyapatite with the chemical formula [$Ca_{10}(PO4)_6(OH)_2$] is one of calcium phosphates family. Its chemical composition is very similar to bone ,where it has a hexagonal structure which allows to host different ions beside to calcium ions and phosphate groups [1].

Bacterial infection of post implantations is common spatially with hydroxyapatite because of its surface features [2]. Doping of hydroxyapatite with antibacterial elements may inhabit bacterial growth and improve hydroxyapatite performance inside the human body. Silver, zinc, copper and other metal elements are widely used bacterial inhibition [3]. No doubt, incorporation of these elements into hydroxyapatite structure will lead to change the dimensions of crystals and the structure order of hydroxyapatite as well [4].

Hydroxyapatite powder can be synthesized following different synthetic routs depending upon the features required like stoichiometric ratio, particle size and particle size distribution, in addition to the morphology. Bulk samples of

hydroxyapatite can be consolidated by using variety of sintering techniques like pressureless sintering method and pressure-assisted techniques [5-7].

High sintering temperatures may cause phase decomposition for the apatite phase at temperatures above than 900°C. This might form secondary phases like **α** or **β** tricalcium phosphate (TCP) and TTCP. Reducing of sintering temperatures may also yield low value of density. Therefore, choosing of appropriate sintering conditions i.e (sintering temperatures and sintering time) are required to get pure apatite phase with high density [8]. Modern sintering techniques attract a lot of attention considering those sintering conditions like cold sintering method. This method is a promising one in the ceramics engineering because it ensures on one side low sintering temperatures (lower than 300 °C); and on the other side low energy consumption which can save cost of production. It involves employing of transient solvent that cause partially dissolution of ceramic particles surface. It is also used to equalize the chemical potential among the particles to be sintered. However, this method is under developing to overcome some drawbacks such as low density. The solvent liquid is evaporated by the end of this method causing precipitation of ceramic species at pores and can lead to form residual nano porosities as a result of escaping the access liquid [9-11].

1.2 Objectives of the Work

The objectives of this study can be summarized as following :

1- Synthesis pure and Co-doped hydroxyapatite powder by incorporation Cu^{2+} and Mg^{2+} into apatite structure with different molar ratios using the wet chemical precipitation method.

2- Investigate the structural features , antibacterial properties, biodegradability , and toxicity of the pure and co-doped hydroxyapatite.

3- Characterize the phase stability, physical and mechanical properties for bulk hydroxyapatite using traditional sintering method and cold sintering method.

4- Low energy consumption and save cost of production .

2.2 Plan of Study

The current study deals with improving the antibacterial properties of HA by incorporation of copper and magnesium ions into HA structure, because hydroxyapatite has a weak antibacterial activity. Besides, investigation the influence of Cu^{+2} and Mg^{+2} ions concentration in the HA lattice on the structural and biological behavior of Co-doped HA with (Cu^{+2}, Mg^{+2}) ions was synthesized using wet chemical co-precipitation method. Biological behavior including antibacterial was made using distinct strains of bacteria which were E.Coli and S.aureu , additionally, cytotoxicity has been calculated. In this investigation, (TEM) used to estimate the particle size and observe the morphology of the starting powders. X-ray diffraction and microstructure of the samples prepared using CSM and traditional sintering have been investigated. In addition, density, hardness and biodegradation behavior of hydroxyapatite has also been studied.

Chapter Two

Theoretical Part and Literature Survey

Chapter Two
Theoretical Background and Literature Survey

2.1 Introduction

During the last two decades, significant advances have been made in the development of biocompatible and biodegradable materials for medical applications. Biomaterials are special materials that have been used in several medical applications. They can be in several kinds like metals, ceramics, polymers and composite etc. Ceramics biomaterials have gained a lot of attention to be used in human body. They were developed to fill and rebuild bone defects: natural coral, bovine porous demineralized bone and human demineralized bone matrix (DBM) [12]. For instance hydroxyapatite material for joins replacement, dental application and drug delivery [13].

Bioceramics are generally classified into three different categories [14]:

- Bioinert ceramics (alumina, zirconia, carbon)
- Bioactive(or surface reactive) bioceramics (hydroxyapatite, Bioglass)
- Bioresorbable ceramics (Tricalcium phosphates) .

2.2 Hydroxyapatite Ceramics

Hydroxyapatite (HA) is widely used as bioceramics due to its compatibility with the chemical and structural bone mineral [15]. It belongs to the family of calcium phosphates as seen in Table (2.1). The chemical formula for pure HA is : $Ca_{10}(PO_4)_6(OH)_2$ which have

a Ca/P ratio of 1.67. It consider as the most stable calcium phosphate compound at room temperatures and at pH between 4 and 12 [16]. Bone is composed of up to 70% HA, 20% collagen, and 10% water [17].

Table (2.1):Calcium phosphate compounds with different ratios of Ca/P [18].

Ca/P molar ratio	Compound	Formula	pH stability range in aqueous solutions at 25°C	Solubility at 25 °C (g/l)
0.5	Monocalcium phosphate monohydrate	$Ca_2(H_2PO_4).H_2O$	0.0-2.0	~18
0.5	Monocalcium phosphate anhydrous	$Ca_2(H_2PO_4)$	Stable at temperatures above 100 °C	~17
1.0	Dicalcium phosphate dihydrate, mineral brushite	$CaHPO_4.2H_2O$	2.5-6.0	~0.088
1.0	Dicalcium phosphate anhydrous, mineral monetite	$CaHP\ O_4$	Stable at temperatures above 100 °C	~0.048
1.33	Octacalcium phosphate (OCP)	$Ca_8(HPO_4)2(PO_4).5H_2O$	5.5-7.0	~0.0081
1.5	α-Tricalcium phosphate (α-TCP)	α-$Ca_3(PO_4)_2$	These compounds cannot be precipitated from aqueous solutions	~0.0025
1.5	ß- Tricalcium phosphate (ß-TCP)	ß-$Ca_3(PO_4)_2$	These compounds cannot be precipitated from aqueous solutions	~0.0005
1.5-1.67	Calcium-deficient hydroxyapatite (CDHA)	$Ca_{10-x}(HPO4)x.(PO4)_{6-x}(OH)_{2-}$	6.5-9.5	~0.0094
1.67	Hydroxyapatite	$Ca_{10}(PO_4)_6\ (OH)_2$	7-11	~0.0003

Studies have shown that synthesized HA promotes osteoblast (bone growth cells) and osteoclast (bone resorption cells) after implantation, thus improve osseointegration. As a result, synthesized HA is widely employed in dentistry and orthopedics, such as dental implants, periodontal treatment, maxillofacial surgery, and otolaryngology [19]. Because it does not exhibit any cytoxic effects[20]. The mechanical properties of HA are low which limits HA use as load

bearing biomaterials in its pure state. Introducing of Al_2O_3, ZrO_2, TiO_2, metal ions, and carbon nanotubes as reinforcement components is the most popular way to deal with this issue [16]. Table (2.2) shows the mechanical properties of dense HA.

Table 2.2: Common mechanical properties of hydroxyapatite [21].

Theoretical density	Tensile strength	Vickers hardness	Bending strength	Compressive strength	Fracture toughness	Young's modulus	Poisson ratio
3.156 g/cm^3	40 - 100 MPa	500 - 800 VH	20 - 80 MPa	100 - 900 MPa	1 MPa.$\sqrt{m}$	30 - 120 GPa	0.3

2.3 Structure of Hydroxyapatite

The most common crystal structure of HA is hexagonal with lattice parameters of (a = b = 9.432 Å, c = 6.881 Å, and γ = 120°). Important structural features of the stoichiometric hydroxyapatite are its structural hydroxyl groups, arranged at the edges of elementary cells, forming the columns–OH–OH–OH– . Hydroxyapatite includes two types of calcium cations, referred to as Ca (I) and Ca (II) as shown in Figure (2.1).The atoms of calcium Ca (I) are located at the edges of a hexagonal unit cell, while the atoms of calcium Ca (II) form equilateral triangles with the column of structural hydroxyl groups in the middle. The structure comprises phosphate ions PO_4^{3-} tetrahedra stuck around each other by calcium ions that are distributed amidst them.
[22].

The space group of the hexagonal HA is $\underline{P6_3/m}$ which allows the unit cells to be placed in a c-axis configuration. This would assign a favored growth that is aligned along with the c-axis to form needle-like shape. Another form of HA is monoclinic that possesses sector group as

$P2_1/b$. This unit cell has lattice parameters a=9.4214(8), b=2a and c=6.88144 (7) Å, γ=120° [23] .

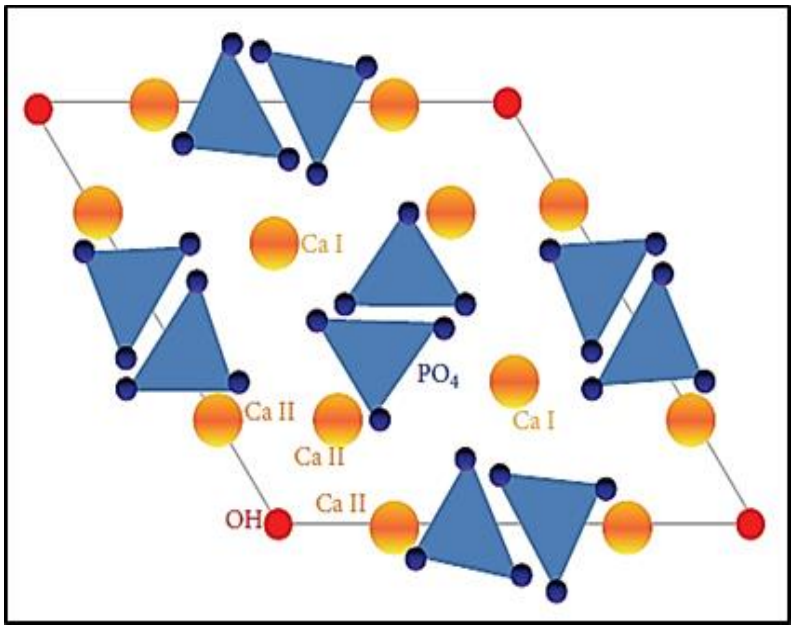

Figure (2.1): Sits of calcium ions and phosphate groups in HA unit cell[22]

The orientations of the hydroxyl (OH) groups are the primary distinction between monoclinic and hexagonal HA [16]. The hexagonal HA is typically precipitated from supersaturated solutions at 25–100°C, whereas the monoclinic HA is generally produced by heating the hexagonal form at 850°C in air and then cooling to ambient temperature [24].

2.4 Modification of Hydroxyapatite Structure

As previously mentioned, HA has a hexagonal structure at room temperature composed of Ca^{2+} ions and PO_4^{3-} tetrahedral arranged on OH^- columns. HA has the ability of one of the main features which is the ion substituting method (i.e., ion exchange) owing to its high structural flexibility, HA can accommodate several anions and cations substitutions within its lattice

see Figure (2.2) . Ions with the same size and charge as hydroxyl ions, like Cl^- or F^-,can take the place of hydroxyl ions. BO_3^{-3} ions take the place of phosphate ions, and Mg^{+2}, Mn^{+2}, or Sr^{+2} ions take the place of calcium cations [22, 25].

The ions substitution is unlimited where there is a total exchange capacity depending on the size difference ions and ions charges [26].

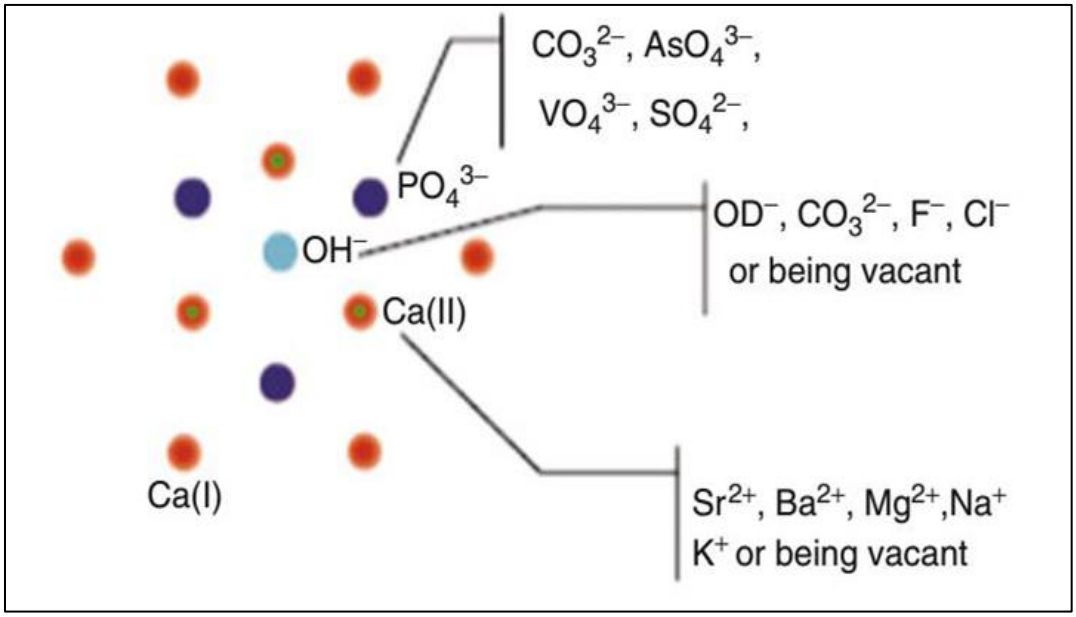

Figure (2.2): Ionic substitution for hydroxyapatite [26]

Most cases necessitate changes compensation as well as the volume of unit cell [27]. The following aspects can outline the effect of doping on the structure of hydroxyapatite:

2.4.1The Effect of Doping on The Crystallinity of HA

The degree of structural order in a solid refers to the crystallinity which it has a significant impact on its properties. The doped ions seems to have no influence on the main phase composition of synthesized HA ,but it has an effect on the crystallinity of the material. Incorporating of exogenous ions in the HA lattice will modify the structure and unit cell dimensions of HA [28]. Most

biological apatites replace Ca^{+2} with Mg^{+2}. Mg-replaced HA materials are anticipated to be biocompatible and have good biological characteristics, on the other hand has smaller atomic radius in comparison to Ca^{+2} ion. This leads to the reduction of the unit cell volume of HA and crystal lattice deformation, as well as the crystallinity of HA will reduce due to Mg ion replacement [29, 30]. In addition , to inhibit the nucleation and growth of HA crystals [28]. Furthermore, putting Zn ions in place of calcium ions was observed to reduced Crystallinity and alters the lattice parameters of Zn-HA by decreasing both a and c, because Zn^{+2} has a lower ionic radius than Ca^{+2} [2, 31].

2.4.2 The Effect of Doping on The Thermal Stability of the Apatite Phase

The phase instability of HA has been well documented when sintering and calcination temperatures becomes high. It takes four steps for HA to become thermally unstable including dihydroxylation (steps 1 and 2) involves the loss of water, which proceeds via the interim formation of firstly oxyhydroxyapatite, OHAP and then oxyapatite OHA , decomposition (steps 3 and 4) of OHA then proceeds to secondary phases such as tricalcium phosphate, tetracalcium phosphate and calcium oxide, and hydroxyapatite was found to undergo decomposition at range of 1100-1400°C [23]. The crystal structure of HA can be stabilized or destabilized by the incorporation of ions into its lattice. It is well documented that the dopants has a big effect on the HA thermal stability and relative density [32]. According to Paluszkiewicz thermal stability and decomposition of MnHA is proportional to the amount of Mn injected into the structure and the calcination temperature. At 800°C, HA with 0.1–1.0 wt. % Mn additions did not exhibit decomposition. also, it was found that MnHA containing (5.0 wt% Mn) decomposed at 800°C to α-TCP and β-TCP [33].

Among substituting cations, magnesium is widely studied, Because Mg is a necessary element for all living beings, Mg ion insertion into the HAp lattice is of significant importance in the development of synthetic bones. Cacciotti [34] and Stipniece [35] have found that the existence of Mg^{2+} inside the HA lattice influences hydroxyapatite thermal stability and crystallization. It promotes decomposition of Mg-substituted hydroxyapatite to Mg-substituted β-TCP after thermal treatment. Furthermore, the inclusion of Mg^{2+} increase the stability of β-TCP phase at elevated temperatures by postponing the phase transition of β to α. In addition, the replacement of the Zn ion inhibits the formation of Zn-HA crystals and reduces the thermal stability of HA, depending on the quantity of Zn integrated into the HA lattice [31].

2.4.3 Effects of Doping on Antibacterial Properties of HA

One of the most important problems after orthopedic surgery are bacterial infections. Most orthopedic infections are caused by Gram-positive bacteria like (S. aureus) and (S. epidermidis) [36]. Bacterial adhesions at implant surfaces represent an initial crucial step of infection [37]. It has been noticed that synthesized HA powder does not have the ability to resist the bacterial infection since it contains only calcium and phosphate [38]. Antibacterial characteristics advantages of some ions , for example Cu^{+2}, Ag^{+}, Zn^{+2}, Ce^{+3}, Fe^{+2},Mn^{+2}, Ti^{+4}, and Sr^{+2} etc. may transferred to HA by incorporating them into structure of HA as dopants [39]. Additionally, magnesium (Mg^{2+}) can be incorporated to improve HA's antimicrobial activity [29]. Combinations of these ions increases their effects on bacteria .For instance,(Ag, Cu-HA) powder was found to be more effective against the bacteria (E.coli and S. mutans) in comparison to single ion doped hydroxyapatite i.e. Ag-HA or Cu-HA [3]. The process of getting rid of bacteria by Cu^{+2} is distinguished into a four-step process as

illustrated in Figure (2.3). This process begins with a release of Cu^{+2} from the Cu-HA surface. Second, the rupture of the cell membrane results in the loss of cytoplasmic content which is the beginning of cell damage. In the third stage the subsequent generation of ROS (Reactive oxygen species) damages cells even more and engaging with proteins and lipids, finally resulting in DNA fragmentation and cell death as a result [39].

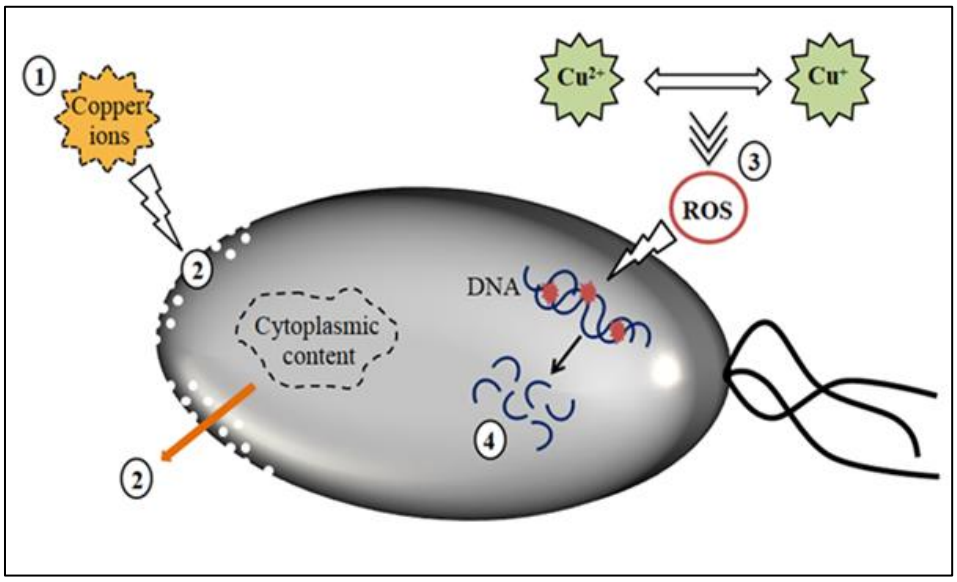

Figure(2.3): The killing procedure for Cu ions [39]

2.5 Methods of Synthesis Hydroxyapatite Powders

The features and characteristics of the hydroxyapatite are critical in the manufacture of HA implants. Phase purity, stoichiometry, grain size, particle shape and orientation, homogeneity, crystallinity, and agglomeration behavior of the powder must all be controlled [23].

There are several methods which have been developed to synthesis HA powders and these can be classified as either dry and wet methods. Synthesising HA using the dry method can be classified into two different methods, solid-

state method and mechanochemical methods[17] . HA can also be synthesised using a high-temperature method where high temperature is used to decompose the materials. The high-temperature processes consists of different methods, namely combustion[27] and pyrolysis [17].

The wet methods are a collection of procedures involving reactions in the presence of liquid media during the synthesis of HA powders. Such methods ensure high purity, uniform particle shape and narrow particle size distribution; in addition to control the crystal growth [27]. Some of the wet methods usually used for the extraction HA include Chemical precipitation method , Sol-Gel method [27, 40] [41] and hydrothermal reactions which it is usually defined as the reaction of chemical regents in an aqueous system at elevated temperature and pressure [17]. The focus will be on the precipitation method because it is the same method utilized in the research.

2.5.1 Wet Chemical Co-Precipitation Method

Precipitation is the most often utilized synthesis process for producing HA powders. Typically, the chemical precipitation procedure involves calcium and phosphate-containing reagents, such as calcium hydroxide $Ca(OH)_2$ or calcium nitrate $Ca(NO_3)_2.4H_2O$ as the Ca^{2+} as a source and acid H_3PO_4 orthophosphoric or diammonium hydrogen phosphate $(NH_4)_2HPO_4$ as the PO_4^{3-} source, are blended according to the molar ratio of the HA [23].

In a brief, it entails the addition of one reagent drop by drop to another while magnetic stirring is maintained at a low speed. This mixture can then be regulated to the desired pH, which is often alkaline, and the temperature of the process is controlled from 25°C to 90°C. Precipitation happens at a fairly slow rate, the solution stirred after that in order to age it, then the precipitated

particles are washed with distilled water , filtered, and then hot dried before being crushed into powder form [17]. Synthesis factors such as temperature, duration, rate of reagent incorporation, pH, and the purity of the chemicals used can all have an impact on the morphological characteristics (shape and size), the stoichiometry of the crystals, and the specific surface area of HA produced via precipitation [27].

To conclude, the chemical precipitation approach requires a number of critical processing parameters to be able to synthesize HA. Firstly, the chemical precursor has to be present chosen based on the HA molar ratio. A chemical precursor with an unequal molar ratio it might lead to synthesis a different phases. Second, the mixture's pH is a critical part that influences HA preparation. Benefits of this method can make nano HA particles; commercial production is possible; and the only by-product is water [17].

2.6 Techniques of Fabrication Bulk Hydroxyapatite

Depending on the temperature of fabrication, hydroxyapatite can be synthesized either at elevated temperature utilizing the diffusion mechanisms. Alternatively, it can be fabricated at temperatures lower than 300°C involving dissolution and precipitation mechanisms [42]. Hereafter the two approaches with details.

2.6.1 Solid Phase Sintering

Sintering is a thermal treatment used to consolidate particles of a powder to dense bulk bodies. Normally it is achieved at 50-75% of melting temperature [42]. It can be run either under pressure or without pressure to close the open pores. In solid-state sintering, a system of three sintering particles, as shown

schematically in Figure (2.4), is utilized to define the mechanisms of sintering, which occurs via at least six possible pathways of matter transport [43].

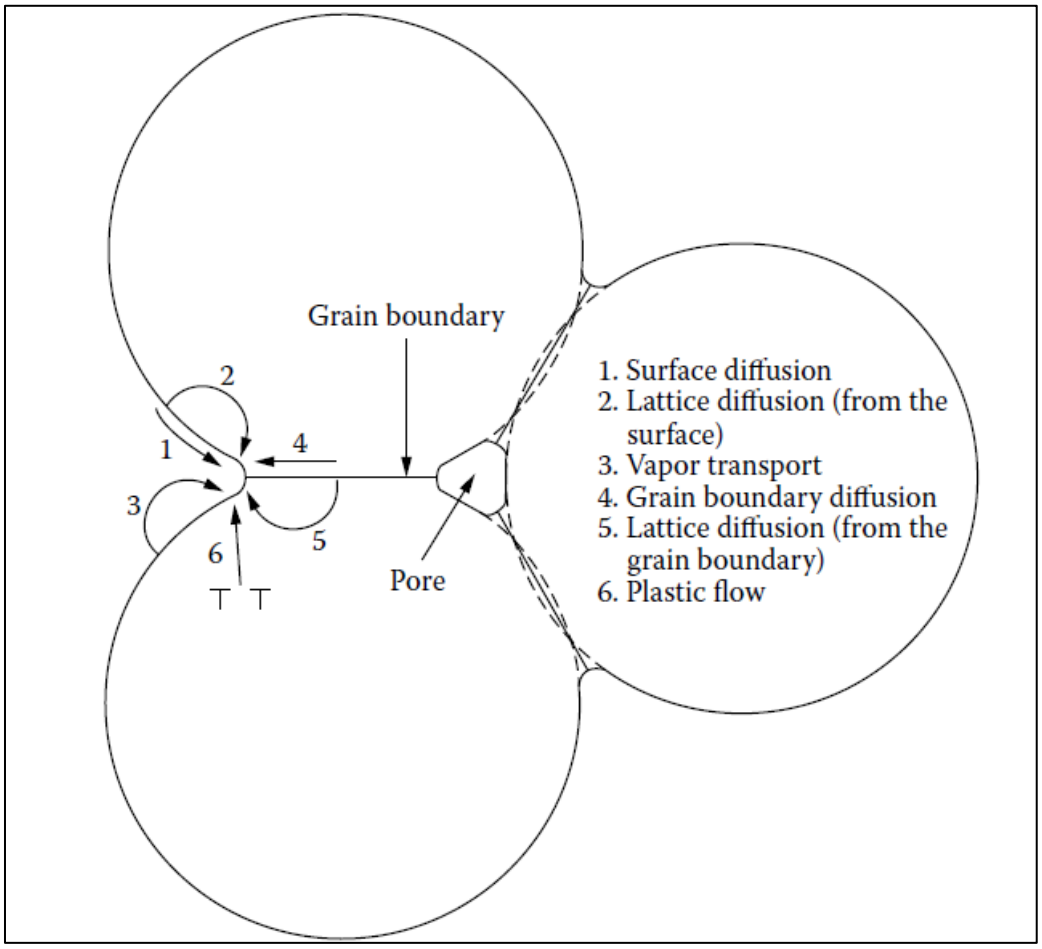

Figure (2.4) : schematic representation of diffusion mechanisms [43].

One of the main signs of sintering is neck formation among the powder particles. Afterwards, the contact region between the particles expand from zero to a certain level, and when equilibrium is attained, the neck development ceases. Another sign of sintering is the secondary or intermediate of grain growth. In this sintering step, grain boundaries are extensively formed besides the interconnected pores .Most densification and microstructure changes take place in this stage of sintering. during the last stage of sintering ,isolated pores appear at grain borders (interfaces), or linear junctures of three grains, and point

junctures of four grains. Density increases to some degree in this stage, but the microstructure develops such as grains growth rate very rapidly in this stage of sintering [44].

2.6.2 Cold Sintering Method (CSM)

CSM is defined as a consolidation method of ceramic particles into one ceramic body by creating new (ionic or covalent) bonds. It's a novel sintering method that allows ceramics to be densified at temperatures ranging from ambient temperature to 300°C using a suitable transient liquid phase (typically water). This will lead to reduce the energy consumed during forming the new bonds as well as reducing the emission of carbon and other harmful gases [45]. It was first utilized to make Li_2MoO_4 ceramics in 2014. Cold sintering has a lot of excellent future possibilities for ceramics because of the extremely low processing temperature, specially unstable ceramics at higher temperatures. In addition, combination of ceramics with other materials, such as metals and polymers, is possible using this technique [46]. Consolidation of thermodynamically unstable materials is another advantage of the CSM . Bang et al [47] have clearly shown this, by using CSM to achieve densification of up to 89 % and keeping phase purity, during the period of 100 minutes at a uniaxial pressure of 350 MPa on SnO, a thermodynamically unstable phase that decomposes thermally to form SnO_2 and Sn at relatively low temperatures. Cold sintering has been used to successfully create a variety of ceramics, including dielectric ceramics, semiconductor ceramics, structural ceramics, ceramic-polymer composites [48-50].

The principle of CSM represents by using a small quantity of a transient solvent (often water) to hydrate or partially dissolve the surface of the starting powders. The solvent serves as a lubricant increasing the particle sliding, while

discharging continuously from the die tolerance. Concurrently, an external pressure of (200 – 500 MPa) is applied at the annealing temperatures. The external pressure assures rearrangement of the ceramic particles in addition to close the pores. Besides, the applied pressure increases the solubility of the particles having sharp edges, and generally causing a better compaction [9]. Heating is necessary to create a supersaturated solution around each particulate due to the evaporation of the liquid phase. A sketch of this method can be seen in Figure (2.5) [51].

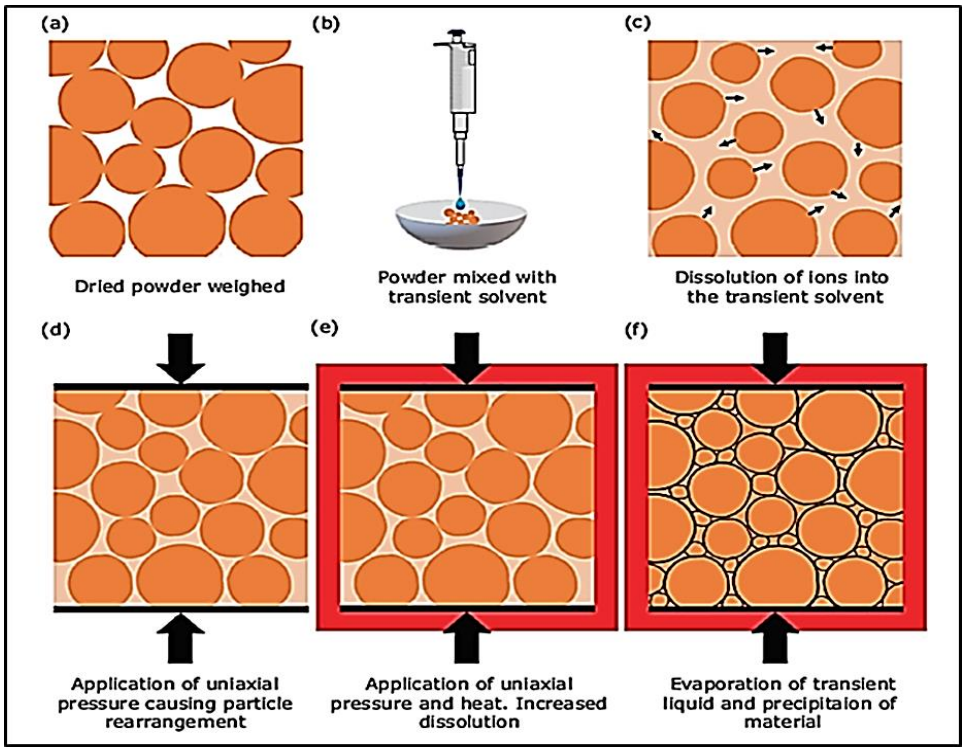

Figure (2.5): Schema of CSM compaction mechanism [10]

The density achieved after finishing CSM depends upon different parameters such as temperature, liquid phase, ratio of liquid phase to powder, and mixing time of the powder with solvent, and can be reached up to 80% to 99% of theoretical density [11]. Table (2.3) shows the densities of some ceramic compounds prepared by CSM [52-60].

Table (2.3): Examples of ceramics densified by cold sintering method

Ceramic materials	Sintering temperature	Relative density (%)	Reference
Al_2O_3-NaCl	120 °C	96	[52]
$BaTiO_3$	180 °C	~80–97	[53]
CeO_2	180°C	~70	[54]
MoO_3	120–150 °C	77	[53]
ZnO	25–305 °C	~65–99	[55]
ZrO_2	180 °C	~56–96	[56, 57]
TiO_2	150 °C	68	[58]
IO- $Ca_{10}(PO_4)_6(OH)_2$	200C	96.8%	[59]
$Ca_{10}(PO_4)_6(OH)_2$	200C	87%	[60]

2.6.2.1 Mechanism of Cold Sintering

Sintering is a kinematic procedure requiring mass transfer to condense particle materials. High temperatures are typically required in case of traditional hot sintering and additional sophisticated solid-state sintering techniques to promote molecular diffusion during particle interactions between solids [11]. The cold sintering process is distinct from regular elevated sintering temperature considering the processing parameters, and the sintering processes. CSM happens at a solid-liquid interface as opposed to suggesting a high-temperature solid-state diffusion to produce a thick material [61].

Two cold Sintering methods have been presented based on the chemistry of the particle-solvent interaction and the dissolving nature of material systems [11, 62]:

- Easy dissolved compounds (congruent dissolution): compounds with high water solubility include hygroscopic KH_2PO_4, $NaNO_2$, NaCl, and alkali molybdates and phosphates. In this case the Cold Sintering Process is relatively simple and takes place in a direct way, since the surface of the materials can be easily dissolved into the water with a homogenous chemical stoichiometry.

- Compound with passive surface (incongruent /negligible dissolution): the appearance of a passive surface separates the aqueous and crystalline phases, hence preventing the precipitation process and further densification, as proven in $BaTiO_3$ ceramics .

An early cold sintering model consists of stages 1 and 2. Mechanical forces and the rearranging of particles dominate the first stage, and a second stage dominated by dissolution and precipitation aided by pressure and temperature [9]. Figure (2.6) depicts a sketch timeline for CS procedure. The initial steps of the cold sintering process often entail particle rearranging, “dissolution of materials (if the materials are soluble), hydrothermal crystal regrowth, or glass/intermediate phase production. similar to traditional pressing, uniaxial mechanical force is used to promote densification; but, there is some aid from the liquid phase due to increased particle lubricity. At the beginning of the first step, after particle-particle interactions, a liquid phase is introduced on purpose which has been moistened with the right amount of a watery solution, and the liquid phase lubricates the particle surface and aids particle rearrangement by partially dissolving the sharp edges of the particles, resulting in greater interstitial space available for particle sliding [9, 11].

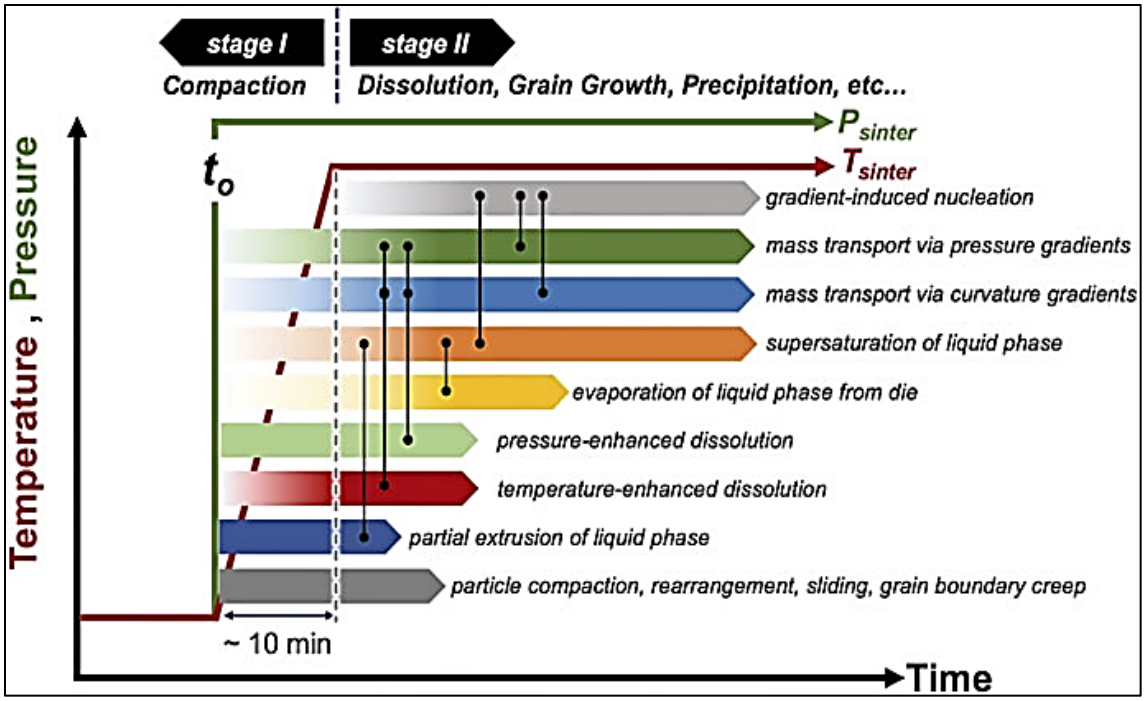

Figure (2.6): Schematic illustration the stage that occur during the cold sintering process [9]

Stage 2 is a hypothesized state in which increased temperatures are supplied under steady high pressure promoting the particle rearrangement. Under these conditions, solubility is enhanced also external pressure is anticipated to enhance solubility at the inter-particle contact site, and a super-saturated liquid is preferred to occur. The super saturation rises throughout time as a result of liquid phase evaporation [9].

It is important to keep in mind that sintering is controlled by each atomic mobility (kinetic factor) and driving force (thermodynamic). The driving force is a variation in the chemical potential of atoms induced by microstructural difference in pressure, which forces the substance to the neck surface. Surface tension and curvature produce these pressure gradients in traditional sintering. The use of an external pressure during room-temperature consolidation in CSM has the effect of increasing this driving force [45]. An external uniaxial load, on

the other hand, is superimposed on the system, producing the strain that promotes densification. The existence of this stress is crucial because it performs as a driving force in bringing particle centers together. Additionally, the uniaxial load induces stress gradient at grain contacts, effectively boosting the mass transport driving force [9].

For a dense material there are a variety methods for obtaining dense materials in cold sintering which are as follows [62]:

1- In the most frequent pathway (A→A), a compound A leads to the same compound A since the original powder and densified material use the same crystallographic phase and composition.

2- route (A→B), a substance A results in a product B with a different chemical composition or crystallographic phase than the starting powder or via allotropic transformation or the production of a new substance.

3- Lastly, there is the potential of (A + B→ C), a reactive pathway, which occurs if a combination of precursors that could interact mutually under cold sintering environments lead in the creation of a new substance or a compound that has been doped after CSM.

2.7 Literature Review

2.7.1 Preparation of Hydroxyapatite by Wet Chemical Co-Precipitation

In (2008) Eslami et al. [63] successfully used diammonium hydrogen phosphate ($(NH_4)_2HPO_4$) and calcium nitrate 4-hydrate ($Ca(NO_3)_2.4H_2O$) to prepare nano HA by using a chemical precipitation technique. Calcium nitrate 4-hydrate was dissolved in water and diammonium hydrogen phosphate was slowly added to the calcium nitrate solution , The pH of solution was adjusted to be 11. The precipitate was aged overnight at room temperature and washed

with de-ionized water . The resulting powder was dried for 10 h. Finally, the dried powder was calcined at 900 ºC for 1 h. The crystallites of manufactured powder were nanosized and had a needle-like morphology, as illustrated by TEM.

In (2013) Abidi et al. [64] utilizing Ca $(OH)_2$ and H_3PO_4 as precursors, hydroxyapatite (HA) nano powder was synthesized using a wet chemical approach in a precipitation reaction, with a different calcination temperature ranging from (100-800° C). H_3PO_4 was added to Ca $(OH)_2$ solution at a rate of 1.5 ml/min. The reactants were stirred for 24 hrs to aid the maturation stage and the reaction temperature was 20 °C. the precipitate was dried in a drying oven for 1hr at 100° C. They investigated that HA powder have a mole ratio of Ca/P is 1.667. with the increase of calcination temperature the crystallite size also increases in which the crystallite size of HA powder was found to be in the range 8.47-24.47 nm .

In (2014) Y. C. Teh, et al. [65] used a wet chemical method to prepare HA powder from an watery medium by slowly adding of (H_3PO_4) solution to a calcium hydroxide $(Ca(OH)_2)$ with different calcination temperatures(700°C , 800°C , 900°C and 1000°C) at a rate of $10°C \cdot min^{-1}$ and, after a dwell time of 2 hours, cooled to room temperature at a rate of $10°C \cdot min^{-1}$. Calcination of HA powder at low temperatures (700 to 900°C) before sintering has no influence on the sintering ability of compacted HA, whereas calcination of the powder at 1000°C prior to sintering has detrimental effects on the characteristics of sintered HA.

In (2016) Mondal et al. [1] Successfully fabricated HA nanoparticles with spherical shape through a simple reaction of tetrahydrated calcium nitrate ($Ca(NO_3)_2.4H_2O$) and di-ammonium hydrogen phosphate ($(NH_4)_2HPO_4$) . The pH of the final mixture was adjusted to be 11 by drop-wise addition of ammonia solution at low temperature (40°C). the formed precipitate was dried at 80°C for 1 h and then calcinated at 600°C for 1 h in air. The creation of spherical nanoparticles was confirmed by SEM and EDS, with a Ca/P ratio of 1.70 ,the average size of the resulting HA was around 23 nm.

In (2018) Yelten-Yilmaz et al. [66] synthesized HA with spherical shape where calcium hydroxide ($Ca(OH)_2$ was utilized as a source of calcium and orthophosphoric acid (H_3PO_4) as the phosphorus source. The process parameters studied were acid addition rate rapid (5.5 ml/min) and slow (1.5 ml/min , and reaction temperature (30°C, 50 °C, and 85 °C). The precipitates were dried at 110 °C for 7 h. Subsequently the semi-dry precipitates were heat-treated at two (950 °C and 1250 °C) for 2 h .The results showed that a low reaction temperature of 30°C and a quick acid addition rate of (5.5 ml/min) are optimal conditions for producing homogenous and spherical HA powders with a mean particle size of 0.2–0.3 μm.

2.7.2 Doping of Hydroxyapatite

Doping of HA is common to change or add some features. It can achieve by inserting or substituting one or more (positive or negative) ions. The unit cell of hydroxyapatite has the ability to accommodate more than one ions besides the calcium ions, phosphate groups and hydroxyl groups. This gives motivation to substitute the above mentioned constitutes with double or triple ions to enhance the physicochemical and biological characteristics of HA.

Here are some of the previous literature that involve single and Co-doping of HA by introducing either metal ions or negative groups along with the phosphate or hydroxyl group .

In (2010) Yan Li et al. [67] Cu^{2+} and Ti^{4+}doped HA powders have been synthesized by using wet chemical method. CuHA and TiHA were effectively synthesized by the ion exchange technique in aqueous solution at several molar ratios (M_{added}/Ca_{added} = 0.01, 0.05, 0.10, and 0.15). $Ca(OH)_2$,H_3PO_4 and metal salt [$Cu(CH_3COO)_2 \cdot H_2O$] and $TiBr_4$ were used as sources for Ca ,P ,Cu^{2+} and Ti^{4+} respectively . 3.71 g $Ca(OH)_2$ was first suspended in 250ml deionised (DI)water , the suspension was stirred at 500 rpm and 98.5°C for 30 min. H_3PO_4 was then added at 4 ml/min into the suspension. The addition of acid was ceased when the resultant slurry reached pH 6. The precipitates were dried overnight in a furnace at 100 °C. The XRD result shown that hydroxyapatite having a hexagonal shape was found in the pure HA, CuHA, and TiHA specimens.
the antibacterial effect of CuHA increased as Cu content increased and have a significant antibacterial activity against E.coli. this was due to the leaching of Cu^{2+} ions which caused the lysis of bacteria. increasing the Ti content in HA can effectively kill bacteria without the acute toxic effect.

In (2010) Vojislav et al. [37] by using Copper and zinc the antimicrobial effects of doped HA nanopowders versus pathogen bacterial strains were tested against (E. coli) and (S. aureus). Doped HA was produced using the neutralization process, which involves dissolving CuO or ZnO in solution of $0.5MH_3PO_4$, The solution is then added dropwise at rate of about 0.5–1 mL/min to a slurry of $Ca(OH)_2$ in order to get a monophasic product. after the aging, the precipitates were filtered off, washed with water and dried at 105°C. The

quantitative elemental analysis showed that the copper and zinc ions fully incorporated into the hydroxyapatite. Copper and zinc-doped samples have the potential to reduce live cells, as demonstrated by antibacterial tests.

In (2016) Gayathri et al. [68] have been synthesized magnesium incorporated hydroxyapatite nanoparticles by using a microwave irradiation method, magnesium chloride hexahydrate ($MgCl_2.6H_2O$) calcium nitratetetra hydrate ($Ca(NO_3)_2.6H_2O$) and disodium hydrogen phosphate (Na_2HPO_4) were used as magnesium, calcium and phosphorous sources to prepare hydroxyapatite nanoparticles. The pH of the solution was adjusted to lie in the range of 9–11. The obtained white precipitate was dried in a muffle furnace at 600°C for 3 h. Due to the incorporation of Mg, the crystallinity becomes smaller, and Mg substitution for Ca causes a reduction in the lattice parameters of hydroxyapatite. The gram negative bacteria E. coli of synthesized nanoparticles showed excellent antibacterial activity.

In (2017) Álvarez et al. [69] hydroxyapatite doped with magnesium oxide nanoparticles (nHAMg) were successfully synthesized by the solvothermal technique. Calcium nitrate tetrahydrate $Ca(NO_3)_2.4H_2O$, diammonium phosphate $(NH_4)_2HPO_4$, magnesium chloride hexahydrate $MgCl_2.6H_2O$, were used as sources for calcium (Ca), phosphorus (P) and Magnesium (Mg) . the pH of the solution was adjusted to 11 by adding 25 % ammonium hydroxide solution. After the solvothermal process, the obtained precipitate was dried at 60 °C for 14h, and the resulting material was calcined at 600 °C for 2h. Antibacterial experiments revealed that (nHAMg) inhibits the growth of S.mutans by exhibiting a halo of inhibition surrounding the discs.

In (2019) in the study of **Daniela et al. [70]** hydroxyapatite doped with magnesium Mg-HA ($Ca_{10-x}Mg_x$ $(PO_4)_6$ $(OH)_2$, x_{Mg} = 0.1), were prepared using chemical precipitation method at room-temperature using calcium nitrate tetrahydrate ($Ca(NO_3)_2.4H_2O$), ammonium hydrogen phosphate $(NH_4)_2HPO_4$,magnesium nitrate hexahydrate ($Mg(NO_3)_2.6H_2O$) as starting material. ammonium hydroxide (NH_4OH) was used to kept the pH of the solution constant at 11 throughout the synthesis process. The antibacterial activity of the Mg-HA suspension against gram-positive strains (S. aureus ATCC 25923, E.faecalis ATCC 29212), gram-negative strains (E.coli ATCC 25922, P. aeruginosa ATCC 27853) were evaluated. The Mg-HA suspensions show antimicrobial efficacy against P. aeruginosa and S. aureus, microbial strains and it might be utilized as biocompatible antimicrobial coatings of medical devices.

In (2017) Mariappan et al. [71] studied the antimicrobial activity of synthesized HA nanopowders integrated Cu^{2+} and Zn^{2+} which it was prepared by simple sol-gel method at room temperature. In this technique, the initial ingredients were calcium acetate ($Ca(C_2H_2O_2)_2$), orthophosphoric acid (H_3PO_4), copper oxide (CuO), and zinc oxide (ZnO). Ethanol and double distilled water were used as solvents . the pH of the solution was maintained at 10.5 by adding aqueous ammonia. Then powders were annealed at 500˚C in a muffle furnace atmosphere for about 1hr. On Muller-Hinton agar, the antimicrobial activity of produced HA versus harmful bacteria in humans was evaluated using the agar diffusion disk technique. HA pure powder shows antimicrobial action, and the antimicrobial rate rises progressively when the concentrations of Cu and Zn in the HA nanopowders are increase.

In (2018) Helen et al. [72] by using the precipitation method hydroxyapatite substituted with Mg/Zn anion was synthesized. Using (Ca $(NO_3)_2.4H_2O$), $(NH_4)_2HPO_4$, ($MgCl_2$ $.6H_2O$) and (Zn Cl_2. H_2O) was used as sources for Ca ,P ,Mg and Zn . maintain pH of the solution at 9 using NH_4OH and the obtained precipitate was dried at 80°C. Co-dopants Mg/Zn alter the structure of hydroxyapatite, as evidenced by XRD. Two bacterial strains, E. coli and S. aureas, were examined for antibacterial activity using the well diffusion technique using Mueller-Hinton agar. Antibacterial testing revealed that co-dopands Mg/Zn HA display 18-24 mm in E.Coli and 15-20 mm in S.aureaus, allowing them to be utilized in a variety of applications.

In (2019) Houria et al. [73] used the precipitation process to create HA doped and co-doped with two metal cations (zinc and magnesium) using $CaCl_2$, Na_2HPO_4, $ZnCl_2$, and $MgCl_2$ aqueous solutions as reactant agents. The solution was adjusted to pH 9 with an aqueous ammonia solution and at a temperature of 90 °C . the precipitates was washed several times with distilled water, followed by drying at 105°C for 24 h and then calcined in a muffle furnace at 900 °C for 1h. the concentrations of (Zn) and/or (Mg) cations ranging from 5 to 15 mol% . All samples containing greater than 10 mol% percent of doping ions were determined to be HA. The antimicrobial property of such nanopowders was evaluated against five microorganisms in vitro (E.coli, Klebsiella pneumoniae, and Pseudomonas aeruginosa as Gram-negative; S.aureus and Bacillus subtilis as Gram-positive). The findings demonstrate that for all HA specimens doped with Zn or co-doped with Zn and Mg ions up to 15 mol% percent, the inhibitory area for every bacteria has significantly expanded, showing a high antibacterial activity .

2.7.3 Cold Sintering of Hydroxyapatite

Cold sintering of hydroxyapatite is interesting because of lowering the challenge of HA decomposition at high temperature treatment. Another interesting thing about cold sintering of HA is using water as trans-solvent which make it cheap method.

In (2017) Hassan et al. [60] have been successfully synthesized bulk HA by wet chemical precipitation and subsequently cold sintering methods. They used di-ammonium hydrogen phosphate [$(NH_4)_2HPO_4$] and calcium nitrate [$Ca(NO_3)_2 \cdot 4H_2O$] as starting materials. pH of the solutions was adjusted at 10.5 by using concentrated ammonia [NH4(OH)2], temperature of the reaction was maintained at 35°C. Sintering of HA powder was achieved at 200 °C and under an applied external pressure of 300MPa. The relative density reached was 87% .

In (2019) Hassan et al. [59] by using the same chemical route they succeeded to fabricate iodate-substituted hydroxyapatite (IO-HA) with single phase and nanocrystals. The molar ratios of Ca, P and I were taken as 10, 6 and 2,respectively. The synthesis was carried out under continuous stirring of 200 RPM with the temperature maintained at 70°C and aging for 12 h. The precipitate was filtered and washed with double-deionized water. Finally, the filtrate was dried for 12 h in a vacuum oven at 110 °C. At 200°C, the dried iodate-substituted hydroxyapatite containing up to 7 % iodine as iodate was sintered. As much as 96.8% of the relative density of the sintered material was reached. The cold sintering conditions (200 C, 500 MPa, 10 min) didn’t cause the iodates to evaporate, which proved that this process is safe and that the substituted iodine is stable.

In (2020) Nosrati et al. [74] reported about fabrication of hydroxyapatite doped with reduced graphene oxide (HA-rGO) powder by using hydrothermal method and then sintered at temperatures lower than 300°C. Calcium nitrate tetrahydrate($Ca(NO_3)_2.4H_2O$), Diammonium hydrogen phosphate ($(NH_4)_2HPO_4$) and Graphene oxide (GO) (CO_xH_y) are the primary chemicals used as source for Ca, P and GO. The amount of rGO used in this study is 1.5% by weight. The solution containing Ca^{2+} was added dropwise to a 20 mL stirred suspension of GO (HA/1.5% rGO) with stirring continued for 1 h. After that the solution containing phosphate ions was added dropwise to the solution. The pH of the solution was adjusted to >10 with ammonium solution(NH_4OH). The powders were dried in an oven for 12 h at 60 °C and then ball milling (250 rpm, 12 h). The powders were mixed with water, dimethylformamide(DMF) ($(CH_3)_2NC(O)H$), and brushite to make the solvent which was added to the powders in different amounts. The results of this study showed that a temperature of 200°C, a holding time of >30 min, and a pressure of 500 MPa were the best conditions for sintering rGO-HA nanopowders.

In(2021) Hassan et al [75]. demonstrated the ability to manufacture dense HA at temperatures as low as 200 °C with no liquid additive using a new densification technique. HA was synthesized using a wet precipitation method the pH of the solutions was adjusted to 10.5 using a 28% ammonia solution and the temperature of reaction was maintained 30 °C. Cold sintering parameters of (200 °C, 500 MPa) were applied to two types of synthesized nanocrystalline HA and compared thoroughly : dry (110 °C, 12 h) and calcinated (1000 °C, 2 h). it was found that CSM was only successful for the only dried HA samples . the calcinated sample, did not undergo sintering even when additional deionized 10 wt% water. In the case of dried HA powders at 110 °C that had compacted at

low temperatures (in the range of 50–300 °C), under uniaxial pressures of 100 to 500 MPa, and for different holding times of up to 60 min. Bulk densities of up to 98.8 g/cm^{3}were achieved at an optimal temperature of 200°C under 500MPa uniaxial pressure.

2.8 Summary of Literature Survey

The literature survey has shown that many researchers have studied about doped and co-doped HA produced by wet chemical precipitation method which is widely used to prepare HA powders. These studies has declared that different metal ions such as Ti, Zn, Se, Sr, Cu and Mg can be substituted in to hydroxyapatite structure to improve the properties like antibacterial property. It is widely found that metal ions like Cu ,Mg was used as single doping because they have a good antibacterial properties, while the effect of combining Cu,Mg ions as doping elements on the structural and biological features of HA has been studied in this research. From the literature survey it was declared that using a modern sintering method (cold sintering) to fabricate a bulk samples from the prepared co- doped(Cu+Mg) HA powders and study the biodegradation behavior wasn't highlighted in previous studies.

Chapter Three

Experimental Part

Chapter Three

Experimental Part

3.1. Introduction

In two stages, this chapter defines the experimental procedures , the first part deals with the preparation of pure and Co-doped HA powders and the analytical techniques that used to characterize and study the structural properties and microbiological effect of HA prepared powders. The other part of this chapter deal with the methods used to fabricate bulk samples of HA, where two sintering methods were applied (Cold sintering and Traditional sintering) and the analytical techniques that used to characterize and study the structural, physical and mechanical properties of fabricated samples.

3.2.The Starting Materials

The starting materials employed in this study are demonstrated in Table (3.1):

Table (3.1): The chemical formula, purity and source of the materials used.

Material Name	Chemical Formula	Purity	Source
Calcium hydroxide	$Ca(OH)_2$	> 98 %	Fluka AG, Germany
O-phosphoric acid	H_3PO_4	> 98%	Thomas Baker, India
Magnesium Oxide	MgO	99.9%	Sigma Alrditch, Germany
Copper Oxide	CuO	> 99%	Sigma Alrditch, Germany
Tris-HCL	$C_4H_{12}NO_3Cl$	> 99%	Bio-Basic Inc, Canada
Muller-Hinton Agar	CAT:1058	>99.9	Conda Lab., Spain

3.3. Characteristics of Starting Materials

3.3.1. Particle Size Distribution Measuring

The particle size and distribution of the starting materials was determined using Bettersize2000 laser particle size analyzer (Bettersize instrument Ltd., China) in Ceramic Department. Engineering materials. University of Babylon.

Figure (3.1) illustrates the particle size distribution (PSD) as a histogram and as an accumulative curve of $Ca(OH)_2$ powder. The average particle size of $Ca(OH)_2$ is 7.70 µm. It shows that the accumulative curve is not smooth. This can be attributed to the existence of agglomerates with different sizes. On the other hand, the PSD of the CuO is seen in Figure (3.2).

The d_{50} of the copper oxide is 3.12 µm. The other candidate oxide (MgO) has a d_{50} of 4.07 µm and a PSD as shown in Figure (3.3), which exhibits an orderly curve in comparison to the others.

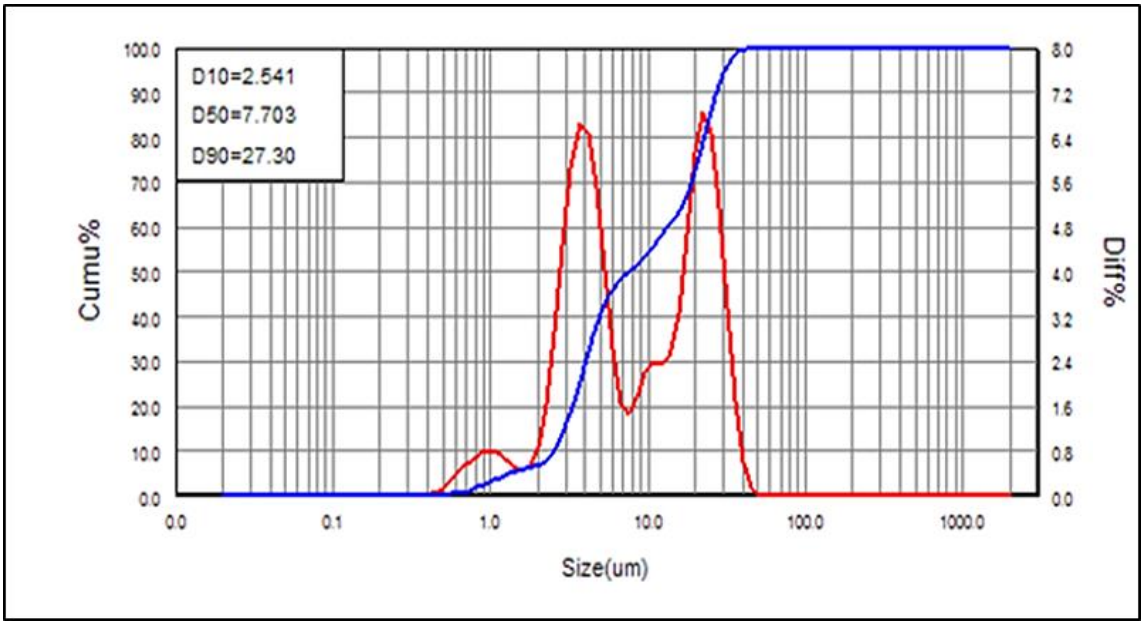

Figure (3.1): Particle size distribution of $Ca(OH)_2$ powder

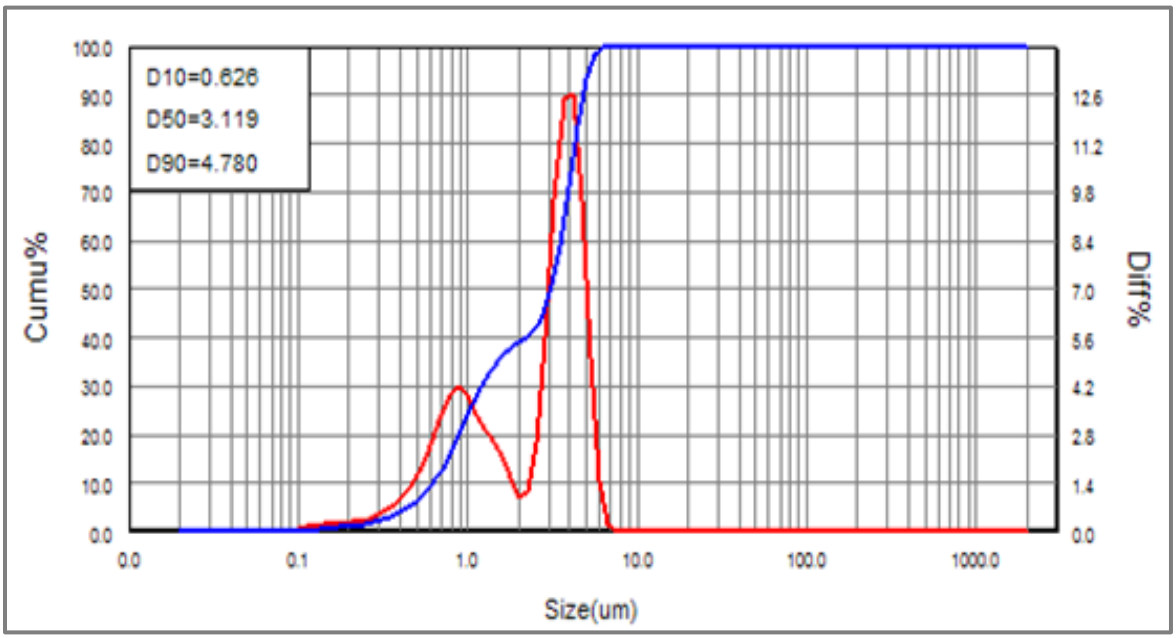

Figure (3.2): Particle size distribution of CuO powder

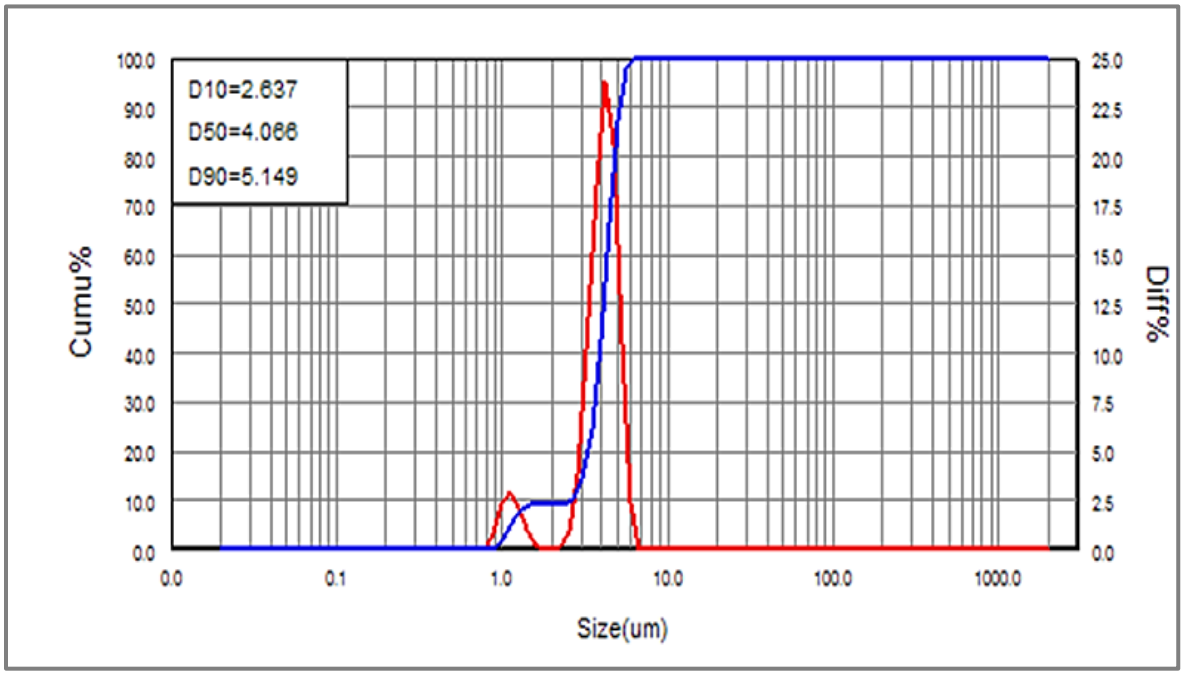

Figure (3.3): Particle size distribution of MgO powder

3.3.2 XRD of $Ca(OH)_2$ Starting Powder

Figure (3.4) exhibits the phase structure pattern of calcium hydroxide involved in this work. The resulting peaks in the range from 20° to 60° . This analysis provides phase purity of calcium hydroxide powder, were all peaks are matched to the card No. 72-0156.

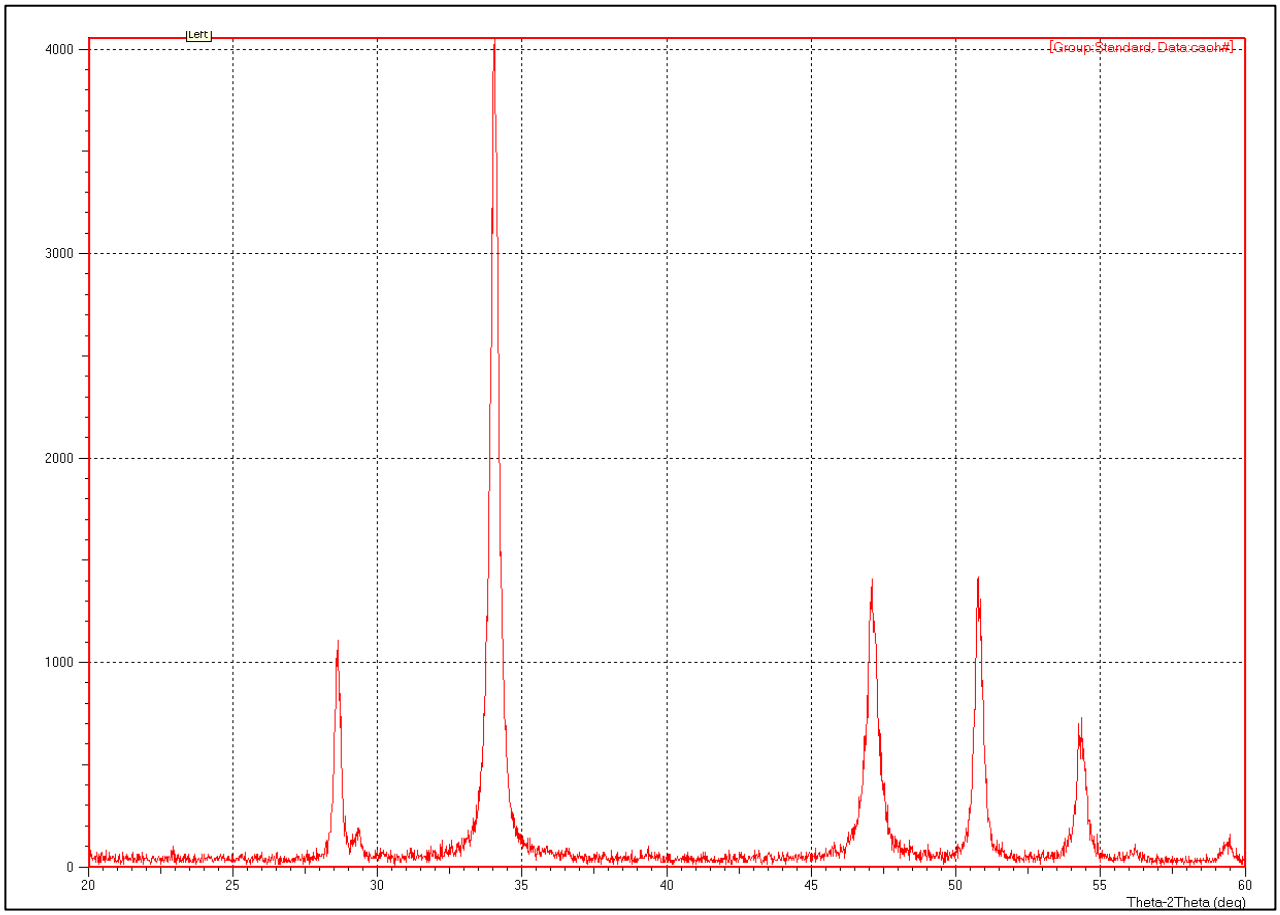

Figure (3. 4): X-ray Diffraction Pattern of the $Ca(OH)_2$

A summary of experimental work are depicted in the following flowchart (Figure 3.5) :

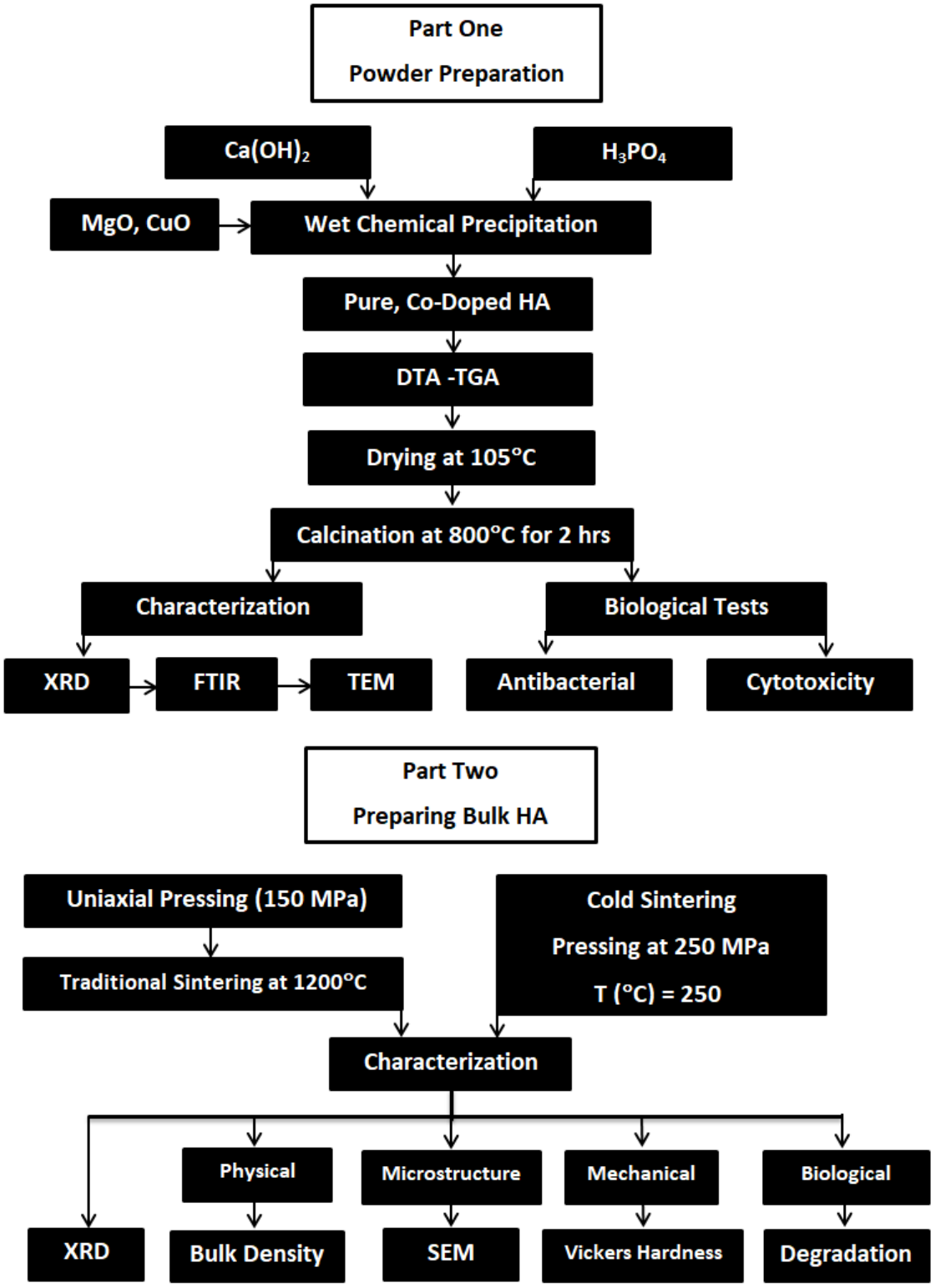

Figure (3.5): Flow chart describing the experimental work of this study

3.4. Part One

3.4.1.Preparation of Hydroxyapatite Powders:

The wet chemical Co-precipitation method was used to obtain ultrapure HA- and (Cu, Mg)HA powders as shown in Figure (3.6). In accordance to the following chemical reaction [64] :

$$10Ca(OH)_2 + 6H_3PO_4 \rightarrow Ca_{10}(PO_4)_6(OH)_2 + 18H_2O \quad \ldots\ldots\ldots\ldots (3.1)$$

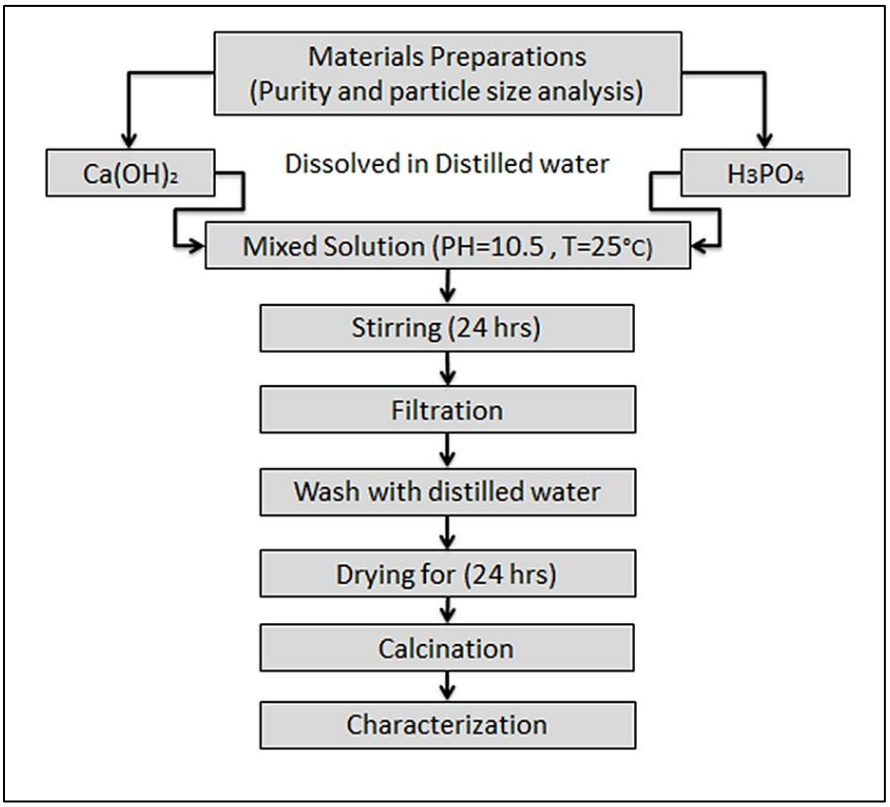

Figure (3.6): Layout of Pure HA powder preparation

All of the reagents' concentrations were calculated considering the mole ratio of Ca/P which equals to 1.67 in HA and was kept as it is for the co-doped HA i.e. (Mg+Cu+Ca)/P = 1.67.

In the chemical method, $Ca(OH)_2$ 0.1 M was prepared by mixing $CaOH_2$ with water using an overhead stirrer at 25°C. Then diluted solution of H_3PO_4 0.06 M was added drop-wise (1.5 ml/min) to the slurry with continuous stirring

(800 rpm) at the room temperature. The pH of the solution was maintained to 10.5. The reactants were continuously stirred (400 rpm) for further 24 h at the room temperature.

Copper oxide CuO and magnesium oxide MgO were used as a source for copper (Cu^{2+}) and magnesium (Mg^{2+}) ions. The required amounts of CuO and MgO were dissolved in H_3PO_4 while stirring at 400 rpm for about 1 h. Then, the same above conditions were adapted for preparing co-doped HA. After finishing the aging for about 24hours, the precipitated particles were then filtered and rinsed with deionized water for three times, finally, it was grained in a mortar after being dried at 105°C. Table (3.2) shows the amounts of reactants used in the preparation method of HA and co-doped HA. The formation reaction of the Cu/Mg-substituted HA is expressed as follows:

$9Ca(OH)_2 + 6H_3(PO_4) + (1\text{-}X)CuO + XMgO \rightarrow Ca_9Cu_{(1-X)}, Mg_X (PO_4)_6(OH)_2$ (s) $+ 18H_2O$ …….... (3.2)

Table (3.2): Amounts of reactants used for preparing (20 g) of HA and co-doped HA.

Samples code	(H_3PO_4) (gram)	($CaOH_2$) (gram)	(CuO) (gram)	(MgO) (gram)	Chemical formula
HA-1	11.705	14.750	0	0	$Ca_{10}(PO_4)_6(OH)_2$
HA-2	11.705	13.274	0.791	0.401	$Ca_9 (Cu_{0.5},Mg_{0.5}) (PO4)_6 (OH)_2$
HA-3	11.705	13.274	0.395	0.601	$Ca_9(Cu_{0.25},Mg_{0.75}) (PO4)_6(OH)_2$
HA-4	11.705	13.274	1.1	0.200	$Ca_9(Cu_{0.75},Mg_{0.25}) (PO4)_6(OH)_2$

Figure (3.7) and Figure (3.8) shows the prepared powders before and after calcination. As a result of doping, the color of HA has changed according to the mole ratio of dopants introduced after calcination the powders at 800°C for 2 h as seen in the optical image below.

Figure (3.7): HA powders before heat treatment at 800°C

Figure (3.8): HA powders after 800°C thermal treatment

3.4.2 Characterizations of Prepared Powders

3.4.2.1 Thermal Investigation

The TGA (thermo gravimetric analysis) equipped with differential thermal analysis (DTA) apparatus at (Tehran University, Tehran - Islamic Republic of Iran) was utilized to study thermal behavior of synthesized HA and Co-doped HA. The analysis was done at air condition and 10°C / minute heating rate. The heat treatment was non-isothermal and the specimens have been heated to 850°C.

3.4.2.2 Phase Identification

The XRD (X-ray diffraction) was utilized to determine the resulting phases and composition of prepared HA powders. The powders were ground and sieved (using sieve no.200.), then scanned using X-Ray diffractometer (XRD 6000, Shimadzo, Japan) in the (ceramics laboratories. College of Material Engineering. University of Babylon) with a Cukα X-ray was involved as a radiation source using 30 mA , 40 kV and the speed of scanning was 5°/min. Nickel-based filter was utilized. Difraction data was collected over a wide range of 2θ = 20 - 50° with a scan speed of 0.05°. The degree of crystallinity (degree of structure order) for prepared powders was calculated following the simple equation[76]:

$$X_c \approx 1 - \frac{V112/300}{I_{300}} \quad \text{..... (3.3)}$$

Where:

I_{300} represents the intensity of plane (300) and V112/300 is the magnitude of the hollow intensity between the (112) and (300) reflections.

3.4.2.3. Fourier Transform Infrared Spectrometer (FTIR)

The Fourier transform infrared (FTIR) (Shimaduz 1800, Japan, at the Department of Polymers Engineering and petrochemical industries, College of Materials, University of Babylon) was utilized to evaluate the structural groups of the HA and co-doped HA powders. The test carried out according to ASTM E1252 . The investigation was done in the range (3600 - 400 cm^{-1}) at 4 cm^{-1}. The test were carried out at room temperature.

3.4.2.4.Transition Electron Microscopy (TEM)

In order to confirm the particle morphology and the particle shape and size of as-synthesized HA powder and Co-doped HA calcined at 800°C. An examination by the transmittion electron microscope (TEM) were done through using (Philips CM120) apparatus at Tehran University, Tehran- Islamic Republic of Iran.

3.5. Biological Characterizations of Powders

3.5.1. Antibacterial Activity Test

The antibacterial activity of as synthesized powders was investigated by the standard agar well diffusion method versus two strains of bacteria which are E. coli and S. aureus. The diffusion test was conducted using Müller-Hinton agar. Pouring agar into Petri plates to generate 4mm thick layers and injecting dense inoculum of the examined microorganisms to achieve semiconfluent growth constitutes the diffusion technique. In order to prepare the test solutions, HA powders were soluble in purified water with a(250 µg/ml)as a concentration. Samples of solutions were put on agar and incubated for 24 hr at 37˚c.

3.5.2. Cytotoxicity Test

MC3T3-E1 osteoblast cell line was obtained from the American Type Culture Collection (ATCC, Manassas, VA, USA). Cells were grown and maintained in alpha-Minimum Essential Medium (α-MEM; Gibco, Life Technologies, Waltham, MA, USA) supplemented with 10% fetal bovine serum (FBS; BioWest SAS, Nuaille, France) and 1% PSF (antibiotic antimycotic solution, Sigma-Aldrich®, St. Louis, MO, USA) in a humidified incubator with 5% CO_2 in air at 37°C. After reaching ~75% confluency, cells were detached using 0.25% trypsin (Gibco, Invitrogen, Waltham, MA, USA) and 0.1% ethylenediaminetetraacetic acid (Merck, Darmstadt, Germany) in phosphate-buffered saline (PBS) at 37°C. Cells were then re-suspended in α-MEM with 10% FBS, 1% PSF. Cells were seeded onto the 96-well plates at a density of 5000 cells per well and incubated for 24h prior to the experiments. The Cells were washed with PBS (phosphate Buffered saline, pH 7.4) and incubated in fresh medium containing different concentrations of samples (1000, 750, 500, 250, 125, 0 µg/ml) for 72h. The cell viability assay was measured using the 3-(4, 5dimethylthiazol-2-yl)-2, 5-diphenyltetrazolium bromide (MTT) dye reduction assay. MTT was performed to determine the cytotoxic effect of the samples at various concentrations. After 72h of incubation (37℃, 5% CO2 in a humid atmosphere), MTT (0.5 mg/mL in PBS) was added to each well, and the plate was incubated for a further 4h at 37℃. The Resulting formazan was dissolved in 100 µl of DMSO with gentle shaking at 37℃, and absorbance was measured at 570 nm with an ELISA reader. The Results were given as the mean of three independent experiments. Epi Fluorescence microscopes was used to see fluorescence micrographs of the live osteoblasts cells.

3.6. Part Two

3.6.1.Fabrication of Bulk Samples:

Two methods were employed in this study to fabricate bulk HA that are :

1- Cold sintering method at 250°C.

2-Traditional sintering method at 1200°C.

Bulk samples of HA were fabricated by cold sintering method which considered a modern method to produce ceramic bulk samples at temperature lower than 300°C. In this method, the prepared HA powders were mixed with an appropriate amount of dilute solution of 10% O-phosphoric acid (H_3PO_4) that was used as solvent. The mixing was lasted for 5 min. After that, the wetted powders was transferred to stainless steel mold that have 12.88 mm diameter. The pressing was achieved at room temperature for 10 minutes by a hand-made setup, containing (frame, heater, temperature controller, manual hydraulic press, and a thermocouple) as illustrated in Figure (3.9). Thermocouples were employed during the pressing phase to control the sintering temperatures.

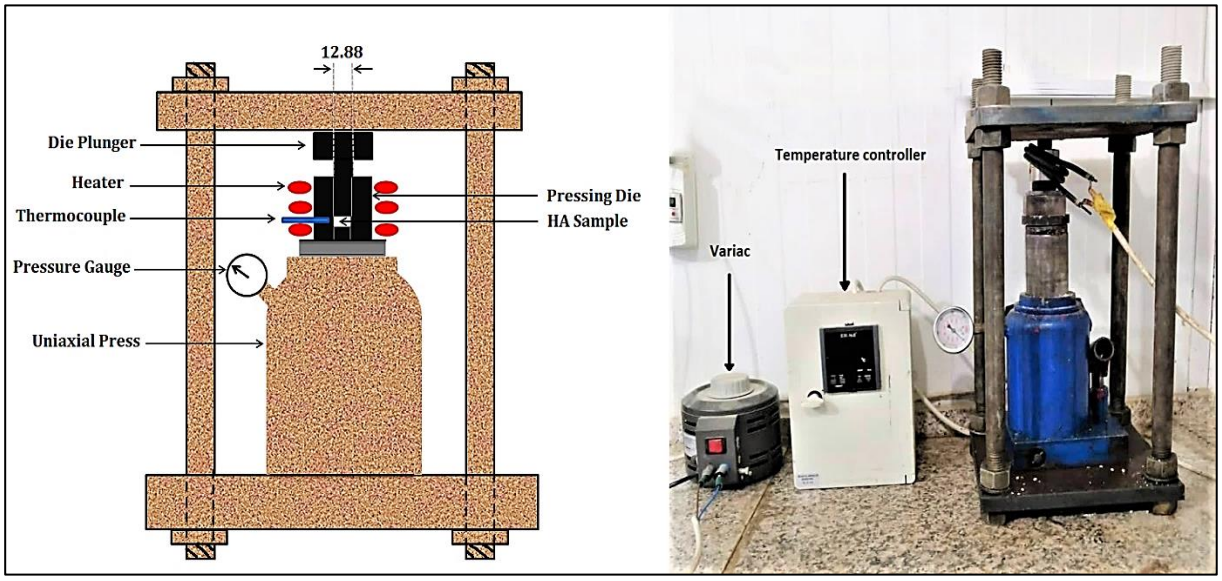

Figure (3.9): Cold sintering method setup

The thermal cycle is sketched as in Figure (3.10). In which the pressing time was divided into three steps. At the begging, the powders were pressed at room temperature for 10 minutes. Next, the temperatures were increased to 250°C with a heating rate of (8°C/min). while keeping the applied pressure for another 120 min .Finally the pressure was also maintained during the cooling phase for 50 minutes.

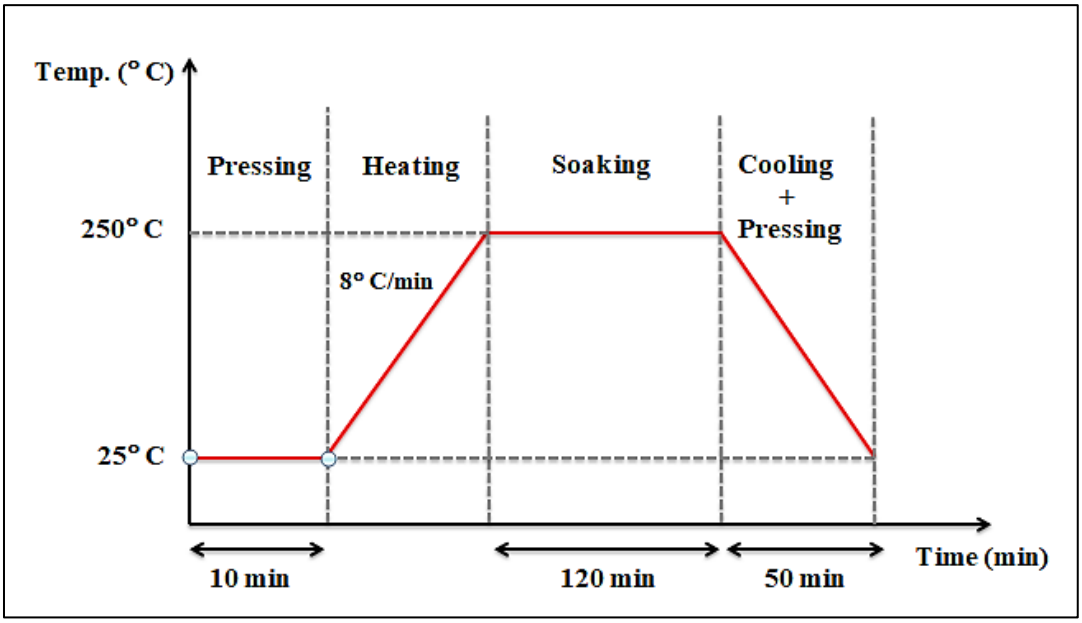

Figure (3.10): Heating cycle for cold sintering method

Other groups of HA samples were fabricated following the pressure less sintering method. This method involves mixing the powders with 2 wt% polyvinyl alcohol (PVA) that was used as a binder material. They were uniaxially pressed under an applied pressure of 150 MPa. The compacts were heat treated at1200°C for 1 h with heat rate (5°C/min). The mold have a 10 mm diameter. The profile of sintering is shown in Figure (3.11).

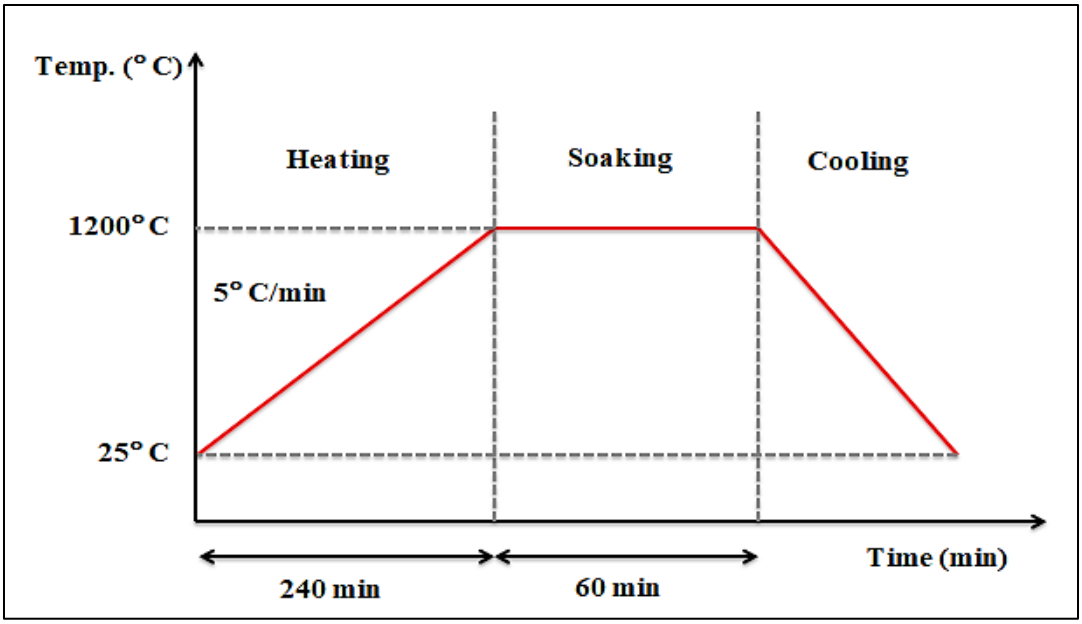

Figure (3.11): Heating cycle for the pressure less sintering method

3.6.2. Characterizations of Bulk Samples

3.6.2.1 Phase Identification

The XRD (X-ray diffraction) was utilized to determine the resulting phases and composition of synthesized bulk HA samples, utilizing the same device that was used to analyze the prepared powders.

3.6.2.2 Density Calculation

The density was measured according to Archimedes method. Where a scale (type GP-120 S) with digital accuracy up to ± 0.0001 g/cm³ was used. The test was carried out at normal atmosphere .

3.6.2.3. Microstructure Observation

Scanning electron microscope (SEM)-Energy dispersive X-ray, (FEI, FP 2017/12 inspect S50, Czech Republic) in Al-Nahrain University / College of

Sciences / Department of Physics laboratories was employed to observe the yield microstructure of the prepared HA samples.

3.6.2.4. Hardness Determination

The test was achieved in accordance with the ASTM standard C1327-90 utilizing a digital Vickers microhardness tester (TH-717) in the (ceramics laboratories. College of Material Engineering. University of Babylon). The test was run at 1 kg load force at a dwell time of 15 second.

3.6.2.5. Biodegradation Test

Samples HA-1, HA-2,HA-3, HA-4 were prepared for the biodegradation test. The test was run according to the ISO 10993-14: 2009. The samples were immersed in Tris-HCl buffer solution of 7.4 pH. The loss in weight was evaluated at a temperature of 37°C. The occupation time may take several days up to 10 days. Using the solution volume / surface area (SV /SA) ratio of 0.5 ml/mm^2, the amount of solution in each specimen is recorded. At every time point, specimens were withdrawn from the immersion medium, rinsed, and then dried at 100 ° C. The weight change of specimens was determined using the equation below [77]:

$$\textbf{Weight loss} = \frac{\Delta W}{S.A} \quad \text{- - - - - - - - - (3.4)}$$

Where : ΔW the weight loss of sample(g), S.A. the surface area (mm^2)

Chapter Four

Results and Discussion

Chapter Four
Results and Discussion

4.1 Introduction

This chapter has been dedicated to display and discuss the results of this study. Characterizations of the starting materials and the synthesized powders will come first and then characterizations of samples will be discussed .

4.2. Characteristics of Prepared Powders

4.2.1.Thermal Analysis

TGA curves illustrated in Figure (4.1A) depicts the weight loss in relation to the temperature of a non-isothermal heat treatment for undoped and co-doped HA after the chemical precipitation. It shows that the mass loss during heating could be classified into three different stages. First, the weight loss at a temperature 200°C is corresponding to remove physically absorb water. Next, the decomposition of HPO_4^{-2} occurs in the temperatures between 200°C up to 650 °C according to the reaction[78]: $2HPO_4^{2-} \rightarrow P_2O_7^{4-} + H_2O$ ……..(4.1) .

Increasing the temperature above 700°C, $P_2O_7^{4-}$ and OH^- ion might have reacted to form PO_4^{3-} and H_2O, according to the reaction

$P_2O_7^{4-} + 2OH^- \rightarrow 2\ PO_4^{3-} + H_2O$ ……(4.2) .as reported by Lee et al. [79] and Mardziah et al [80].

Eventually, the weight loss continuously occurs up to 850°C which is corresponding to adsorbed H_2O in the powders and interstitial water in the structure. The total mass loss in the samples HA-1, HA-3 and HA-4 is about 10%. HA-2 has a weight loss of about 12%. Beyond 850°C, no significant weight loss was observed.

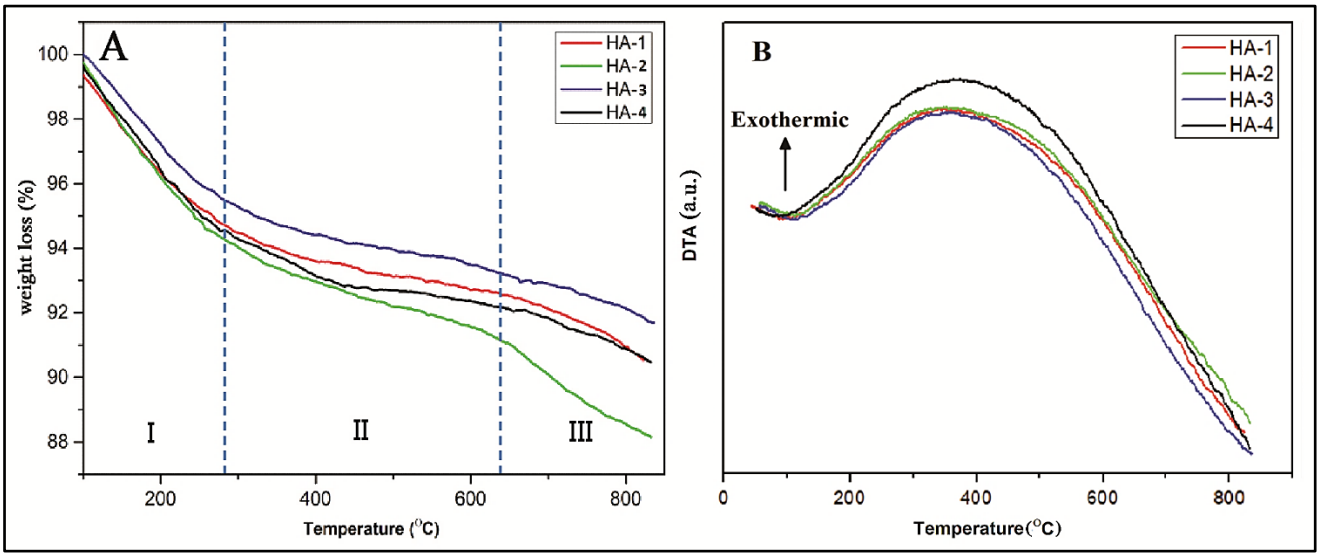

Figure (4.1): Thermal behavior of as prepared hydroxyapatite before the heat treatment; A) TGA curves; B) DTA curves

The DTA analysis shown in Figure (4.1B) was done for the freshly prepared undoped and co-doped HA. Elimination of physically adsorbed water of the hydroxyapatite powder is the cause of the endothermic peak that can be seen in the range of 100 - 200 ° C for all the DTA curves [35]. The exothermic reaction observed in the 200–800 °C range indicates the decomposition of HPO_4^{-2} and H_2O, which is accompanied by weight loss.

4.2.2. Structural Characteristics of Powders after Calcination

The results of the X-ray diffraction are illustrated in Figure (4.2). It is clear that the yield compound has a pure hexagonal apatite phase without any secondary phases (pattern HA-1). The co-doped hydroxyapatites do not show

other secondary calcium phosphate phases nor oxides of the dopants. Patterns (HA-2, HA-3, and HA-4) confirm that the substituted of Cu^{2+} and Mg^{2+} into HA have incorporated well into the apatite crystals where no traces of those oxides have appeared. The data in Table (4.1) has been measured from the XRD information using the origin program. It exhibits that the cell dimensions as well as the crystallinity of the undoped and co-doped hydroxyapatite crystals are incompatible because of the ions substitution.

The crystal dimensions (**a** plus **b**) of the undoped HA are about 9.4348 Å, while it is about 6.8847 Å for **c** as shown in Table 4.1. They are comparable to those of synthesized HA [37, 81]. Introducing divalent ions (Cu^{2+} and Mg^{2+}) into HA lattice changed the crystal dimensions as a result of variation in the ions radii among Ca^{2+}, Mg^{2+} and Cu^{2+} (114pm, 86pm, 87pm, respectively). As a matter of fact, the single substitution of ions were exempted in this work because it has intensively covered in other literature [69-71] and the effort was focused on the double ions substitution to fabricate functional HA.

Table (4.1): Alteration of the unit cell dimensions and crystallinity of undoped- and (Cu, Mg) co-doped HA

Composition	a, b (Å)	C (Å)	Volume ($Å^3$)	X_c, (%)
$Ca_{10}(PO_4)_6(OH)_2$	9.4348	6.8847	530.74	81.5
$Ca_9(Cu_{0.5},Mg_{0.5})(PO4)_6(OH)_2$	9.3723	6.8911	524.22	82.2
$Ca_9(Cu_{0.25},Mg_{0.75})(PO4)_6(OH)_2$	9.4277	6.8649	528.42	75
$Ca_9(Cu_{0.75},Mg_{0.25})(PO4)_6(OH)_2$	9.3448	6.8780	520.16	79.3

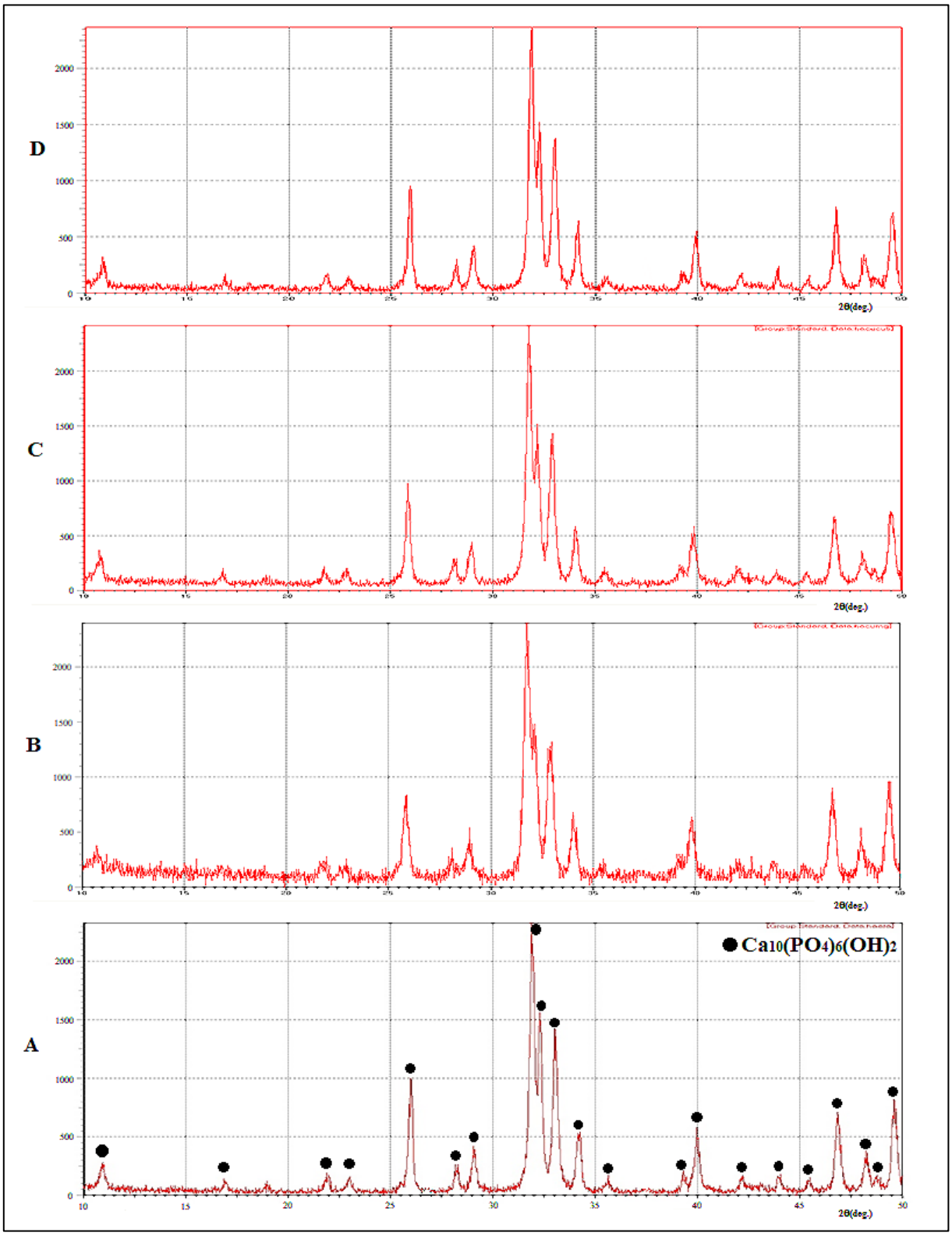

Figure (4.2): X- Ray diffraction patterns of prepared powders (A) HA-1 ,(B) HA-2 , (C) HA-3 ,(D) HA-4 calcinated at 800°C

As illustrated in Table (4.1), that increasing the substituted mole ratio of copper and decreasing that of magnesium decreases the HA crystal dimensions (**a**, **b**) where they recorded to be 9.3448 Å. The dimension (**c**) slightly changed where no remarkable trend has noticed for with the additions. Vojislav et al. reported that (**a**, **b**) lattice dimensions decreased with increasing doped fraction of Cu^{2+} alone. A possible reason for this alteration is owing to the difference of ionic radii [37]. The shift of the main peaks of HA due to the Mg and Cu doped ions in the powders causes a slight contraction in the (a,b)-axis dimensions as shown in Figure (4.3), The shift of the HA peaks occurs owing to differences in atomic radii between Mg^{2+} and Cu^{+2} ions with Ca^{2+} ions, which allows doping ions to enter the HA structure [82]. Doping of HA with Mg^{2+} ions causes contraction in the hexagonal unit cell volume as well [81].

In fact, adding equal mole ratio of 0.5 of each element did not make that change in **a-** and **b**-dimensions, where they were recorded to be 9.4348 Å before and 9.3723Å after doping. However, **c** dimension was a slight increased from 6.8847 Å to 6.8911Å after doping. The crystallinity of prepared powders was also calculated as shown in Table 4.1.

The doping ions have also decreased the crystallinity of HA. Sharp peaks in Figure (4.2) confirms that they are highly ordered. The crystallinity of as-prepared HA-1 was about 81.5%. The same degree of order can be seen in HA of the chemical formula$[Ca_9(Cu_{0.5},Mg_{0.5})(PO4)_6(OH)_2]$ for about 82.2% as shown in figure (4.2B). Increasing of Cu^{2+} and lowing Mg^{2+} content led to lowering the crystallinity below 79.3% shown in figure (4.2D), and the minimum crystallinity was recorded to $[Ca_9(Cu_{0.25},Mg_{0.75})(PO4)_6(OH)_2]$ of about 75% shown in figure (4.2C). This may cause high distortion in the lattice configuration of hydroxyapatite. It is known that the crystallinity of

hydroxyapatite depends upon the fabrication method. With respect to the wet chemical precipitation, the crystallinity is precipitation temperature and aging time dependent [37]. Lazi´c et al. have found that the crystals of hydroxyapatite show high crystallinity at precipitation temperature range of 22°C – 95°C in addition to the maturing time of 20h [78].

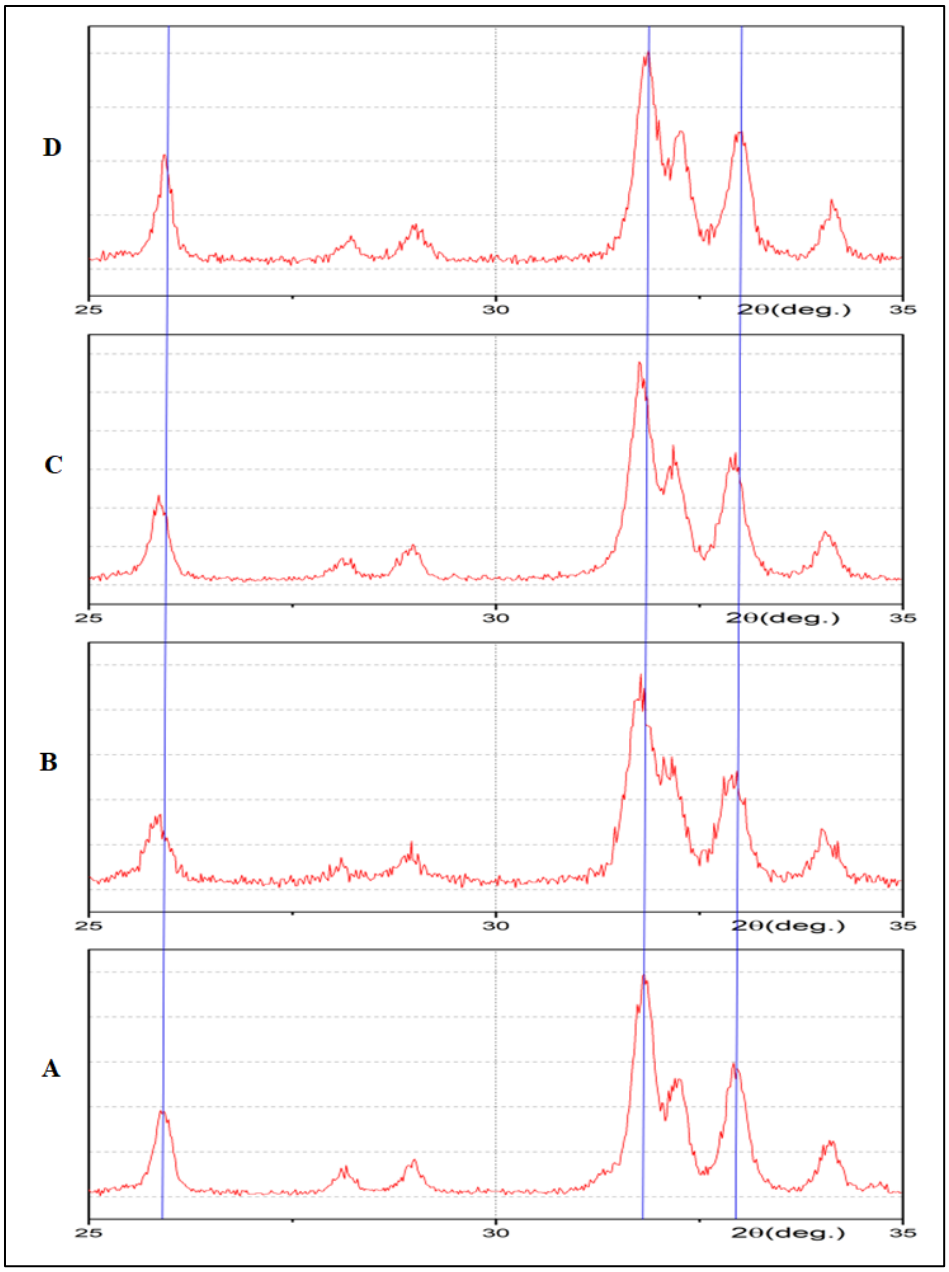

Figure (4.3): Shifting of the main peaks for the x- ray diffraction patterns for powders (A) HA-1 ,(B) HA-2 ,(C) HA-3 ,(D) HA-4.

4.2.3. Fourier Transform Infrared Spectrometer (FTIR)

Another noticeable influence of doping is shifting of the functional groups band of hydroxyapatite. Figure (4.4) reveals FTIR spectra of the functional groups (PO_4^{3-} and OH^-) in the HA lattice. In the spectra of specimen HA-1 are the characteristic bands of absorbed water (hydroxyl group) at around 570 cm^{-1} and at the range 3471-3417 cm^{-1}. Band at 1041cm^{-1} and 462 cm^{-1} associate with the stretching modes of the PO_4^{-3} related to HA. The band at 1620 cm^{-1} is assigned for the stretching modes of H_2O bond. The bands attributed to CO_3^{-2} was observed in (1427, and1458 cm^{-1}), while that at 2468 cm^{-1} was attributed to CO_2 according to Álvarez et al [69].

These bands (PO_4^{3-} , OH^- , CO_2 , H_2O)are found in all specimen with different intensities. The influence of the co-doping is indicated by the band shifts of PO_4^{-3} group at 1041 cm^{-1} where it increases as the mole ratio of substitutions is 50% each.

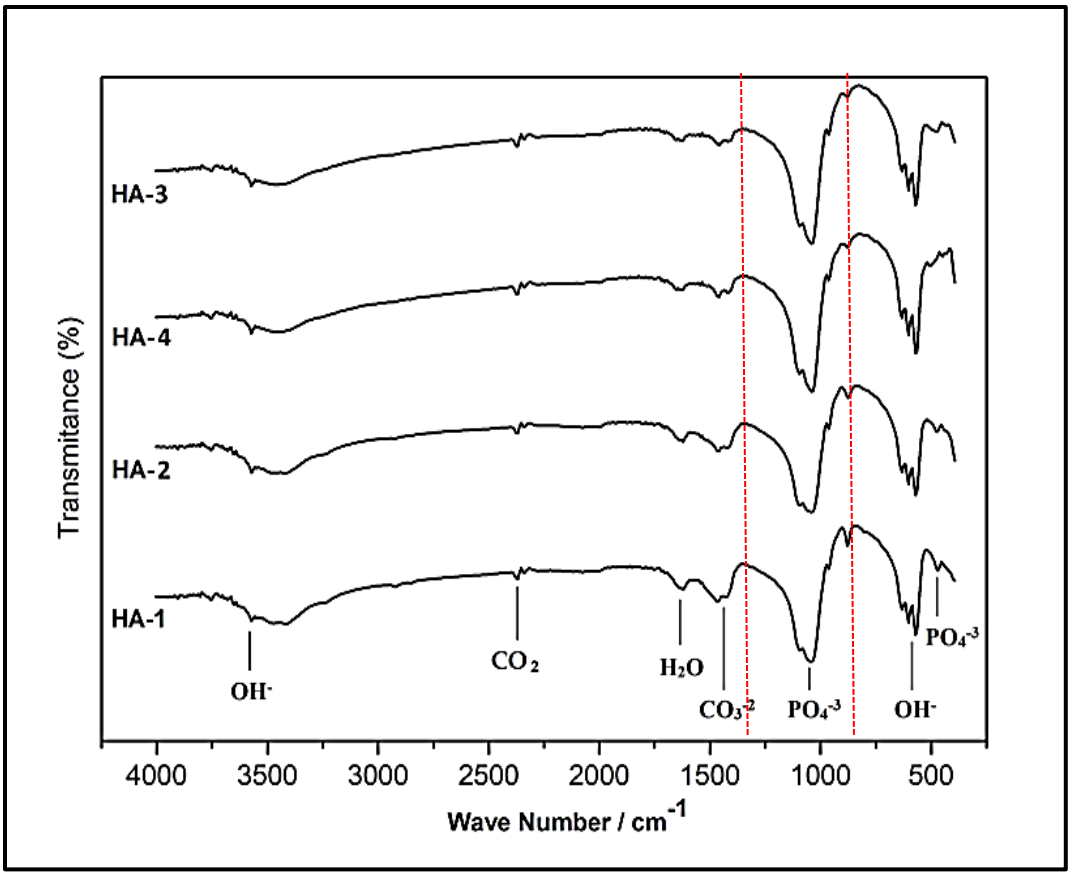

Figure (4.4) : Functional groups of precipitated hydroxyapatite with different compositions.

4.2.4. Transition Electron Microscopy (TEM)

The shape of HA particles are depicted in the TEM micrographs before and after HA doping as seen in Figure (4.5). All specimen were heat treated at 800°C for 2h. Two compositions were chosen to be optically observed depending on the inhibition impact on bacteria i.e pure HA and $[Ca_9(Cu_{0.75},Mg_{0.25})(PO_4)_6(OH)_2]$. Figure (4.5) reveals that most of the particle size of the prepared HA is lower than 100 nm. Moreover, their shape has retained the hexagonal (longitudinal) after the substitution. The TEM micrographs are

support the X-ray diffraction results that have showed decrease in **a-** and **b-** dimensions of HA crystals.

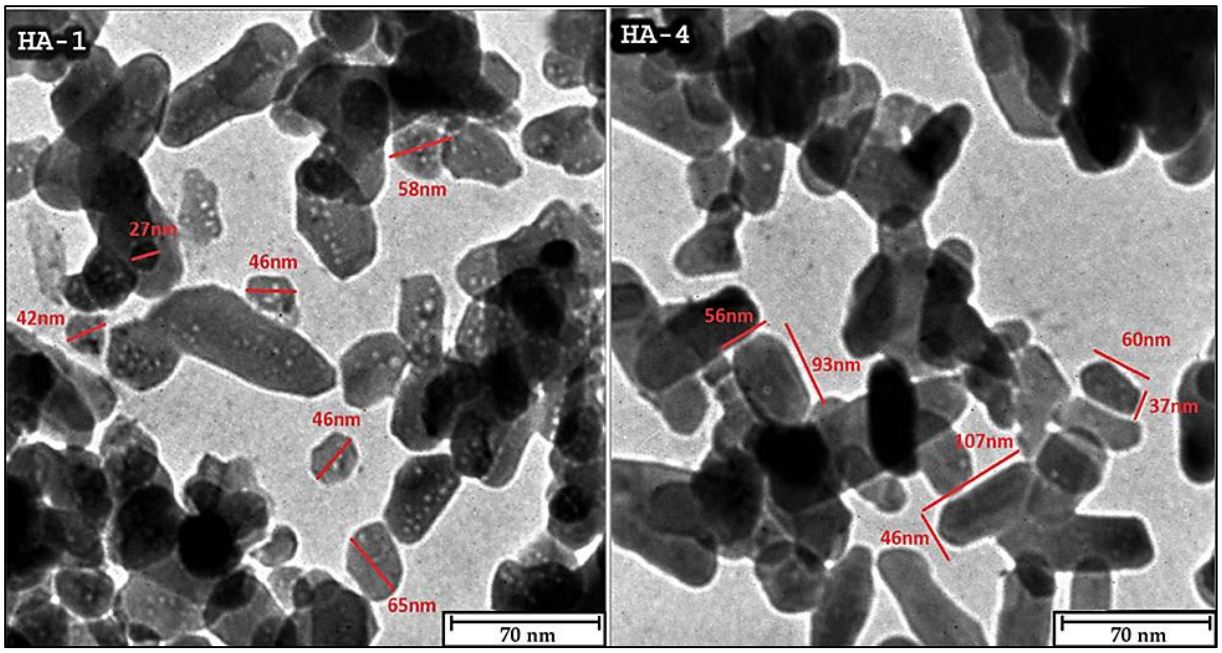

Figure (4.5): TEM micrograph of the hydroxyapatite powders, HA-1 (pure HA), HA-4 (co-doped HA)

4.3.Biological Result

4.3.1 Antimicrobial Activity

The findings of bacterial inhibition showed that the antimicrobial activity has varied according to the chemical modifications as shown in table (4.2). Figure (4.6) exhibits different responses of the synthesized hydroxyapatite. HA-1 didn't show any effect against either Gram(+) as S.aureus or Gram(-) as E.coli bacteria. This means that these composition cannot fight the effect of bacterial media. On the other side, the composition denoted as HA-3 shows remarkable effect on the E.coli, while on the S. arueus the behavior was slightly different.

The gray inhibition ring is small which indicates that increasing the mole ratio of Cu^{2+} on the account of Mg^{2+} in HA increases the zone diameter of inhibition. It is around 30 mm in E.coli bacteria and is 14mm in S.aureus bacteria. The results also indicates that Mg^{2+} has lower influence on the inhibition of bacteria activity. In this context, composition denoted as HA-3 [$Ca_9(Cu_{0.25},Mg_{0.75})(PO_4)_6(OH)_2$] shows low inhibition against E.coli and S.aureus bacteria. It exhibited an inhibition zone diameter of 25 mm in E.coli and 9 mm in S.aureus media. This allow us to infer that doped with Cu^{2+} is more valuable for the co-doped HA in fighting infection of implants or other clinical usages. Magnesium, on the other hand, showed little contribution to inhabit the bacteria activity as seen in the gray zone diameter.

Table 4.2. Inhibition diameters of HA and Co-doped HA for E.coli and S.aureus.

Samples code	E.coli Inhibition Diameters (mm)	S.aureus Inhibition Diameters (mm)
HA-1	_	_
HA-2	28	14
HA-3	25	9
HA-4	30	14

One possible reason for that is copper ions interact with bacterial cell membranes of E. coli causing structural change, eventually, death of cell [83]. The larger diameter, the larger inhibition effect. Figure (4.6) shows also different responses for HA in E.coli and in S.aureus bacteria. This can belong to

the S. aureus membrane structure of Gram+ which makes it less susceptible to all metal-doped HA than E. coli bacteria [37].

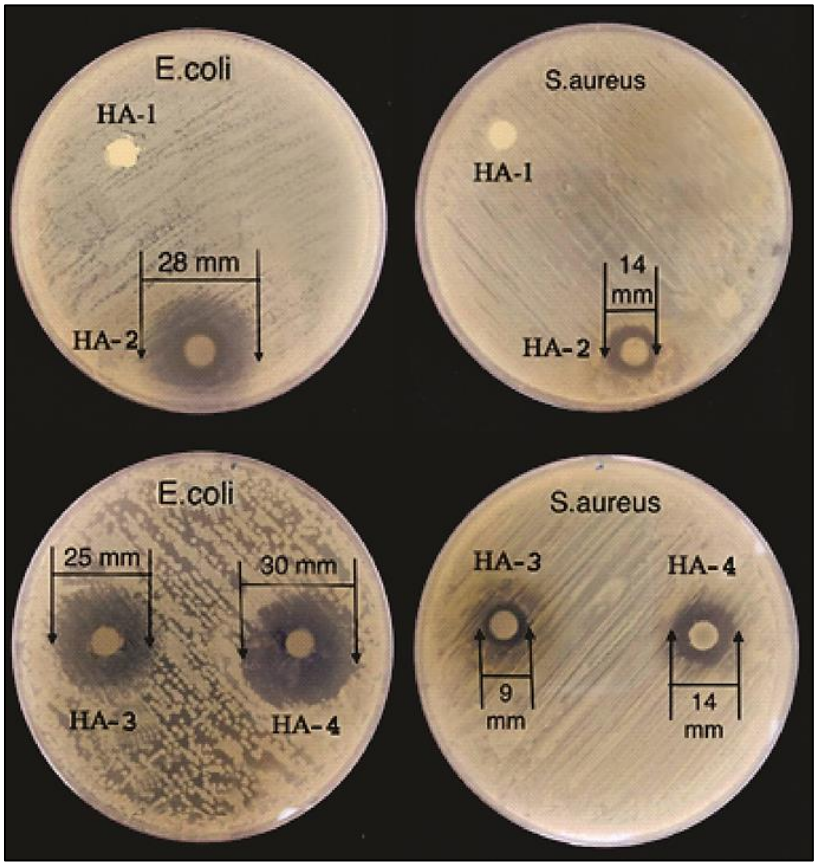

Figure (4.6): Antibacterial response of the synthesized HA against E.Coli and S. Aureus bacteria

4.3.2. Cytotoxicity Investigation

Cytotoxicity is an important feature of biomedical materials because they would be in touch with living tissues. Therefore, investigation of cytotoxicity for the material intended is an essential requirement for biocompatibility. In vitro cytotoxicity test is one of the tests that is suggested and considered acceptable for the biological evaluation of a medical product [84]. The viability of osteoblast cells using MTT assay which is a colorimetric reaction that can easily

be measured from cell monolayers that have been plated in 35 mm dishes or multiwell plates, is shown in Figure (4.7). It reveals that the cells viability are reversely related to the concentration of dissolved HA where it is about 76.8% at 125 mg/ml. The Figure also exhibits that HA alone showed lower performance in comparison to co-doped HA. No matter how the concentration of dissolved HA is, $(Mg_{0.75},Cu_{0.25})$HA shows no toxic effect.

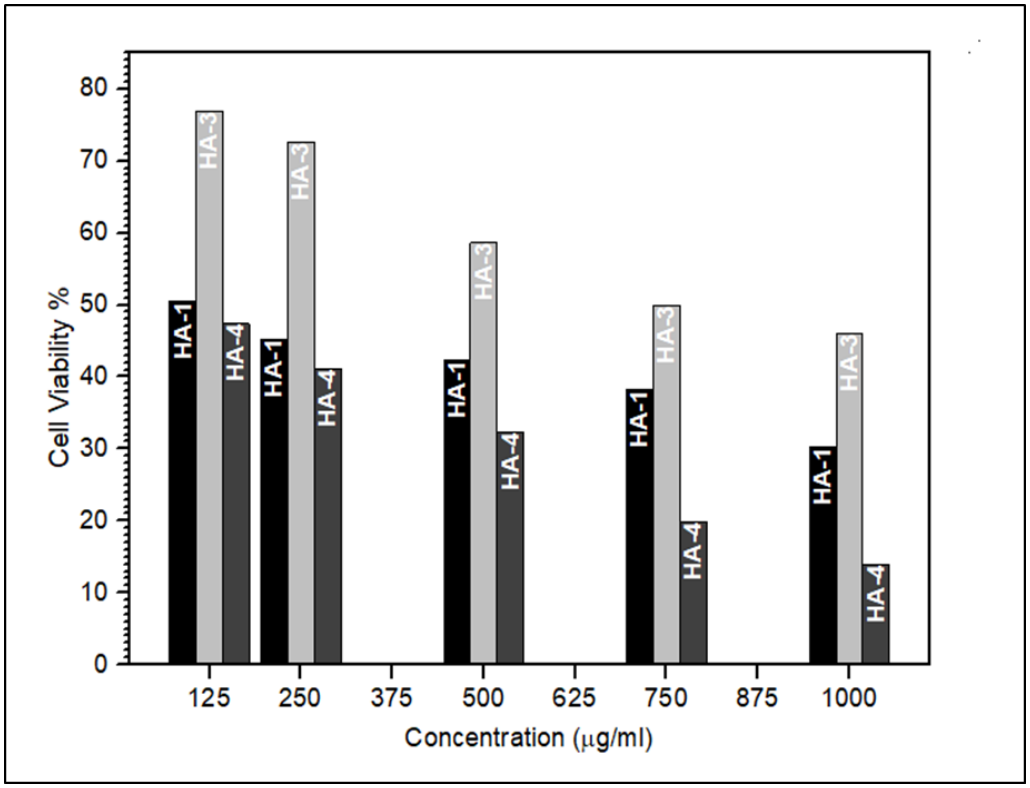

Figure (4.7): Cell viability from MTT assay for different concentrations of pure and co-doped HA

This can be inferred by the abundance of survival cells. In fact, magnesium has high biocompatibility with live cells and an important role in bone healing by stimulating osteoblast proliferation at the early stages of osteogenesis according to Tite [85]. It can enhance osteoblast growth subsequently bone regeneration by accelerating mineral metabolism. However, low concentration

of copper can well do as antibacterial agent. HA-4 exhibits the lowest live cells all the intended concentrations which indicates a toxic effect which contains 0.75 %Cu^{2+}. Figure(4.8) represents the viability of cells at concentration of 250 (µg/ml) which is the same concentration that was used in the antibacterial test.

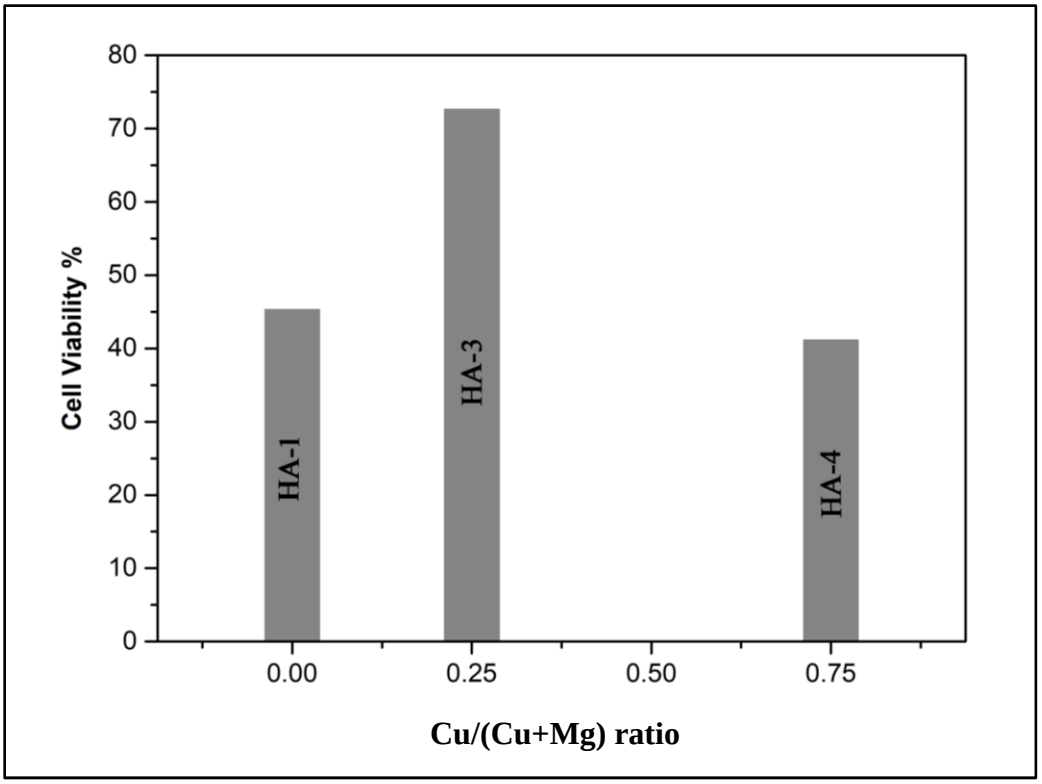

Figure (4.8): Cell viability from MTT assay for 250 (µg/ml) concentrations only of HA-1, HA-3 and HA-4 specimen

Figure (4.9) illustrates the fluorescence microscopic images of the live and healthy cells after 3 days of cultural periods for different HA concentrations. It has been noticed that the choice of dopant ions influences the cells environment. Figure (4.9) supports the results of MTT assay, where the density of live cells vary according to the amount of doping elements added and to the concentration of the dissolved hydroxyapatite. The image also revealed that increasing the release of Mg^{2+} into the body fluids during the bone remodeling phase will boost

the osteoblasts to grow faster and help bones to heal compared to HA-1 and HA-4. As known already that Mg^{2+} exists in natural dentin and bones at concentration of 1.23 wt% and 0.73 wt%, respectively [69] It means that Mg^{2+} acts similar to a growth factor during the early stages of osteogenesis and promotes bone formation [86]. This effect can be seen by increasing the number of the blue spots as shown in Figure (4.9). Controversially, increasing the concentration of copper in the HA lower the number of osteoblasts where the cell underwent lysis. Therefore, the cytotoxicity assay reveales that osteoblast cell is killed when high concentration of Cu^{2+} exists in their environment [67]. In fact, presence of copper makes confluence and proliferation of live cells at minimum as inferred from Figure (4.9).

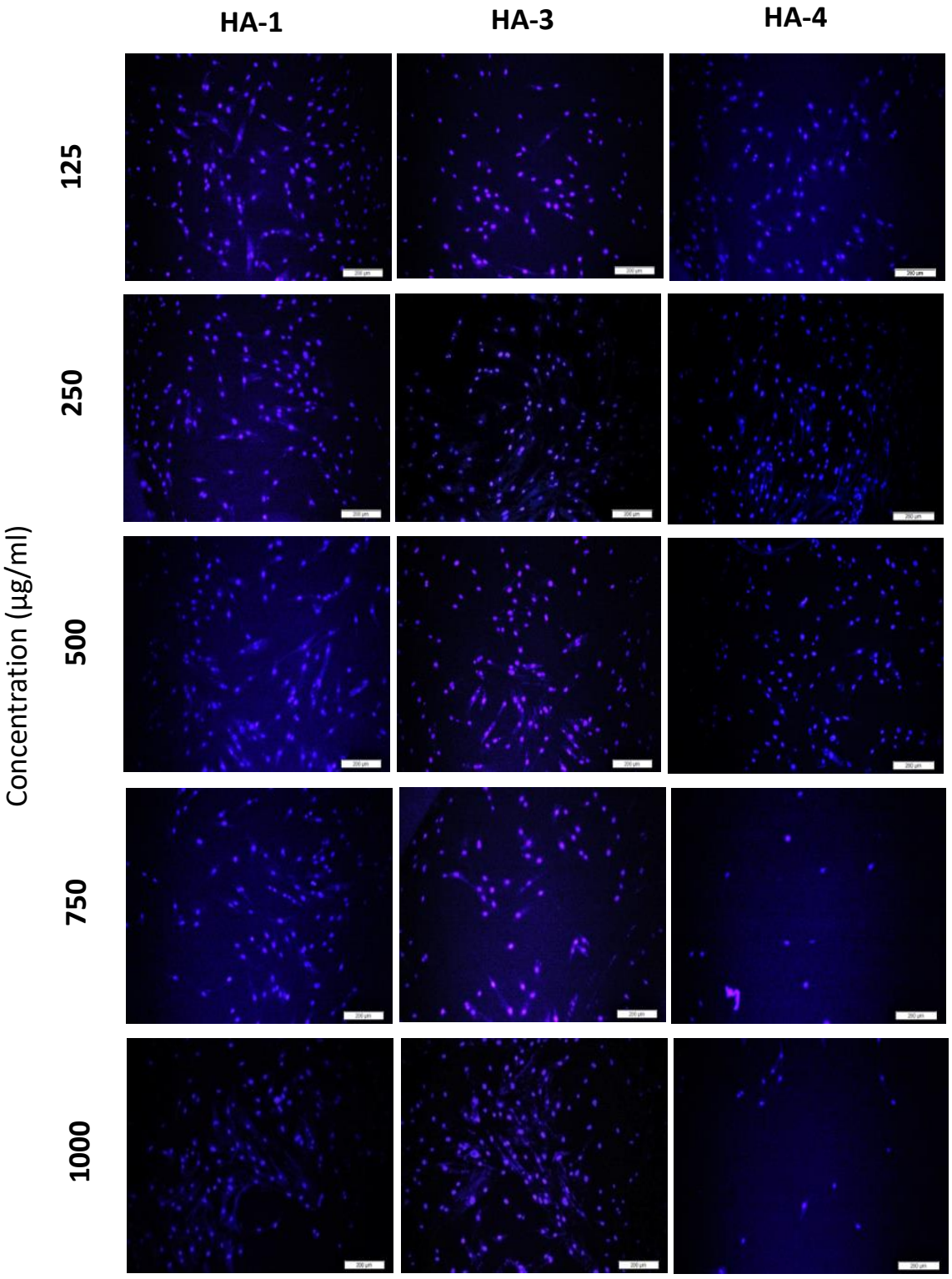

Figure (4.9): Microscopic images of osteoblast cells in different concentrations of pure and co-doped HA (Scale Bar 200µm)

4.4. Characteristics of the bulk hydroxyapatite

4.4.1. Phase Identification

The patterns in Figure (4.10) represent the x-ray reflections of sintered Pure and co-doped hydroxyapatite using traditional sintering method at 1200°C. It has been widely described in several studies that sintering of HA at a temperature range of 1000°C to 1300°C exhibits thermal instability which leads to decompose HA into TCP, CaO and H_2O vapor. The presence of CaO in the sintered specimen could be assigned to the reaction described below [23, 87]:

$$Ca_{10}(PO_4)_6(OH)_2 \longrightarrow 3Ca_3(PO_4)_2 + CaO + \uparrow H_2O$$

The findings of diffraction analysis refer to slightly decomposition of HA-1 into CaO where its main peak at 37.360 (JCPDS no. 00-002-1088). The decomposition occurs in all sintered samples at 1200°C; however, the intensity of the resulting phases varies depending on the mole ratio of doping. The other bulk samples i.e. HA-2 and HA-3 exhibits noticeable decomposition of HA into β-TCP (JCPDS no. 09-0169) and other phases as seen in Figure (4.10B, 4.10C). Presence of Mg^{2+} ions in the initial solution slows apatite crystallization and favors its thermal conversion into the TCP phase. Increasing the Mg^{2+} concentration increases the decomposition tendency into β-TCP.

This result is consistent with the findings in the literature [28, 88]. Fadeev et al. reported that the destabilizing is because of the lattice distortion which leads to increase the strain inside the lattice and favoring HA to β-TCP transition [89].

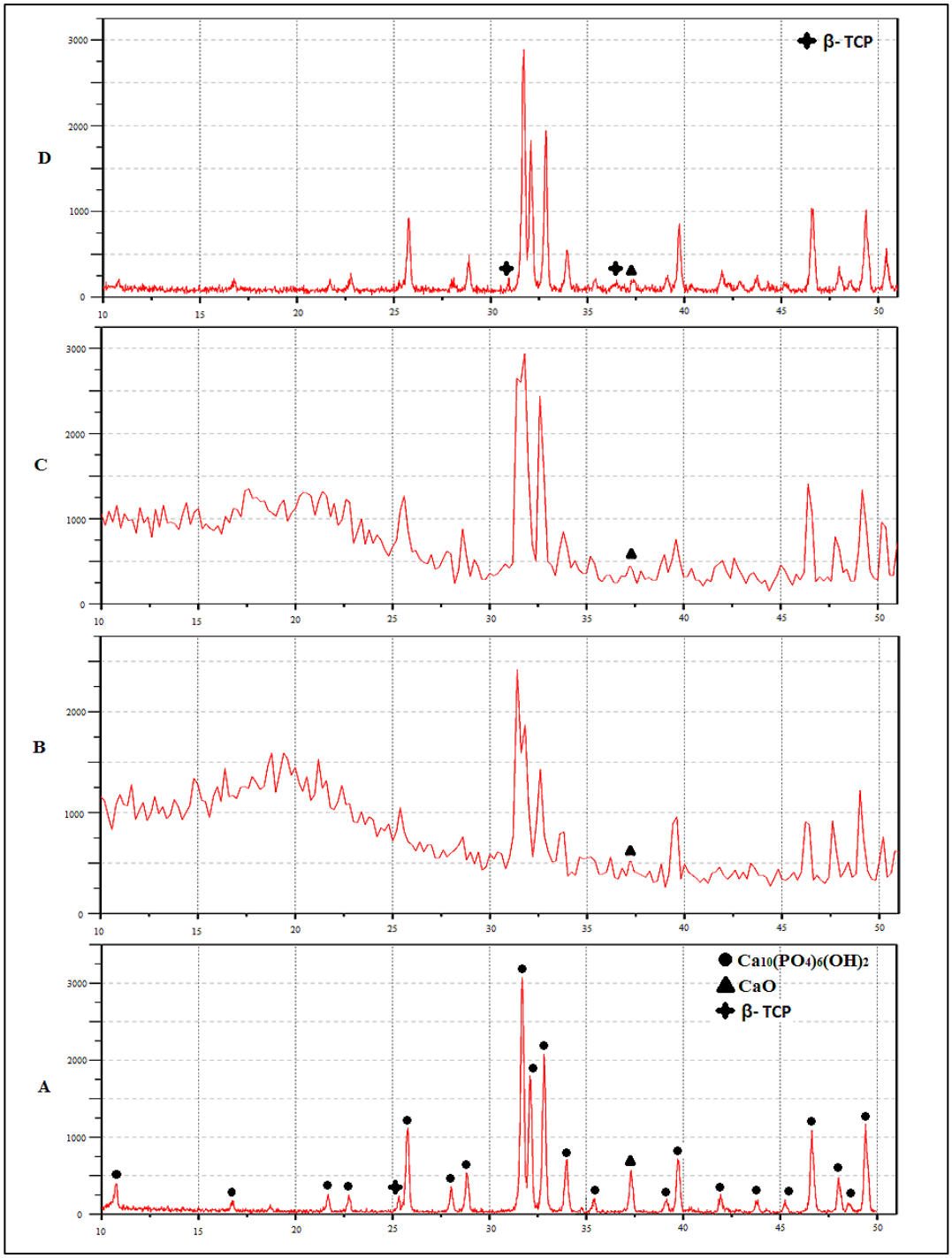

Figure (4. 10): XRD patterns of samples (A) HA-1 , (B) HA-2 , (C) HA-3, (D) HA-4 prepared by traditional sintering at 1200°C.

Introducing of Cu^{2+} ions will cause similar tendency of HA transition into β−TCP as seen in the XRD pattern of HA-4 shown in Figure (4.10D). Figure (4.10) shows also that there is no other compounds involving Mg^{+2} or Cu^{+2} ions appeared in the X-ray reflections.

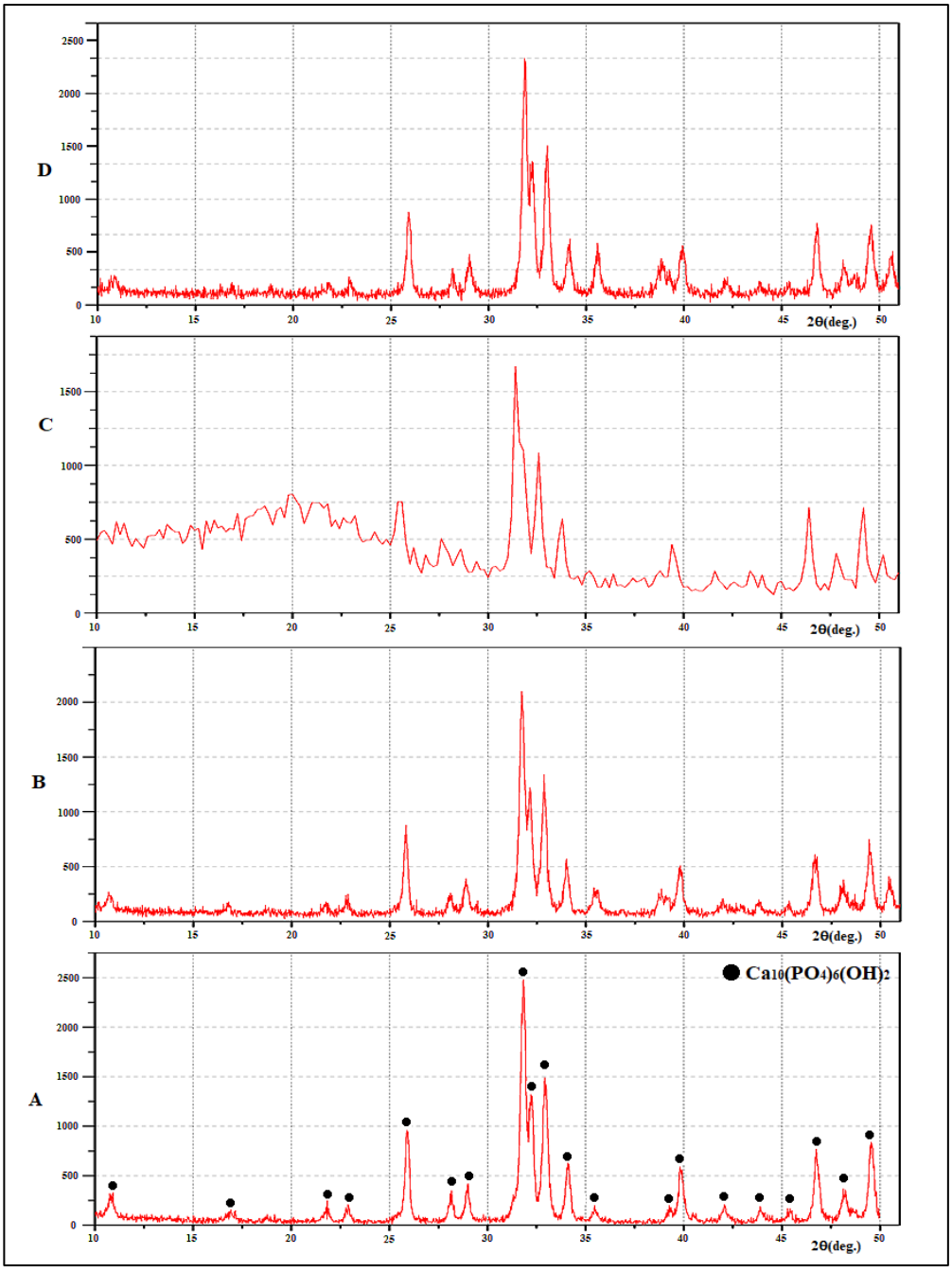

Figure (4. 11): XRD patterns of samples (A) HA-1 , (B) HA-2 , (C) HA-3, (D) HA-4 prepared by cold sintering at 250°C

One of the suggested solutions to stop the thermal instability of hydroxyapatite is lowering the sintering temperature to that of decomposition that is around 900°C [90]. In this context, sintering at temperatures lower than 300°C using cold sintering method would be perfect for this material. Figure (4.11) exhibits the X-ray diffraction patterns of hydroxyapatite specimen before and after doping prepared by cold sintering. These specimen were cold sintered at 250°C. The patterns of (Mg,Cu) co-substituted hydroxyapatites are in excellent accordance with the standard card (ICDD Card No. 01- 084-1998), where no secondary phases of TCP and/or CaO are formed in addition to stabilize the hexagonal structure of apatite. Such positive results are comparable to those in Refs [59] and [74].

4.4.2. Bulk Density

The density of fabricated HA is influenced by the doping and by the sintering method. Generally, it is expected that the density of the HA powder is changed according to the doping ions density, where the density of Cu^{2+} is 8.96 g/cm^3 and that of Mg^{2+} is 1.73 g/cm^3 in comparison to 1.55 g/cm^3 for Ca^{2+}. Figure (4.12) explains the effect of sintering method on the density of compacted samples in relation to the mole ratio of $\frac{Cu}{Cu+Mg}$ rather than the sintering temperature. Because it was determined to be constant at 250 °C for all the experiments.

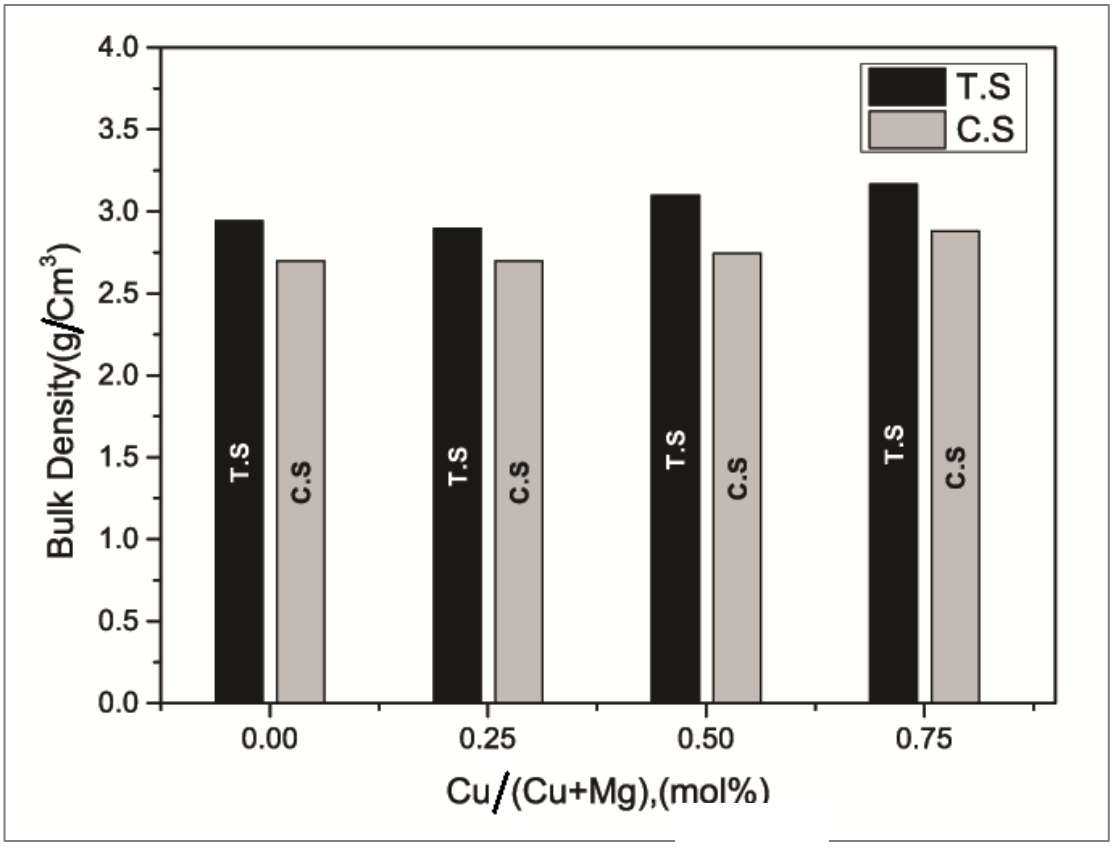

Figure (4. 12): Bulk Density of HA Prepared by traditional (at 1200°C) and Cold Sintering(at 250°C)

In fact, the HA-1 sintered at 1200 °C has a density about 2.9433 g/cm^3, about 93% theoretical density of HA which is 3.156 g/cm^3. While cold sintered HA-1 has a value of 2.6972 g/cm^3. The difference in density returns to the mechanism of closing the pores inside each specimen. Table (4.3) shows the density values of undoped and co-doped hydroxyapatite. For the traditional sintering diffusion of matter and creep are the main mechanisms for densifications. This, of course, leads to transport huge amount of species to the neck area which contributes to full and contract the overall specimen volume. On the other side, the crucial step in CSM is the partially surface dissolving of particles that create slurry-like media around the particles. This, however, will

leave tiny (meso-) pores after evaporation the transesolvent. The situation can get worse if insufficient external pressure applied [90]. In our case, the solvent (water) worked well but the maximum applied pressure of the machine (250 MPa) was not high enough to close the pores. Hassan et.al. [75] demonstrated that density of HA increases with pressure. In the same study (500 MPa) uniaxial pressure were found to be ideal for achieve a bulk densities of up to 98.8% . The sintering temperature of cold sintering is considered remarkable advantage of the method that is < 300 °C.

Table (4.3): Density (g/cm^3) values of the samples prepared by traditional (TS) and cold sintering

Sample Code	TS	CS
HA1	2.9433	2.6972
HA2	3.0978	2.7441
HA3	2.8959	2.6648
HA4	3.1658	2.8792

This temperature plus the applied pressure makes a combined effect on powder consolidation. Controlling the other parameters i.e. kind and concentration of liquid phase as well as sintering time is demanded to get as high as density. It is clear from Figure (4.10) and Table (4.3) that the yield density of the co-doped HA increases with $\frac{Cu}{Cu+Mg}$ ratio. In which, ($Cu_{0.75}$, $Mg_{0.25}$)HA has a value of 2.8792 g/cm^3 among the CSed ones. The result may return to the copper which is heavier than the other divalent ions. Another reason which was reported by Radovanovic [91] as copper reduces the porosity of the ceramic.

4.4.3. Microstructure After Sintering

Figure (4.13) represents SEM images of fracture surface of the sintered HA-1 by both methods. The microstructures of both specimen reflect the mechanism of each sintering method. In Figure (4.13B), it is seen that powder particles are connected to each other forming cohesive agglomerates, necking and grain growth. Residual pores are seen in the microstructure. Controversially, the image in Figure (4.13D) exhibits densified microstructure of cold sintered HA. Where no clear grains or grain boundaries appear on the image.

This can be attributed to densification mechanism that implies particles rearrangement, precipitation and epitaxial growth of new crystals [59]. Residual pores are still seen in the microstructure. Nevertheless, this structure contains higher pore contain than they appear which may be reflected in the number of density as stated in Table (4.3).

The SEM images in Figure (4.14) are of cold sintered co-doped HA that shows other morphologies depending on the doping elements. A closer view of Figure (4.14-A,B) for the fractured surface of HA-3 ($Ca_9Cu_{0.25}Mg_{0.75}(PO_4)_6(OH)_2$) cold sintered shows cracks. Probably they are a mixture of intergranular and transgranular crack. However, the crack propagation is predominantly intergranular. Fracture surfaces become rougher and subsurface microcrack formations.

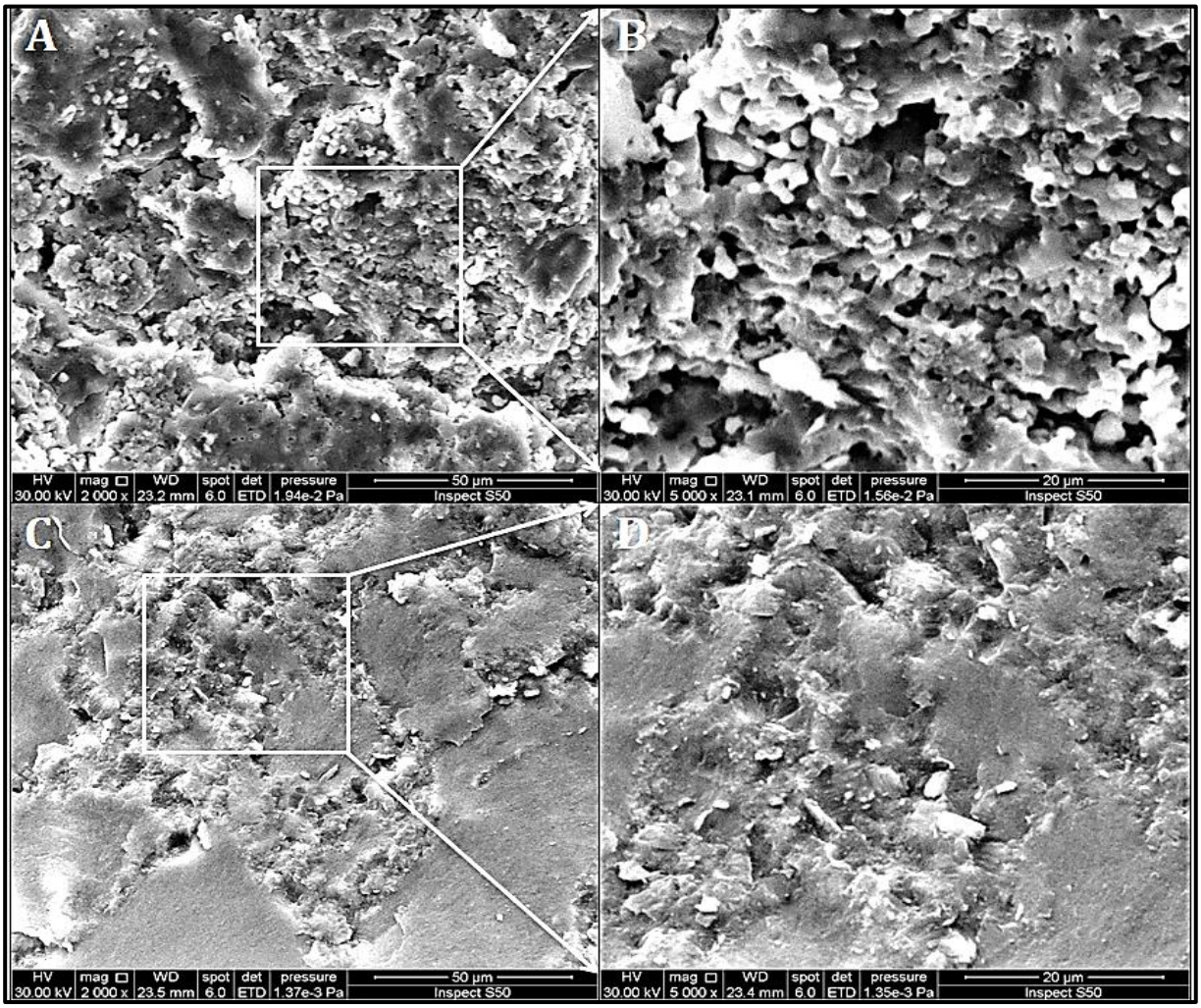

Figures (4.13): SEM images of undoped HA. A,B) sintered by traditional method at 1200°C; C,D) sintered by CSM at 250°C

The specimen HA-4 $(Cu_{0.75},Mg_{0.25})Ca_9(PO_4)_6(OH)_2$ in Figure (4.14D) reveals that the mode of fracture is nearly entirely transgranular. The microcrack, once developed, swiftly expands across the grain, but rarely through the neighboring grains.

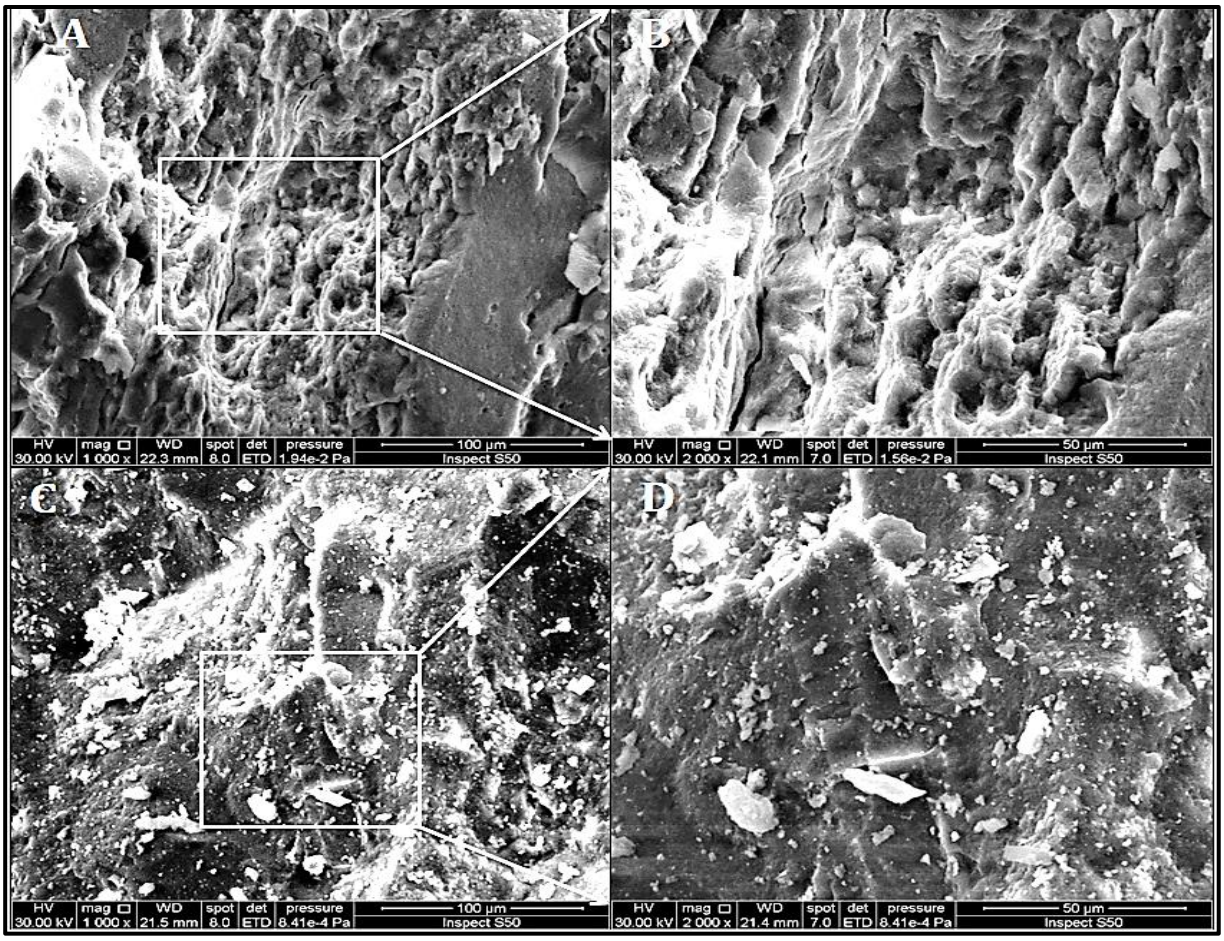

Figures (4.14): SEM image of co-doped HA sintered by cold sintering at 250°C. A,B) $Ca_9(Cu_{0.25},Mg_{0.75})(PO_4)_6(OH)_2$; C,D) $Ca_9(Cu_{0.75},Mg_{0.25})(PO_4)_6(OH)_2$

Figure (4.15) illustrates EDX line-scan of 10 µm length which shows that there is no big difference in the distribution of Ca^{2+} and P^{5+} which may refer to homogeneous structure after the finishing of the cold compacting. The doped HA also showed acceptable distribution of the Ca and P ions over the scanned line. Figure (4.16) and Figure (4.17) depicts the semi-equal distribution of Ca and P ions. The slightly deviation in distribution in Figure (4.17) may belong to the morphology of the specimen surface or the test itself. The reason may be that all the compacted HA have no divergent regions in the chemical composition since the transsolvent has the same ions of the base hydroxyapatite.

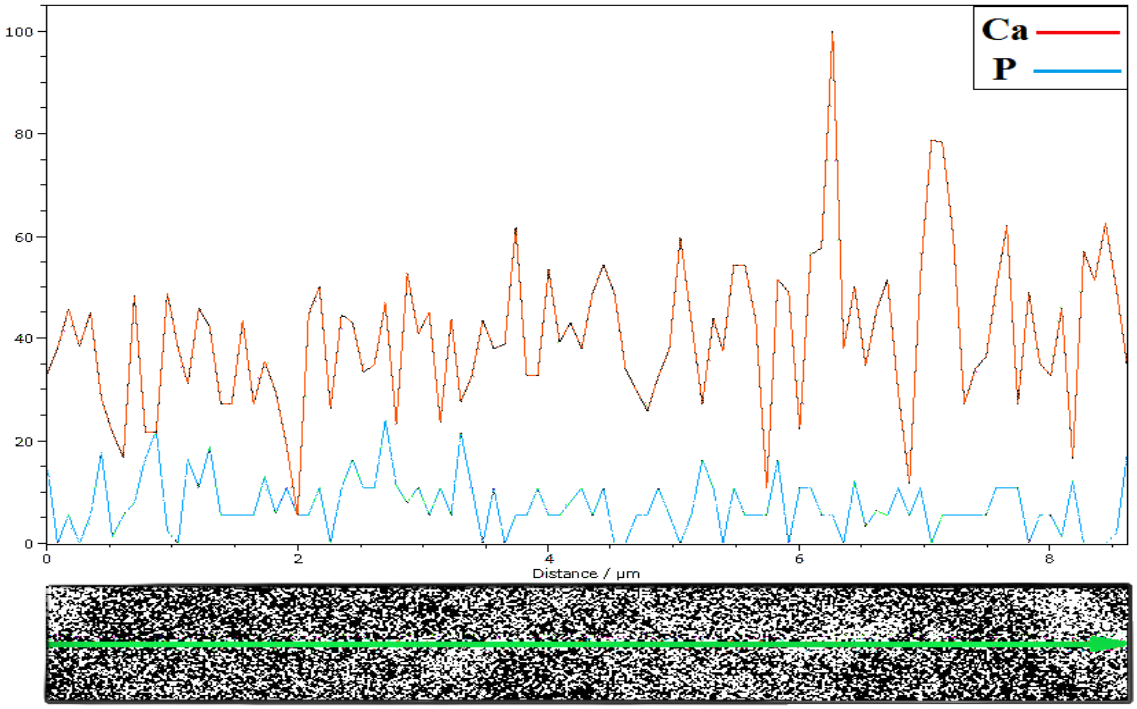

Figure(4.15): Line-scan EDX result of pure HA prepared by CSM at 250°C

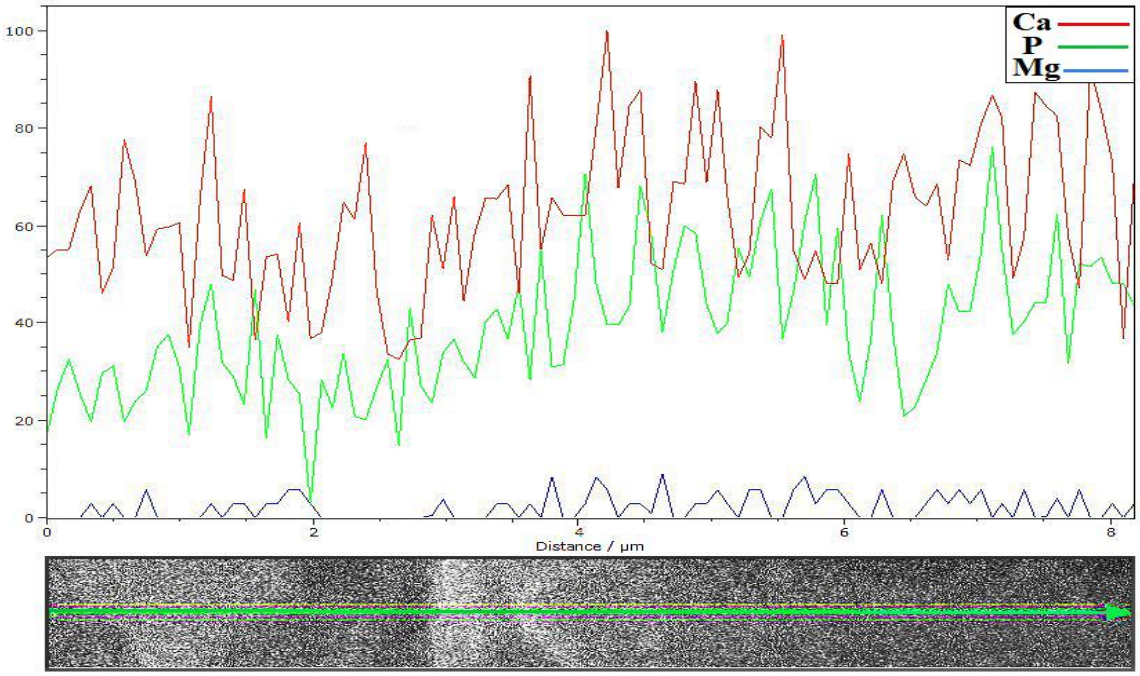

Figure (4.16): Line-scan EDX result for $Ca_9(Cu_{0.25},Mg_{0.75})(PO_4)_6(OH)_2$) sintered by CSM at 250°C

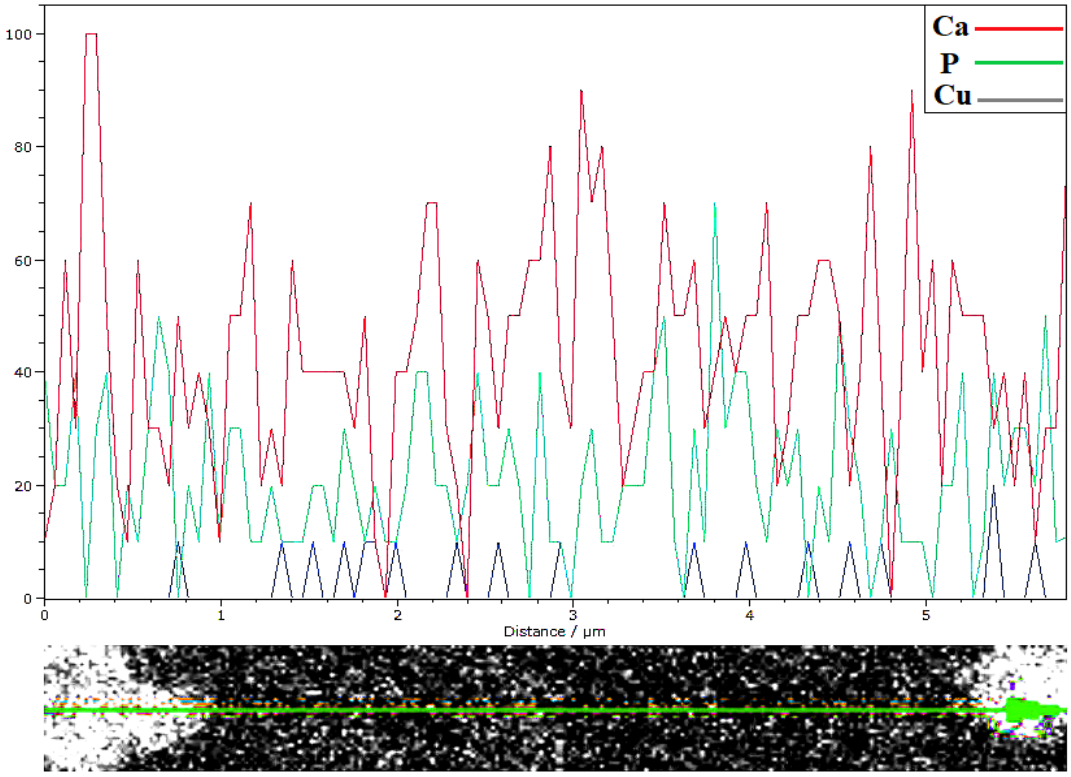

Figure (4.17): Line-scan EDX result for $Ca_9(Cu_{0.75},Mg_{0.25})(PO_4)_6(OH)_2$ sintered by CSM at 250°C

4.4.4. Vickers Microhardness

This test was conducted to depict the quality of cold sintering in comparison to the traditional one. The results of microhardness test for all the prepared samples are shown in bar chart (4.18). In order to get accurate hardness values, the test was repeated three times in distinct regions and then an average value was calculated. In general, all HA samples sintered by traditional method have superior hardness compering with cold sintered specimen , which may be attributed to the densification mechanism that drives high density after sintering. Increase the copper ratio above than 0.25 has led to decrease the hardness of cold sintered co-doped HA. The reason may belong to decreasing the tendency

of sintering as copper lowers HA dissolubility in the transsolvent which probably weakens the bonds between particles of HA in comparison to magnesium [92]. In traditional sintering method, doping elements caused positive effect on the hardness of HA in all doping ratios. These results are comparable to those reported by C.Y. Tan [93] and Noviyanti [82].

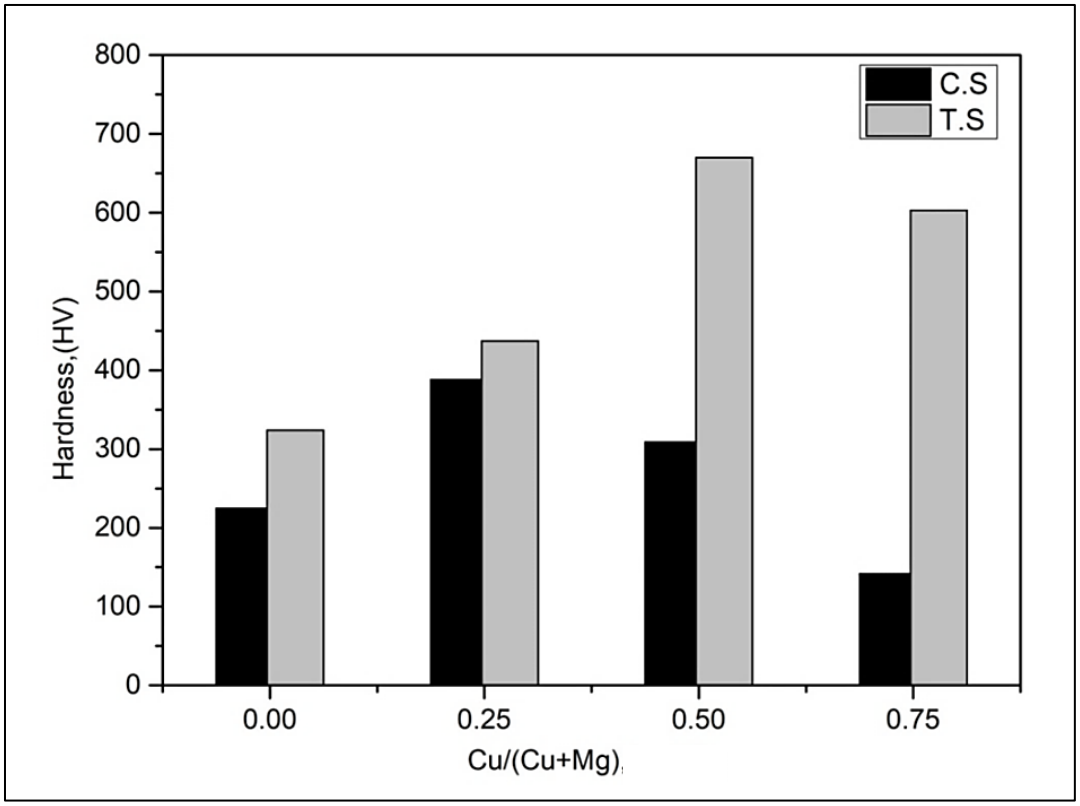

Figure (4.18): Vickers micro hardness of HA samples prepared using traditional sintering at (1200°C) and CSM method at (250°C).

4.4.5. Biodegradation Behavior of Hydroxyapatite

Material composition and sintering conditions are two important factors that affect the activity and dissolution behavior of ceramic implants in the biological environment. Degradation of HA is one of the most essential aspects, where the surface degradation appears to be linked to their osteoconductive

(bioactive) characteristics and plays a significant role in the early implant fixation according to various publications [94]. Ducheyne and Cuckler [95] mentioned that the greater the rate of dissolution of HA, the greater the effect of bone-ingrowth fixation. This meaning was also confirmed by Dhiraj Mehta et al. [96].Therefore, it is necessary to investigate the degradation tendency of undoped and co-doped hydroxyapatite. The prepared specimens were subjected to an in vitro degradation in Tris–HCl buffer (pH 7.4) for 1, 3, 7 and 10 days. This test can provide information about the degradation behavior of biomaterials in vitro to predict the rate of degradation in vivo. It is also one of the most critical tool for determining the suitability of material to be implants for bone repairing or scaffolds for bone tissue engineering. The degradation behavior of traditional sintered HA is shown in Figure (4.19).

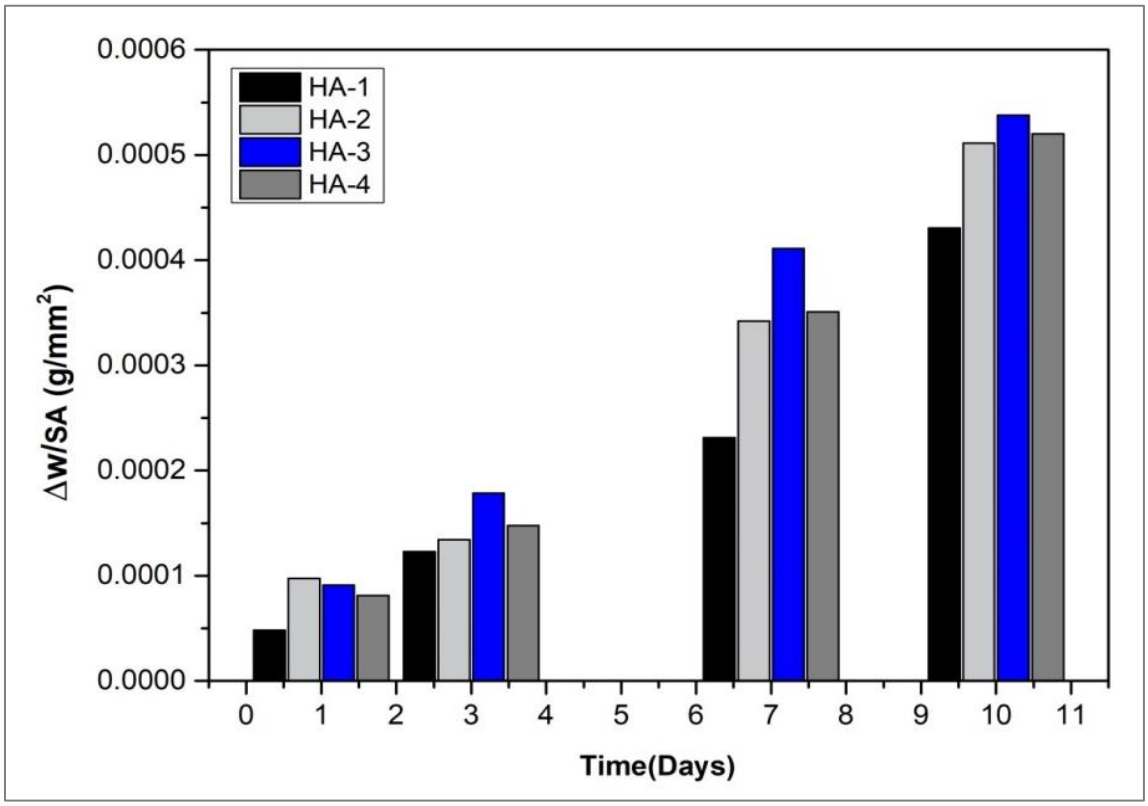

Figure(4. 19): Degradation of hydroxyapatite pellets fabricating using traditional method at 1200°C

In general, it is shown that the biodegradability of HA increased as the number of immersion days increases. It is also clear that high content of Mg^{2+} increases the biodegrability of HA as seen for all the immersion periods. This may belong to the distortion of HA crystals that magnesium bring with. The tendency of biodegrability of cold sintered HA is shown in Figure (4.20).

The results displayed in Figures (4. 19) and (4.20) indicate that HA-1 has the lowest rate of degradation in comparison to the other compositions as indicated somewhere in Ref. [16]. It is obvious that doping with Mg and Cu has raised the degradability of HA. Investigations of single and co-doped HA have shown that incretion metal ions into HA structure causes decreasing of crystallinity; and thus improves degradation and biological activity of HA.

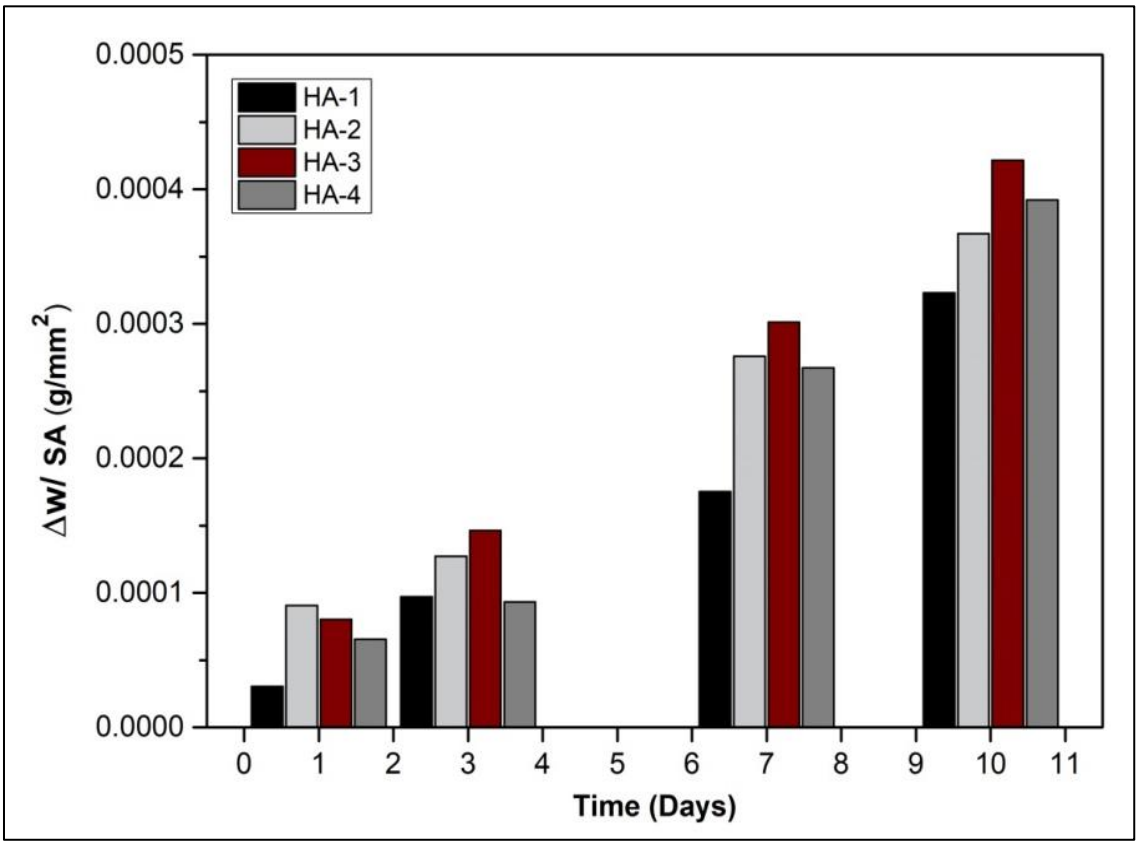

Figure(4.20): Degradation of HA and co-doped HA consolidated by CSM at 250°C

As stated in the work of Ying and Liu [77] which implies raising the rate of degradation as the amount of doping elements increase, especially strontium. They also reported that materials with more doping amount have the most potential for bone degradation and regeneration. A noticeable degradation behavior is detected for HA-2 and HA-3 comparing to the undoped HA. Particularly, $Ca_9(Cu_{0.25},Mg_{0.75})(PO_4)_6(OH)_2$ (HA-3) has the higher rate of degradation since it had the higher concentration of magnesium in the prepared hydroxyapatite.

Previous research has indicated that magnesium improves HA solubility, and the reason for this could be due to difference in size among possible $Ca^{+2}$and cations, and it may causes HA crystal deformation, altering their solubility and biodegradability in physiological fluids [97, 98]. Other research has suggested that the enhanced solubility of Mg-doped HA could be due to decreased crystallinity and/or increased surface hydration [88].

With respect to the sintering method, the outcomes do not refer to a great difference between both methods. Indeed HA compacted using CS method has slightly lower degradation rate than the traditional compacted HA. It seems that density was not the crucial factor that controlled HA degradation. The other factor that led to this discrepancy is the phase decomposition of hydroxyapatite. As indicated in the findings of x-ray diffraction Figure (4.10) that secondary phases (TCP and CaO) were identified besides the apatite phase. This case was not seen in the cold sintered HA. Such phases may boost the degradation of HA because they are more soluble in aqueous solution than HA; therefore, they lead to faster solubility [28] [99].

Chapter Five

Conclusions and Recommendations

Chapter Five

Conclusions and Recommendations

This chapter covers the main conclusions of this work. In addition, it presents some recommended futuristic work that might develop this research.

5.1. Conclusions

The results of this study may lead to infer the following points:

1. Ultrapure, homogeneous and very fine hydroxyapatite and co-doped hydroxyapatite can be prepared by wet chemical precipitation method.
2. Small additions of metal ions has changed the structure and main features of hydroxyapatite. Where decreasing in the unit cell volume was recorded to be 520.16 ($Å^3$)in HA-4 comparing to the 530.74($Å^3$) of pure HA .
3. The substituted of Cu^{+2} and Mg^{+2} to HA improves the antibacterial property significantly. As the increasing in Cu^{+2} concentration has superior inhibition effect.
4. This study confirmed that the cold sintering method is able to fabricate bulk HA with a relative density up to 87% at 250^{o} C and an external applied pressure of 250MPa.
5. The effects of doping elements are reflected in the behavior of HA. In this context, magnesium increases the degradation and densification of HA. While, Cu increases the antibacterial features of HA.

6. An increase of copper concentration has negative effect on the in vitro cell culture of HA using osteoblasts. On the other hand, existing of Mg^{2+} ions can enhance osteoblast growth.

5.2. Recommendations

The following are some recommendations that may be made on the basis of the findings obtained from the current study:

1. Study the effect of Triple-doping ions , such as selenium, cerium and strontium on the structure, mechanical and biological behavior of HA .

2. Densification improvement of cold sintered HA by moderating the sintering parameters i.e. temperature, time, solvent and pressure.

3. Study the effect of different sintering methods on densification behavior of (Mg, Cu) doped HA.

4. Carry out more biological tests like (quantification of cell number and collagen secretion) to investigate if doped HA induce bone formation.

References

References

[1] S. Mondal, A. Dey, and U. Pal, "Low temperature wet-chemical synthesis of spherical hydroxyapatite nanoparticles and their in situ cytotoxicity study," *Advances in nano research*, vol. 4, p. 295, 2016.

[2] E. Thian, T. Konishi, Y. Kawanobe, P. Lim, C. Choong, B. Ho, *et al.*, "Zinc-substituted hydroxyapatite: a biomaterial with enhanced bioactivity and antibacterial properties," *Journal of Materials Science: Materials in Medicine*, vol. 24, pp. 437-445, 2013.

[3] B. Yilmaz, A. Z. Alshemary, and Z. Evis, "Co-doped hydroxyapatites as potential materials for biomedical applications," *Microchemical Journal*, vol. 144, pp. 443-453, 2019.

[4] A. Bigi, E. Foresti, M. Gandolfi, M. Gazzano, and N. Roveri, "Inhibiting effect of zinc on hydroxylapatite crystallization," *Journal of Inorganic Biochemistry*, vol. 58, pp. 49-58, 1995.

[5] H. W. Kim, Y. M. Kong, Y. H. Koh, H. E. Kim, H. M. Kim, and J. S. Ko, "Pressureless sintering and mechanical and biological properties of fluor-hydroxyapatite composites with zirconia," *Journal of the American Ceramic Society*, vol. 86, pp. 2019-2026, 2003.

[6] S. Kobayashi, W. Kawai, and S. Wakayama, "The effect of pressure during sintering on the strength and the fracture toughness of

hydroxyapatite ceramics," *Journal of Materials Science: Materials in Medicine*, vol. 17, pp. 1089-1093, 2006.

[7] J. Wang and L. L. Shaw, "Transparent nanocrystalline hydroxyapatite by pressure-assisted sintering," *Scripta Materialia*, vol. 63, pp. 593-596, 2010.

[8] M. Prakasam, J. Locs, K. Salma-Ancane, D. Loca, A. Largeteau, and L. Berzina-Cimdina, "Fabrication, properties and applications of dense hydroxyapatite: a review," *Journal of functional biomaterials*, vol. 6, pp. 1099-1140, 2015.

[9] J.-P. Maria, X. Kang, R. D. Floyd, E. C. Dickey, H. Guo, J. Guo, *et al.*, "Cold sintering: current status and prospects," *Journal of Materials Research*, vol. 32, pp. 3205-3218, 2017.

[10] J. Andrews, D. Button, and I. M. Reaney, "Advances in cold sintering: Improving energy consumption and unlocking new potential in component manufacturing," *Johnson Matthey Technology Review*, vol. 64, pp. 219-232, 2020.

[11] H. Guo, A. Baker, J. Guo, and C. A. Randall, "Cold sintering process: a novel technique for low-temperature ceramic processing of ferroelectrics," *Journal of the American Ceramic Society*, vol. 99, pp. 3489-3507, 2016.

[12] L. Le Guéhennec, P. Layrolle, and G. Daculsi, "A review of bioceramics and fibrin sealant," *Eur Cell Mater*, vol. 8, p. 1e11, 2004.

[13] J. TU and M. Senthilkumar, "PREPARATION AND CHARACTERIZATION OF PURE AND SILVER NITRATE DOPED NANO HYDROXYAPATITE FOR BIOMEDICAL APPLICATIONS," *International Journal of Technical Research and Applications,* pp. 32-37, 2016.

[14] P. De Aza, A. De Aza, and S. De Aza, "Crystalline bioceramic materials," *Bol. Soc. Esp. Ceram,* vol. 44, pp. 135-145, 2005.

[15] S. Gomes, C. Vichery, S. Descamps, H. Martinez, A. Kaur, A. Jacobs, *et al.*, "Cu-doping of calcium phosphate bioceramics: From mechanism to the control of cytotoxicity," *Acta Biomaterialia,* vol. 65, pp. 462-474, 2018.

[16] M. Mucalo, *Hydroxyapatite (HAp) for biomedical applications*: Elsevier, 2015.

[17] N. M. Pu'ad, R. A. Haq, H. M. Noh, H. Abdullah, M. Idris, and T. Lee, "Synthesis method of hydroxyapatite: A review," *Materials Today: Proceedings*, vol. 29, pp. 233-239, 2020.

[18] S. V. Dorozhkin, "Calcium orthophosphates as bioceramics: state of the art," *Journal of functional biomaterials,* vol. 1, pp. 22-107, 2010.

[19] D. Campoccia, L. Montanaro, and C. R. Arciola, "The significance of infection related to orthopedic devices and issues of antibiotic resistance," *Biomaterials,* vol. 27, pp. 2331-2339, 2006.

[20] I. Mobasherpour, M. S. Heshajin, A. Kazemzadeh, and M. Zakeri, "Synthesis of nanocrystalline hydroxyapatite by using precipitation method," *Journal of Alloys and Compounds,* vol. 430, pp. 330-333, 2007.

[21] M. M. H. Jasim, "Experimental and Numerical Investigation of Crack Propagation and Opening in Bioceramic Materials " MSc, Non Metallic Materials Engineering University of Babylon Babylon 2018.

[22] J. Kolmas, E. Groszyk, and D. Kwiatkowska-Różycka, "Substituted hydroxyapatites with antibacterial properties," *BioMed Research International,* vol. 2014, 2014.

[23] V. S. Gshalaev and A. C. Demirchan, *Hydroxyapatite: synthesis, properties, and applications*: Nova Science Publishers, 2012.

[24] M. Markovic, B. O. Fowler, and M. S. Tung, "Preparation and comprehensive characterization of a calcium hydroxyapatite reference material," *Journal of research of the National Institute of Standards and Technology,* vol. 109, p. 553, 2004.

[25] S. V. Dorozhkin, "Calcium orthophosphates in nature, biology and medicine," *Materials,* vol. 2, pp. 399-498, 2009.

[26] S. Kannan, F. Goetz-Neunhoeffer, J. Neubauer, and J. Ferreira, "Ionic substitutions in biphasic hydroxyapatite and β-tricalcium phosphate mixtures: structural analysis by Rietveld refinement," *Journal of the American Ceramic Society,* vol. 91, pp. 1-12, 2008.

[27] D. Gomes, A. Santos, G. Neves, and R. Menezes, "A brief review on hydroxyapatite production and use in biomedicine," *Cerâmica*, vol. 65, pp. 282-302, 2019.

[28] M. Askari Louyeh, "Silver, magnesium and zinc substituted hydroxyapatite for orthopaedic applications," University of Birmingham, 2017.

[29] I. Cacciotti, "Multisubstituted hydroxyapatite powders and coatings: The influence of the codoping on the hydroxyapatite performances," *International Journal of Applied Ceramic Technology*, vol. 16, pp. 1864-1884, 2019.

[30] Y. Oshida, *Hydroxyapatite - Synthesis and Applications*, 2015.

[31] M. O. Li, X. Xiao, R. Liu, C. Chen, and L. Huang, "Structural characterization of zinc-substituted hydroxyapatite prepared by hydrothermal method," *Journal of materials science: Materials in medicine*, vol. 19, pp. 797-803, 2008.

[32] S. Bodhak, S. Bose, and A. Bandyopadhyay, "Influence of MgO, SrO, and ZnO dopants on electro-thermal polarization behavior and in vitro biological properties of hydroxyapatite ceramics," *Journal of the American Ceramic Society*, vol. 94, pp. 1281-1288, 2011.

[33] C. Paluszkiewicz, A. Ślósarczyk, D. Pijocha, M. Sitarz, M. Bućko, A. Zima, *et al.*, "Synthesis, structural properties and thermal stability of Mn-doped hydroxyapatite," *Journal of Molecular Structure*, vol. 976, pp. 301-309, 2010.

[34] I. Cacciotti, A. Bianco, M. Lombardi, and L. Montanaro, "Mg-substituted hydroxyapatite nanopowders: synthesis, thermal stability and sintering behaviour," *Journal of the European Ceramic Society*, vol. 29, pp. 2969-2978, 2009.

[35] L. Stipniece, K. Salma-Ancane, N. Borodajenko, M. Sokolova, D. Jakovlevs, and L. Berzina-Cimdina, "Characterization of Mg-substituted hydroxyapatite synthesized by wet chemical method," *Ceramics International*, vol. 40, pp. 3261-3267, 2014.

[36] A. Ewald, D. Hösel, S. Patel, L. M. Grover, J. E. Barralet, and U. Gbureck, "Silver-doped calcium phosphate cements with antimicrobial activity," *Acta biomaterialia*, vol. 7, pp. 4064-4070, 2011.

[37] V. Stanić, S. Dimitrijević, J. Antić-Stanković, M. Mitrić, B. Jokić, I. B. Plećaš, *et al.*, "Synthesis, characterization and antimicrobial activity of copper and zinc-doped hydroxyapatite nanopowders," *Applied Surface Science*, vol. 256, pp. 6083-6089, 2010.

[38] A. Rajendran, R. C. Barik, D. Natarajan, M. Kiran, and D. K. Pattanayak, "Synthesis, phase stability of hydroxyapatite–silver composite with antimicrobial activity and cytocompatability," *Ceramics International*, vol. 40, pp. 10831-10838, 2014.

[39] A. Jacobs, G. Renaudin, C. Forestier, J.-M. Nedelec, and S. Descamps, "Biological properties of copper-doped biomaterials for orthopedic applications: A review of antibacterial, angiogenic and osteogenic aspects," *Acta Biomaterialia*, vol. 117, pp. 21-39, 2020.

[40] M. Sadat-Shojai, M. T. Khorasani, E. Dinpanah-Khoshdargi, and A. Jamshidi, "Synthesis methods for nanosized hydroxyapatite with diverse structures," *Acta Biomater*, vol. 9, pp. 7591-621, Aug 2013.

[41] X. Wang, "Preparation, synthesis and application of Sol-gel method," 10/28 2020.

[42] S. Faouri, A. Mostaed, J. Dean, D. Wang, D. Sinclair, S. Zhang, *et al.*, "High quality factor cold sintered Li2MoO4-BaFe12O19 composites for microwave applications," *Acta Materialia*, vol. 166, 03/01 2019.

[43] A. M. Abdullah, "Optimization of Lead Dioxide Powder Densified by Cold Sintering Process," Master, College of Materials Engineering/Cermaic department Babylon Iraq, 2019.

[44] R. L. Coble, "Sintering Crystalline Solids. I. Intermediate and Final State Diffusion Models," *Journal of Applied Physics*, vol. 32, pp. 787-792, 1961.

[45] S. Grasso, M. Biesuz, L. Zoli, G. Taveri, A. I. Duff, D. Ke, *et al.*, "A review of cold sintering processes," *Advances in Applied Ceramics*, vol. 119, pp. 115-143, 2020/04/02 2020.

[46] L. li, W. Hong, S. Yang, H. Yan, and X. Chen, "Effects of water content during cold sintering process of NaCl ceramics," *Journal of Alloys and Compounds*, vol. 787, 02/01 2019.

[47] S. H. Bang, T. Herisson De Beauvoir, and C. A. Randall, "Densification of thermodynamically unstable tin monoxide using cold sintering

process," *Journal of the European Ceramic Society*, vol. 39, pp. 1230-1236, 2019/04/01/ 2019.

[48] H. Guo, T. J. M. Bayer, J. Guo, A. Baker, and C. A. Randall, "Current progress and perspectives of applying cold sintering process to ZrO2-based ceramics," *Scripta Materialia*, vol. 136, pp. 141-148, 2017/07/15/ 2017.

[49] D. Wang, H. Guo, C. S. Morandi, C. A. Randall, and S. Trolier-McKinstry, "Cold sintering and electrical characterization of lead zirconate titanate piezoelectric ceramics," *APL Materials*, vol. 6, p. 016101, 2018.

[50] D. Wang, D. Zhou, S. Zhang, Y. Vardaxoglou, W. G. Whittow, D. Cadman, *et al.*, "Cold-Sintered Temperature Stable Na0.5Bi0.5MoO4–Li2MoO4 Microwave Composite Ceramics," *ACS Sustainable Chemistry & Engineering*, vol. 6, pp. 2438-2444, 2018/02/05 2018.

[51] R. Boston, J. Guo, S. Funahashi, A. L. Baker, I. M. Reaney, and C. A. Randall, "Reactive intermediate phase cold sintering in strontium titanate," *RSC Advances*, vol. 8, pp. 20372-20378, 2018.

[52] I. J. Induja and M. T. Sebastian, "Microwave dielectric properties of cold sintered Al2O3-NaCl composite," *Materials Letters*, vol. 211, pp. 55-57, 2018/01/15/ 2018.

[53] C. Vakifahmetoglu and L. Karacasulu, "Cold sintering of ceramics and glasses: A review," *Current Opinion in Solid State and Materials Science*, vol. 24, p. 100807, 2020/02/01/ 2020.

[54] T. Charoonsuk, U. Sukkha, T. Kolodiazhnyi, and N. Vittayakorn, "Enhancing the densification of ceria ceramic at low temperature via the cold sintering assisted two-step sintering process," *Ceramics International*, vol. 44, pp. S54-S57, 2018/11/01/ 2018.

[55] S. Funahashi, J. Guo, H. Guo, K. Wang, A. L. Baker, K. Shiratsuyu, *et al.*, "Demonstration of the cold sintering process study for the densification and grain growth of ZnO ceramics," *Journal of the American Ceramic Society*, vol. 100, pp. 546-553, 2017.

[56] H. Guo, J. Guo, A. Baker, and C. A. Randall, "Cold sintering process for ZrO2-based ceramics: significantly enhanced densification evolution in yttria-doped ZrO2," *Journal of the American Ceramic Society*, vol. 100, pp. 491-495, 2017.

[57] H. Guo, T. Bayer, J. Guo, A. Baker, and C. Randall, "Cold sintering process for 8 mol%Y2O3-stabilized ZrO2 ceramics," *Journal of the European Ceramic Society*, vol. 37, 01/12 2017.

[58] V. Medri, F. Servadei, R. Bendoni, A. Natali Murri, A. Vaccari, and E. Landi, "Nano-to-macroporous TiO2 (anatase) by cold sintering process," *Journal of the European Ceramic Society*, vol. 39, pp. 2453-2462, 2019/07/01/ 2019.

[59] M. u. Hassan and H. J. Ryu, "Cold sintering and durability of iodate-substituted calcium hydroxyapatite (IO-HAp) for the immobilization of radioiodine," *Journal of Nuclear Materials*, vol. 514, pp. 84-89, 2019/02/01/ 2019.

[60] M. u. Hassan and H. J. Ryu, "Sintering of Hydroxyapatite at Extra Ordinary Low Temperature of <200 deg C - A Way Forward to the Effective Immobilization of Radioiodine," in *Proceedings of the KNS 2017 Spring Meeting*, Korea, Republic of, 2017, pp. 1CD-ROM.

[61] T. Hérisson de Beauvoir, K. Tsuji, X. Zhao, J. Guo, and C. Randall, "Cold sintering of ZnO-PTFE: Utilizing polymer phase to promote ceramic anisotropic grain growth," *Acta Materialia*, vol. 186, pp. 511-516, 2020/03/01/ 2020.

[62] A. Ndayishimiye, M. Y. Sengul, T. Sada, S. Dursun, S. H. Bang, Z. A. Grady, *et al.*, "Roadmap for densification in cold sintering: Chemical pathways," *Open Ceramics*, vol. 2, p. 100019, 2020/07/01/ 2020.

[63] M. Tahriri, M. Solati-Hashjin, and H. Eslami, "Synthesis and Characterization of Hydroxyapatite Nanocrystals via Chemical Precipitation Technique," *Iranian Journal of Pharmaceutical Sciences*, vol. 4, pp. 127-134, 2008.

[64] S. S. A. Abidi and Q. Murtaza, "Synthesis and Characterization of Nano-hydroxyapatite Powder Using Wet Chemical Precipitation Reaction," *Journal of Materials Science & Technology*, vol. 30, pp. 307-310, 2014/04/01/ 2014.

[65] Y. C. The, C. Y. Tan, R. Singh, J. Purbolaksono, Y. M. Tan, H. Thambinayagam, *et al.*, "Effect of calcination on the sintering behaviour of hydroxyapatite," *Ceramics - Silikaty*, vol. 58, pp. 320-325, 01/01 2014.

[66] A. Yelten-Yilmaz and S. Yilmaz, "Wet chemical precipitation synthesis of hydroxyapatite (HA) powders," *Ceramics International*, vol. 44, pp. 9703-9710, 2018.

[67] Y. Li, J. Ho, and C. P. Ooi, "Antibacterial efficacy and cytotoxicity studies of copper (II) and titanium (IV) substituted hydroxyapatite nanoparticles," *Materials Science and Engineering: C*, vol. 30, pp. 1137-1144, 2010.

[68] B. Gayathri, N. Muthukumarasamy, D. Velauthapillai, and S. Santhosh, "Magnesium incorporated hydroxyapatite nanoparticles: preparation, characterization, antibacterial and larvicidal activity," *Arabian journal of chemistry*, vol. 11, pp. 645-654, 2018.

[69] C. Paucar Álvarez, J. S. C. Sarmiento, S. C. Freitas, and C. García, "Solvothermal Synthesis of Magnesium Oxide-Substituted Hydroxyapatite Nanoparticles as Antibacterial Nanomaterial for Biomedical Applications," in *Defect and Diffusion Forum*, 2017, pp. 8-14.

[70] D. Predoi, S. L. Iconaru, M. V. Predoi, G. E. Stan, and N. Buton, "Synthesis, characterization, and antimicrobial activity of magnesium-doped hydroxyapatite suspensions," *Nanomaterials*, vol. 9, p. 1295, 2019.

[71] A. Mariappan, P. Pandi, N. Balasubramanian, R. R. Palanichamy, and K. Neyvasagam, "Structural, optical and antimicrobial activity of copper and zinc doped hydroxyapatite nanopowders using sol-gel method," *Mechanics, Materials Science & Engineering Journal*, vol. 9, 2017.

[72] S. Helen and A. R. Kumar, "Co-Dopands on Hydroxyapatite in Structural, Morphology And in Antibacterial Activity," *Mechanics, Materials Science & Engineering Journal,* vol. 14, 2018.

[73] H. Alioui, O. Bouras, and J.-C. Bollinger, "Toward an efficient antibacterial agent: Zn-and Mg-doped hydroxyapatite nanopowders," *Journal of Environmental Science and Health, Part A,* vol. 54, pp. 315-327, 2019.

[74] H. Nosrati, R. Sarraf-Mamoory, R. Z. Emameh, D. Q. S. Le, M. C. Perez, and C. E. Bünger, "Low temperature consolidation of hydroxyapatite-reduced graphene oxide nano-structured powders," *Materials Advances,* vol. 1, pp. 1337-1346, 2020.

[75] M. ul Hassan, M. Akmal, and H. J. Ryu, "Cold sintering of as-dried nanostructured calcium hydroxyapatite without using additives," *Journal of Materials Research and Technology,* vol. 11, pp. 811-822, 2021.

[76] E. Landi, A. Tampieri, G. Celotti, and S. Sprio, "Densification behaviour and mechanisms of synthetic hydroxyapatites," *Journal of the European Ceramic Society,* vol. 20, pp. 2377-2387, 2000.

[77] Y. Chen, Z. Liu, T. Jiang, X. Zou, L. Lei, W. Yan, *et al.*, "Strontium-substituted biphasic calcium phosphate microspheres promoted degradation performance and enhanced bone regeneration," *Journal of Biomedical Materials Research Part A,* vol. 108, pp. 895-905, 2020.

[78] S. Lazić, S. Zec, N. Miljević, and S. Milonjić, "The effect of temperature on the properties of hydroxyapatite precipitated from calcium hydroxide

and phosphoric acid," *Thermochimica Acta,* vol. 374, pp. 13-22, 2001/06/18/ 2001.

[79] I.-H. Lee, J.-A. Lee, J.-H. Lee, Y.-W. Heo, and J.-J. Kim, "Effects of pH and reaction temperature on hydroxyapatite powders synthesized by precipitation," *Journal of the Korean Ceramic Society,* vol. 57, pp. 56-64, 2020.

[80] C. Mardziah, I. Sopyan, and S. Ramesh, "Strontium-doped hydroxyapatite nanopowder via sol-gel method: effect of strontium concentration and calcination temperature on phase behavior," *Artif. Organs,* vol. 23, pp. 105-113, 2009.

[81] Z. Evis and T. Webster, "Nanosize hydroxyapatite: doping with various ions," *Advances in Applied Ceramics,* vol. 110, pp. 311-321, 2011.

[82] A. R. Noviyanti, I. Rahayu, and R. P. Fauzia, "The effect of Mg concentration to mechanical strength of hydroxyapatite derived from eggshell," *Arabian Journal of Chemistry,* vol. 14, p. 103032, 2021.

[83] W.-L. Du, Y.-L. Xu, Z.-R. Xu, and C.-L. Fan, "Preparation, characterization and antibacterial properties against E. coli K88 of chitosan nanoparticle loaded copper ions," *Nanotechnology,* vol. 19, p. 085707, 2008.

[84] N. Matsumoto, K. Sato, K. Yoshida, K. Hashimoto, and Y. Toda, "Preparation and characterization of β-tricalcium phosphate co-doped with monovalent and divalent antibacterial metal ions," *Acta Biomaterialia,* vol. 5, pp. 3157-3164, 2009.

[85] T. Tite, A.-C. Popa, L. M. Balescu, I. M. Bogdan, I. Pasuk, J. M. Ferreira, *et al.*, "Cationic substitutions in hydroxyapatite: Current status of the derived biofunctional effects and their in vitro interrogation methods," *Materials*, vol. 11, p. 2081, 2018.

[86] A. Farzadi, F. Bakhshi, M. Solati-Hashjin, M. Asadi-Eydivand, and N. A. abu Osman, "Magnesium incorporated hydroxyapatite: Synthesis and structural properties characterization," *Ceramics International*, vol. 40, pp. 6021-6029, 2014.

[87] G. Muralithran and S. Ramesh, "The effects of sintering temperature on the properties of hydroxyapatite," *Ceramics International*, vol. 26, pp. 221-230, 2000.

[88] E. Boanini, M. Gazzano, and A. Bigi, "Ionic substitutions in calcium phosphates synthesized at low temperature," *Acta biomaterialia*, vol. 6, pp. 1882-1894, 2010.

[89] I. Fadeev, L. Shvorneva, S. Barinov, and V. Orlovskii, "Synthesis and structure of magnesium-substituted hydroxyapatite," *Inorganic Materials*, vol. 39, pp. 947-950, 2003.

[90] H. Guo, J. Guo, A. Baker, and C. A. Randall, "Hydrothermal-assisted cold sintering process: a new guidance for low-temperature ceramic sintering," *ACS applied materials & interfaces*, vol. 8, pp. 20909-20915, 2016.

[91] Ž. Radovanović, Đ. Veljović, L. Radovanović, I. Zalite, E. Palcevskis, R. Petrović, *et al.*, "Ag+, Cu2+ and Zn2+ doped hydroxyapatite/tricalcium phosphate bioceramics: Influence of doping and sintering technique on

mechanical properties," *Processing and Application of Ceramics,* vol. 12, pp. 268-276, 2018.

[92] A. Elrayah, J. Weng, and E. Suliman, "Effect of Copper Ions Doped-Hydroxyapatite 3d Fiber Scaffold," *Int. J. Biomed. Biol. Eng,* vol. 13, pp. 255-259, 2019.

[93] C. Tan, A. Yaghoubi, S. Ramesh, S. Adzila, J. Purbolaksono, M. Hassan, *et al.*, "Sintering and mechanical properties of MgO-doped nanocrystalline hydroxyapatite," *Ceramics International*, vol. 39, pp. 8979-8983, 2013.

[94] M. Nagano, T. Nakamura, T. Kokubo, M. Tanahashi, and M. Ogawa, "Differences of bone bonding ability and degradation behaviour in vivo between amorphous calcium phosphate and highly crystalline hydroxyapatite coating," *Biomaterials,* vol. 17, pp. 1771-1777, 1996.

[95] P. Ducheyne and J. M. Cuckler, "Bioactive ceramic prosthetic coatings," *Clinical orthopaedics and related research*, pp. 102-114, 1992.

[96] D. Mehta, S. George, and P. Mondal, "Synthesis of hydroxyapatite by chemical precipitation technique and study of its biodegradability," *International Journal of Research in Advent Technology*, vol. 2, pp. 159-161, 2014.

[97] E. Landi, G. Logroscino, L. Proietti, A. Tampieri, M. Sandri, and S. Sprio, "Biomimetic Mg-substituted hydroxyapatite: from synthesis to in vivo behaviour," *Journal of Materials Science: Materials in Medicine,* vol. 19, pp. 239-247, 2008.

[98] A. Bigi, G. Falini, E. Foresti, A. Ripamonti, M. Gazzano, and N. Roveri, "Magnesium influence on hydroxyapatite crystallization," *Journal of Inorganic Biochemistry*, vol. 49, pp. 69-78, 1993.

[99] H. Wang, *Hydroxyapatite degradation and biocompatibility*: The Ohio State University, 2004.

الخلاصة

يعتبرالهيدروكسي اباتايت (HA) احد اهم المواد السيراميكية التي تكون العظام في الكائنات الفقرية و الذي يتم استخدامة على نطاق واسع في التطبيقات الطبيبة بسبب التوافق الحيوي العالي، كونه غير سام ولة القدرة العالية على خلق ترابطات في العظام و كذلك الانسجة الحيوية. تم تحضير هيدروكسيباتيت نقي ومشوب مع أيونات Cu^{+2}، Mg^{+2} باستخدام طريقة الترسيب الكيميائي الرطب في درجة حرارة الغرفة. في هذه الدراسة تم تحضير ثلاثة تراكيب متكافئة من HA المشوب عن طريق استبدال أيونات الكالسيوم بأيونات المعادن الثنائية التكافؤ وفقًا للنسب :(Mg^{+2} :Cu^{+2}) (٠,٥:٠,٥ , ٠,٢٥:٠,٧٥, ٠,٧٥:٠,٢٥) بعد ذلك تم كلسنة المساحيق المرسبة بدرجة حرارة ٨٠٠ درجة مئوية لمدة ساعتين. تم اجراء عدد من الفحوصات لغرض التاكد من الطور البنيوي الناتج بالاضافة الى تحديد شكل و حجم الجسيمات الجديدة. بينت النتائج ال XRDأن الـ HA المُصنَّع المُشوب مكون من طور واحد، ولم يُظهر أطوارًا ثانوية أخرى أو أكاسيد لمواد التشويب. وايضا من خلال نتيجة تحليل XRD يمكن الاستنتاج الى ان الاطوار الرئيسية لجميع HA المشوب تعرضت لازاحة . بينما أشارت صور TEM إلى حدوث استطالة بسيطة في جسيمات الـ HA بعد التشويب. و كان حجم الحبيبات الناتجة اقل من١٠٠ نانومتر .كما أظهرت النتائج أن جميع النسب المتكافئة من $Cu^{٢+}$ و$Mg^{٢+}$قد حسنت من النشاط المضاد للبكتيريا لـ HA بالاخص [$Ca_9(Cu_{0.75},Mg_{0.25})\ (PO_4)_6\ (OH)_2$] لة نشاط تثبيط للبكتريا أعلى من المركبات الاخرى . من ناحية أخرى ، فإن تبديل النسبة المتكافئة للمغنيسيوم والنحاس ، أي [$Ca_9\ (Cu_{0.25},\ Mg_{0.75})\ (PO_4)_6\ (OH)_2$] أضهر دورًا متفوقًا في تحفيز الخلايا الحيوية Osteoblasts على النمو و التكاثر أكثر من الهيدروكسي ابتايت النقي . لاحقا، تم تلبيد عينات من الـ HAاستخدام تقنية تلبيد حديثة و بسيطة تعرف باسم طريقة التلبيد على البارد (CSM). حيث لا تزيد درجة حرارة التلبيد عن ٣٠٠ درجة مئوية مع تسليط ضغط خارجي. اضهرت نتيجة XRD لعينات HA المصنعة باستخدام CSM عدم وجود اطوار ثانوية لل CaO أو TTC مع طور Hydroxyapatite.

بلغت كثافة هيدروكسيابتايت النقي و المحضر باستخدام CSM ٢,٦٩٧٢ غرام/سم^{٣} مقارنة بـ ٢,٩٤٣٣ غرام/سم^{٣} لـلـ HA المحضر بواسطة التلبيد التقليدي. أدى إدخال ألايونات المعدنية إلى تباين الكثافة وفقًا لنسبها في بنية HA. على سبيل المثال ، يُظهرHA-4 المصنع بواسطة CSM كثافة تبلغ ٢,٨٧٩٢ غرام/سم^{٣}. في نفس السياق ، ان نتائج الصلادة تغيرت اعتمادا على طريقة التلبيد و التركيب الكيميائي من ناحية أخرى. حيث تم قياس صلادة الـ HA النقي المحضر باستخدام التلبيد التقليدي لتكونHV ٣٢٣,٨٣ مقارنة بـ ٢٢٤,٨٦ HV لـلـ HA الملبد بواسطة CSM. كما أظهرت نتائج التحلل الحيوي Biodegradability الى أن تحلل لـلـ HA زاد مع زيادة عدد ايام الغمر. كما تشير النتائج المتحصل عليها إلى أن الـHA النقي كان لديه أقل معدل تحلل، و أن زيادة محتوى Mg في هيكل الـ HA حسن من التحلل بشكل كبير.